Identification of Molecular Targets for the Treatment of the Skeletal Phenotype in Lysosomal Storage Disorders

Thesis

Identification of molecular targets for the treatment of the skeletal phenotype in Lysosomal Storage Disorders

A thesis submitted for the degree of Doctor of Philosophy at

The Open University

By
Rosa Bartolomeo
MSc

Affiliated Research Centre: **Telethon institute of Genetics and Medicine (TIGEM)**

Director of Studies: **Carmine Settembre, Ph.D**

Submission for examination: January 2017

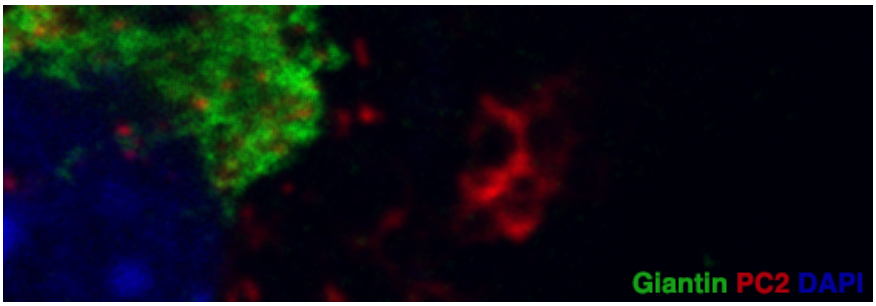

".. and yet it doesn't matter if he's all in bits. The whole is disorganized. But each individual fragment is in order, is a representative of a Higher Order. The Highest Order prevails even in the disintegration. The totality is present even in the broken pieces. More clearly present, perhaps, than in a completely coherent work. At least you aren't lulled into a sense of false security by some merely human, merely fabricated order. You have to rely on your immediate perception of the ultimate order. So in a certain sense disintegration may have its advantages. But of course it's dangerous, horribly dangerous. Suppose you couldn't get back, out of the chaos.."

Aldous Huxley, The Doors of Perception, 1954

(I can't get no) Satisfaction

The Rolling Stones, 1965

LIST OF FIGURES

LIST OF ABBREVIATIONS

A.A.	Amino acid
AMPK	Adenosine monophosphate- activated protein kinase
ANOVA	Analysis of variance
ARSB	Arylsulfatase B
ATG	Autophagy-related gene
ATP	Adenosine 5'-triphosphate
AV	Autophagosome
Bcl-2	Beta cell lymphoma 2
BMP	Bone morphogenetic protein
BSA	Bovine serum albumin
CLEAR	Coordinated lysosomal expression and regulation element
CMV	Citomegalovirus
Coll II-IX-X	Type 2-9-10 collagen
CS	Chondroitin sulfate
Ctr	Control
DMEM	Dulbecco's modified Eagle's medium
DMSO	Dimethyl sulfoxide
DNA	Deoxyribose nucleic acid
DS	dermatan sulfate
E	Embryonic
ECM	Extra-cellular matrix
EDTA	1-(4-aminobenzyl)ethylenediamine-N,N,N'N'-tetra-acetic acid
EO	Endochondral ossification

ERK	Extracellular signal-regulated kinase
ERT	Enzyme replacement therapy
FBS	Fetal bovine serum
FGF	Fibroblast growth factor
FGFR	Fibroblast growth factor receptor
GAG	Glycosaminoglycan
GAP	GTPase activating protein
GDP	Guanosine 5’-diphosphate
GFP	Green fluorescent protein
GTP	Guanosine 5’-triphosphate
Gusb	Beta-glucuronidase
GWAS	Genome-wide association study
h	hour
HCl	Hydrogen cloride
HeLa	Henrietta Lacks
HEPES	4-(2-hydroxyethyl)-1-piperazineethanesulfonic acid
HLH	Helix–loop–helix
HOPS	Homotypic vacuole fusion and protein sorting
HS	Heparan sulfate
HSCT	Hematopoietic stem cell transplantation
IF	Immunofluorescence
IGF	Insulin-like growth factor
IHC	Immunohistochemistry
Ihh	Indian hedgehog
kDa	Kilo-Dalton

KS	Keratan sulfate
Lamp-1	Lysosomal-associated membrane protein 1
LAMTOR	Late endosomal/lysosomal adaptor, MAPK and MTOR activator
LSD	Lysosomal storage disorder
Lys	Lysosome
m	milli
MAP1LC3	Microtubule-associated protein light chain 3
MAPK	Mitogen activated protein kinase
MMP	Matrix metalloproteinase
MPS	Mucopolysaccharidosis
Mr	Marker
mTOR	Mammalian target of rapamycin
mTORC1/2	Mammalian target of rapamycin complex 1/2
Na3VO4	Sodium orthovanadate
NaCl	Sodium cloride
PAGE	Polyacrylamide gel electrophoresis
PBS	Phosphate-buffered saline
PC	Procollagen
PCR	Polymerase chain reaction
PFA	Paraformaldehyde
PI(3,4,5)P_3	Phosphatidylinositol-3,4,5-triphosphate
PI(3)P	Phosphatidylinositol-3-phosphate
PI3K	Phosphatidylinositol 3 kinase
PIER	Proteolytic induced epitope retrieval

POC	Primary ossification center
PTHrP	Parathyroid hormone related peptide
RCS	Rat chondrosarcoma
RFP	Red fluorescent protein
Rheb	RAS homologue enriched in brain
RIPA	Radioimmuno precipitation assay
ROI	Region of interest
Rpt	Raptor
SD	Standard deviation
SDS	Sodium dodecyl sulfate
SEM	Standar error of mean
Ser	Serine
SOX	SRY (sex determining region Y)-box containing gene
SQSTM1	Sequestosome 1
TFEB	Transcription factor EB
ULK	Unc-51-like kinase
UPS	Ubiquitin proteasome system
UVRAG	UV radiation resistance-associated gene
VEGF	Vascular endothelial growth factor
Vps	Vacuolar protein sorting
WT	Wild-type
μ	Micro

TABLE OF CONTENT

Abstract

Autophagy is a lysosomal pathway deputed to the recycling of cellular components. Regulation of autophagy is essential for tissue homeostasis. The mTORC1 kinase tunes autophagy according to nutrient levels and environmental factors. Recently the laboratory in which I performed the experiments used for my thesis has demonstrated that autophagy, by controlling collagen secretion in chondrocytes, is necessary during bone growth. However, whether mTORC1 and autophagy play any role in the pathogenesis of skeletal disorders is still unknown. In this thesis work I show that an altered mTORC1 signaling impairs autophagy and consequently bone growth in lysosomal storage disorders (LSDs). I found that in LSD chondrocytes a proteasome-sensitive increase of mTORC1 signaling inhibits late steps of autophagy through the phosphorylation of the UV radiation resistance-associated gene (UVRAG) protein, a member of the Beclin1/Vps34 complex. Reducing mTORC1 signaling or enhancing Beclin1/Vps34/UVRAG complex activity rescued autophagy flux in LSD chondrocytes. *In vivo,* normalization of mTORC1 signaling or pharmacological induction of Beclin1 rescued collagen levels in cartilage and bone growth in two different LSD mouse models. Taken together, these data unveil a role for mTORC1 and autophagy in the pathogenesis of skeletal disorders and suggest their modulation as new therapy for the skeletal abnormalities observed in LSDs.

Introduction

1. Skeletogenesis.

The process by which bones are formed is called ossification. Ossification is an extremely complex, life-long process. Formation of the adult skeleton is achieved through two independent mechanisms: intramembranous and endochondral ossification[1]. In intramembranous bone formation, mesenchymal cells directly differentiate into osteoblasts. Some of the craniofacial bones are formed this way. Endochondral ossification (EO) is the process responsible for formation of the majority of bones in the vertebrate skeleton. EO starts from mesenchymal cells that condense at the position of future bone, through a complex process of chondrogenesis to form a highly controlled and precisely shaped cartilage template[2].

The cartilage template grows through chondrocyte proliferation and differentiation to establish the cartilage growth plate that ultimately drives the longitudinal growth of the bone. This process eventually determines the adult height. Long bones such as femur and tibia are formed through this process. Finally, a process of growth and remodeling after birth (in a growth and maintenance phase) results in a skeleton which is well adapted to its function as an organ not only for support and protection of internal organs, but also for movement, blood cell formation and regulation of calcium homeostasis.

1.1 Endochondral bone formation.

Endochondral ossification is initiated by aggregation of mesenchymal cells, followed by cell differentiation into chondrocytes through the process of chondrogenesis (**Figure 1**).

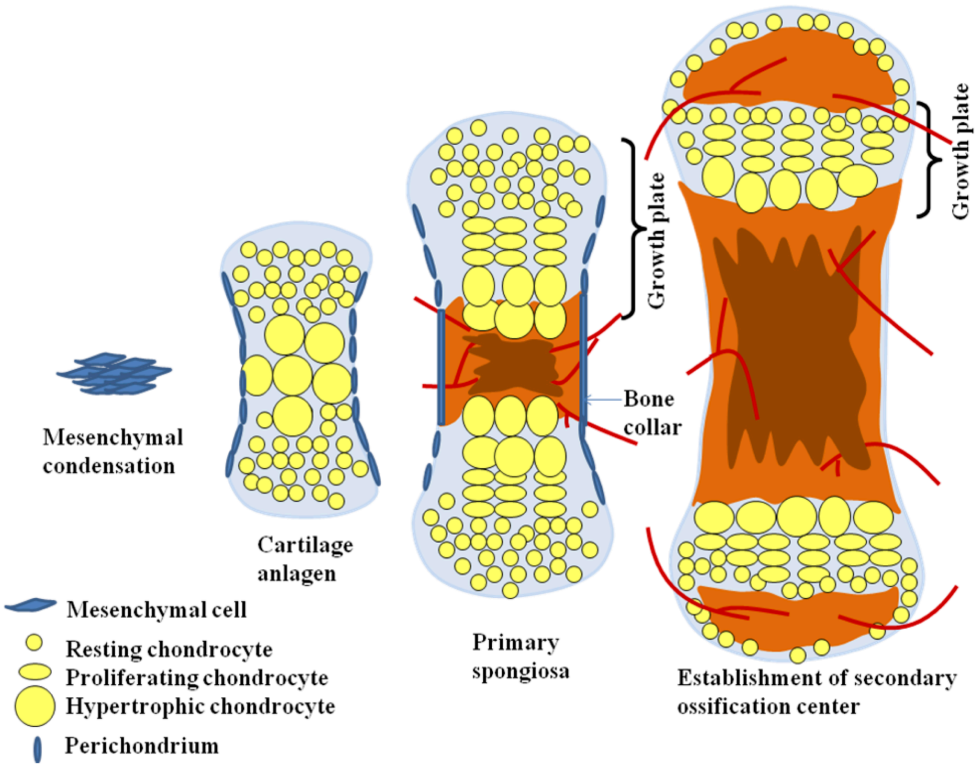

Figure 1. Overview of endochondral ossification.
During embryogenesis, mesenchymal cells start to aggregate and condense at the location of future bone. They then differentiate into chondrocyte in the center of these condensations through chondrogenesis. Chondrocytes proliferate and differentiate within these condensations leading to the formation of cartilage anlagen. At the periphery of the condensations, cells flatten, elongate and form the perichondrium. These chondrocytes also keep proliferating to expand the cartilage template. Eventually, cells at the center of this template terminally differentiate into hypertrophic cells. Perichondral cells adjacent to hypertrophic chondrocyte become osteoblasts, forming a bone collar. Hypertrophic chondrocyte direct mineralization of the surrounding cartilage matrix, attract blood vessel invasion, and then undergo apoptosis. Osteoblasts form early trabecular bone adjacent to the hypertrophic chondrocytes, forming the primary spongiosa. Epiphyseal growth plates form at both ends of the long bone with unique organization of the chondrocytes. At the end of the bone, the secondary ossification center forms through cycles of chondrocyte hypertrophy, vascular invasion and osteoblast activity. (Created according to [1-3])

During embryogenesis, mesenchymal cells start to aggregate and condense at the location of future bone. They then differentiate into chondrocyte in the center of these condensations through chondrogenesis. Chondrocytes proliferate and differentiate within these condensations leading to the formation of cartilage anlagen. At the periphery of the condensations, cells flatten, elongate and form the perichondrium. These chondrocytes also keep proliferating to expand the cartilage template. Eventually,

cells at the center of this template terminally differentiate into hypertrophic cells. Perichondral cells adjacent to hypertrophic chondrocyte become osteoblasts, forming a bone collar. Hypertrophic chondrocyte direct mineralization of the surrounding cartilage matrix, attract blood vessel invasion, and then undergo apoptosis. Osteoblasts form early trabecular bone adjacent to the hypertrophic chondrocytes, forming the primary spongiosa. Epiphyseal growth plates form at both ends of the long bone with unique organization of the chondrocytes. At the end of the bone, the secondary ossification center forms through cycles of chondrocyte hypertrophy, vascular invasion and osteoblast activity[1].

Chondrogenesis is a highly complex process leading to the formation of a cartilage template. Early condensations can be found in the human fetus at 6.5 weeks of gestation and at embryonic (E) 10.5 days (E10.5) of mouse development. At this time point in development, the shape, number and position of future skeletal elements are decided[3]. Members of the Sox family of transcription factors (Sox9, Sox5 and Sox6) are required for this early differentiation[2]. Cells in the condensations differentiate to chondrocytes and deposit an extracellular matrix specific for cartilage, consisting of molecules such as collagens II, IX, and XI and proteoglycans (e.g. aggrecan). At the border of the condensations, chondrocytes differentiate to flattened elongated cells to form the perichondrium[1]. All these events contribute to the establishment of cartilage anlagen for the future bone elements.

1.2 Epiphyseal growth plate.

Once mesenchymal cells commit to the chondrogenic lineage, the subsequent events of EO occur through the epiphyseal growth plate. Longitudinal bone growth dictates the final height of human bodies and is dependent on the activity of the growth plates[4]. The growth plate is a unique structure where specific chondrocyte populations are

organized in distinct zones (e.g. zones of resting, proliferating, and hypertrophic chondrocytes) based on their morphology, cellular activities and gene expression patterns (**Figure 2**). Within these zones, the chondrocytes are organized in distinguishable columnar arrays and express different matrix proteins.

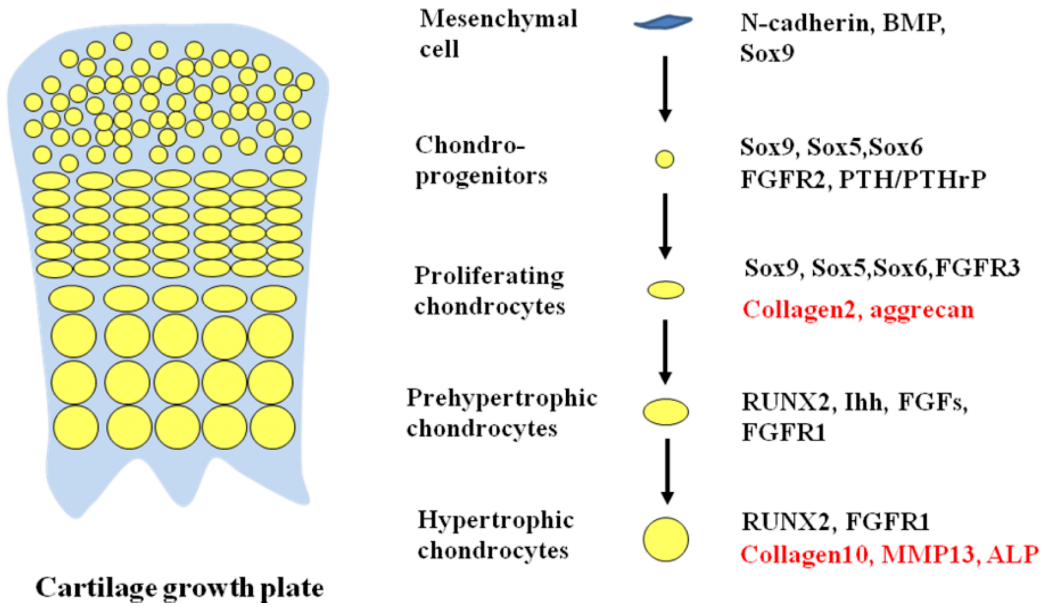

Figure 2. Local regulators of growth plate and life cycle of chondrocyte.
Longitudinal growth of the cartilage growth plate is under control of many secreted factors and endogenous regulators such as transcription factors. Each stage of chondrocyte is characterized by expression of specific molecular markers and matrix proteins (in red): the aggregates of mesenchymal cells express BMPs and Sox family proteins; resting cells express Sox proteins, PTH/PTHrP, FGFR2 and collagen II; proliferative chondrocytes express FGFR3, cell cycle proteins such as Cyclins D1 and A, and collagen II and aggrecan; prehypertrophic cells are under control of the transcription factor RUNX2, and express Ihh and FGFs; hypertrophic cells express collagen X, MMP13 and ALP in bone matrix. (Created according to [1-3])

The resting chondrocytes are small round cells in a relatively quiescent state and located furthest away from the primary ossification center. It is believed that some of these cells have stem-like properties, and can give rise to the neighboring proliferative zone. Within this zone of the growth plate, flattened proliferating chondrocytes are organized in a columnar array, and proliferation of chondrocytes occurs in a unidirectional

manner, resulting in longitudinal growth of the bone. Both resting and proliferating chondrocytes express extracellular matrix (ECM) molecules, such as collagen II and aggrecan[1]. Throughout chondrogenesis, the balance of signaling by growth factors such as bone morphogenetic proteins (BMPs) and fibroblast growth factors (FGFs) determines the rate of proliferation[5].

1.3 Chondrocyte hypertrophy and extracellular matrix production.

Chondrocytes in the center of the cartilage mould then stop proliferating, start to differentiate into prehypertrophic cells, and eventually enlarge to terminally differentiated hypertrophic chondrocytes under the control of several cell cycle genes and different transcription factors[1], [2]. The transcription factor RUNX2 (runt related transcript factor 2) is required for this terminal chondrocyte differentiation[4].

Hypertrophic chondrocytes are the principle regulators of the subsequent events of bone growth[2]. They change their gene expression pattern to synthesize type X collagen, direct the mineralization of their extracellullar matrix, attract blood vessel invasion through the production of vascular endothelial growth factor (VEGF), activate osteoclasts to digest the matrix, and direct adjacent perichondral cells to become osteoblasts, which then secret a matrix rich in type I collagen and form a bone collar around the center of the cartilage template. Hypertrophic chondrocytes then undergo apoptotic cell death. The cartilage matrix provides a scaffold for osteoblasts to lay down bone matrix within it.

1.4 Blood vessel invasion and ossification centers.

VEGF and other angiogenic factors secreted by hypertrophic chondrocytes recruit endothelial cells from the surrounding blood circulation, and trigger vascular invasion from the periosteum[1]. This invasion brings osteoclasts and hematopoietic cells into

the mineralized cartilage. The newly recruited osteoclasts start to degrade the mineralized matrix. Osteoblasts are also recruited from the periosteum, and lay down a new bone-specific matrix on the remains of the hypertrophic cartilaginous matrix. With the formation of the early trabecular bone, the primary spongiosa is established from the middle of the growth plates and eventually develops into a primary ossification center (POC) (**Figure 3**). Another step in endochondral bone formation is the formation of secondary ossification centers (SOCs), which initiate at a late stage of development. These centers form in the middle of epiphyseal cartilage after establishment of the growth plates.

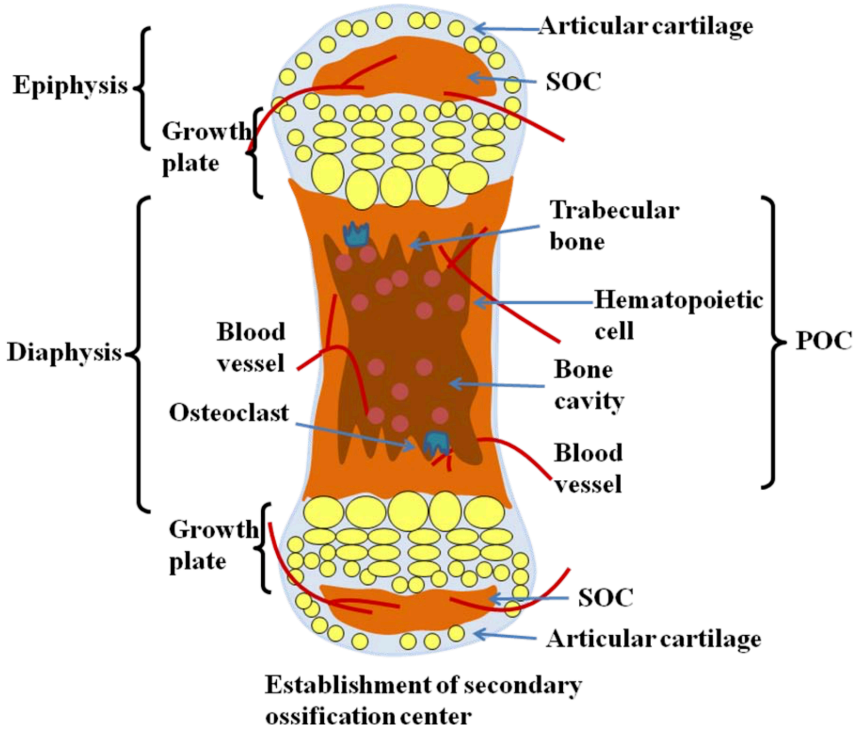

Figure 3. The formation of secondary ossification centers.
The secondary ossification centers (SOC) form in the middle of the epiphyseal cartilage after establishment of growth plates. At this point, the epiphyseal cartilage that is now separated from the growth plate by the SOC will eventually develop into articular cartilage at the far end of bone, which provides an important cushion during the whole adult life. The longitudinal growth of the bone continues to depend on the activity of the epiphyseal growth plates between primary and secondary ossification centers. In humans, the growth plates close during puberty and eventually determine adult height. The mechanisms leading to the formation of the secondary ossification centers are similar to the formation of primary ossification centers. (POC: primary ossification center). (Created according to [1-3].)

After formation of the secondary ossification center, the epiphyseal cartilage is now separated from the growth plate by the SOC and will eventually develop into articular cartilage at the far end of bone, which provides an important cushion during the whole adult life. The longitudinal growth of the bone continues to depend on the activity of the epiphyseal growth plates between primary and secondary ossification centers. In humans, it closes during puberty (when primary and secondary ossification centers fuse) and eventually determines adult height[2].

The mechanisms leading to the formation of the secondary ossification centers are similar to the formation of primary ossification centers.

2. Autophagy.

Autophagy is an important protein degradation pathway playing fundamental roles in tissue homeostasis and energy metabolism. It is defined as a tightly regulated membrane rearrangement process that ensures lysosome-dependent bulk degradation of cytosolic proteins and organelles such as the endoplasmic reticulum, mitochondria, peroxisomes, the nucleus and ribosomes. Evidence indicates that autophagic degradation promotes the recycling and salvage of cellular nutrients, thereby enabling cell survival during starvation or in response to environmental stresses[6].

The term "autophagy" refers to a collection of tightly regulated catabolic processes, all of which deliver cytoplasmic components to the lysosome for degradation, and that are broadly classified into three pathways: macroautophagy, microautophagy and chaperone-mediated autophagy (**Figure 4**)[6], [7]. Macroautophagy involves the formation of double membrane-bound vesicles called autophagosomes that engulf cytoplasmic proteins and organelles; these autophagosomes are trafficked to lysosomes, where the sequestered cargo is degraded. Microautophagy refers to the invagination of the lysosomal or endosomal membrane, resulting in the direct engulfment of substrates that are subsequently degraded by lysosomal proteases. Chaperone-mediated autophagy is distinct from macroautophagy and microautophagy because cargo is not sequestered within a membrane-delimited vesicle. Instead, proteins targeted by chaperone-mediated autophagy contain a peptide motif that, once recognized by a cytosolic chaperone, promotes the translocation of these targets across lysosomal membranes into the lysosome. Macroautophagy (hereafter autophagy) is believed to be the major mode of autophagy, and is the most extensively analyzed in this thesis work.

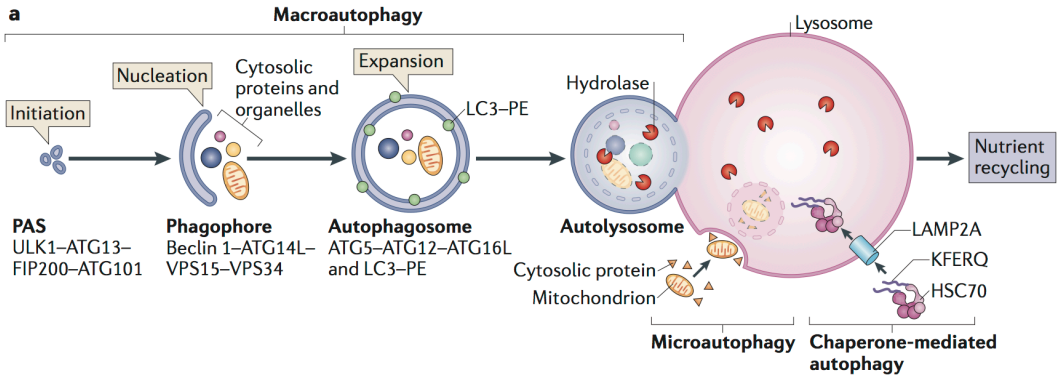

Figure 4. Overview of autophagy pathways.
In macroautophagy, initiation begins with the formation of the phagophore assembly site (PAS). This is mediated by the UNC51-like kinase (ULK) complex, which consists of ULK1, autophagy-related protein 13 (ATG13), FAK family kinase interacting protein of 200 kDa (FIP200) and ATG101. Further nucleation requires the class III PI3K complex, which is composed of the vacuolar protein sorting 34 (VPS34) PI3K, along with its regulatory subunits ATG14L, VPS15 and Beclin 1. Phagophore membrane elongation and autophagosome completion requires two ubiquitin-like conjugation pathways. The first produces the ATG5–ATG12 conjugate, which forms a multimeric complex with ATG16L, whereas the second results in the conjugation of phosphatidylethanolamine (PE) to LC3 (the microtubule-associated protein 1 light chain 3). PE-conjugated LC3 (LC3–PE) is required for the expansion of autophagic membranes, their ability to recognize autophagic cargoes and the fusion of autophagosomes with lysosomes. The resulting autophagosome fuses with endocytic and lysosomal compartments, ultimately leading to formation of the autolysosome. In microautophagy, substrates are directly engulfed at the boundary of the lysosomal membrane. In chaperone-mediated autophagy, substrates with the pentapeptide motif KFERQ are selectively recognized by the heat shock cognate 70 kDa protein (HSC70) chaperone and translocated to lysosomes in a LAMP2A-dependent manner. In all three processes, the autophagic cargo is degraded via lysosomal hydrolases (adapted from [6]).

2.1 Overview of the autophagic pathway.

Two main kinase systems control the autophagic pathway: the mTOR-ULK1 and the Beclin 1 pathways. While the former is required to give the initiation signal to the autophagosome formation, the latter is required for properly vesicle nucleation.

mTOR, or mammalian target of rapamycin, is an evolutionarily conserved Ser/Thr protein kinase central for integrating signaling pathways that regulate cellular homeostasis[8]. mTOR is the catalytic subunit of two functionally and structurally distinct complexes called mTOR complex 1 (mTORC1) and mTORC2 whose molecular

function will be described later.

Beclin 1 is a coiled-coil protein involved in the regulation of autophagy in mammalian cells[9]. Beclin 1 binds to hVps34/class III phosphatidylinositol-3-kinase (PI(3)K) through its evolutionarily conserved domain (ECD). The hVps34/PI(3)K generates phosphatidylinositol-3-phosphate (PI(3)P), which has important roles in several membrane trafficking pathways, including the multivesicular body pathway, retrograde trafficking from endosomes to the Golgi and phagosome maturation[10].

Autophagosome biogenesis.

The earliest step of autophagy is characterized ultrastructurally by the sequestration of portions of cytoplasm into a double membrane-bound vesicle called the autophagosome. The autophagosome subsequently fuses with a lysosome, leading to the degradation of the sequestered cytosolic proteins and organelles. Studies in yeast have identified more than 30 AuTophagy-related Genes (ATGs), many of which have identified mammalian orthologues[7]. As depicted in Figure 1, autophagosome formation comprises three main steps: initiation, nucleation and expansion of the isolation membrane.

Initiation/Nucleation.

The process of autophagosome formation begins at the phagophore assembly site (PAS, also known as the isolation membrane) with the contribution of mTORC1 activity[7]. When activated in the presence of nutrients, the mTORC1 complex associates with the UNC51-like kinase (ULK) complex and hyperphosphorylates its subunits such as ULK1 on Serine 757 (S757) and Atg13, which results in its inactivation and subsequent down-regulation of autophagy. Conversely, nutrients deprivation downregulates mTORC1, which dissociates from the ULK1 complex, leading to its subsequent

dephosphorylation on specific residues and resulting in its activation. Once active, the ULK1 complex (which in addition to ULK1 and ATG13 is composed by FAK family kinase interacting protein of 200 kDa (FIP200) and ATG101) assembles to initiate autophagosome formation. The carboxy-terminal domain (CTD) of ULK1 binds to membranes, and this property might mediate the recruitment of the complex to the site of autophagosome initiation[11]. Furthermore, has been shown that autophagy is promoted by AMP activated protein kinase (AMPK), which is a key energy sensor and regulates cellular metabolism to maintain cellular homeostasis. Under glucose starvation, AMPK promotes autophagy by directly activating ULK1 through phosphorylation of Serine 317 (S317) and Serine 777 (S777). Under nutrient sufficiency, high mTORC1 activity prevents ULK1 activation by phosphorylating ULK1-S757 and disrupting the interaction between ULK1 and AMPK. This coordinated phosphorylation is important for ULK1 in autophagy induction[12].

Equally important for initiating autophagosome formation is the autophagy specific class III PI3K complex (also known as Beclin1 complex), which is composed by a vacuolar protein sorting 34 (Vps34), p150, Beclin1 and ATG14[9]. Once activated and targeted to the site of autophagosome initiation, the PI3K complex produce an autophagosome-specific pool of PI(3)P, an essential membrane component of the elongating phagophore. ULK1 was recently shown to phosphorylate Vps34, and this enhances the activity of the PI3K complex[11]. These events drive the nucleation of the isolation membrane and the recruitment of additional ATG proteins and autophagy-specific PI(3)P effectors, such as DFCP1 (double FYVE-containing protein 1) and WIPI (WD- repeat domain phosphoinositide-interacting), proteins that induce membrane rearrangements that ultimately facilitates the formation of autophagosomes.

The Beclin1 core complex also interacts with UVRAG (UV irradiation resistance-

associated gene). A proportion of UVRAG is present in a Beclin 1– UVRAG–Vps34–Vps15 complex that normally excludes Atg14L. This mutual exclusion of Atg14L and UVRAG for Beclin 1 binding is likely to be due to the overlap of their docking sites on Beclin 1[13]. UVRAG was reported to act together with Beclin 1 to induce autophagosome formation. The expression of UVRAG was also correlated with an increase in Vps34 enzyme activity, suggesting a role for the Beclin 1–UVRAG–Vps34–Vps15 complex in autophagy regulation. Negative regulators of Beclin1 activation has been described: RUN domain Beclin 1-interacting and cysteine-rich containing protein (Rubicon) and Bcl-2 (beta cell lymphoma 2). Rubicon binds Beclin 1, UVRAG and Vps34. In opposition to the role of Atg14L, Rubicon was found to suppress the UVRAG function in stimulating the kinase activity of Vps34 that contributes to autophagosome biogenesis[13].

In addition some antiapoptotic members of the Bcl-2 family, such as Bcl-2 and BclxL, interact with Beclin 1. A series of investigations have shown that antiapoptotic Bcl-2 proteins inhibit the autophagic function of Beclin 1 through binding to its BH3 domain, thereby suggesting that Bcl-2 family members also function as inhibitors for autophagic pathways[14]. A model was proposed that the Beclin 1–Bcl-2 complex is constitutively present and functions as a rheostat to maintain homeostasis of basal levels of autophagy. It has been shown that Bcl2, Beclin1, VPS34, UVRAG are present in the same complex. Protein phosphorylation can modulate the status of the Beclin1 complex, regulating Bcl2-Beclin1 mediated autophagic activity.

Expansion

Following nucleation, the ATG12–ATG5–ATG16L1 complex (also called the ATG16L1 complex) is recruited to the membrane, where it functions as an E3-like ligase to mediate the lipidation of microtubule-associated protein 1 light chain 3

(MAP1LC3; also known as LC3) with phosphatidylethanolamine and its family members GATE16 and GABARAP (GABA receptor-associated protein)[15]. This enables them to associate with the autophagosome membrane. The association of these cytosolic proteins and protein complexes with the membrane occurs while the isolation membrane is expanding. There are two ubiquitin-like systems that are key to autophagy[7]. In the first of these systems, Atg7 acting like an E1 ubiquitin activating enzyme activates Atg12 in an ATP-dependent manner by binding to its carboxyterminal glycine residue. Atg12 is then transferred to Atg10, an E2-like ubiquitin carrier protein that potentiates covalent linkage of Atg12 to lysine 130 of Atg5. Conjugated Atg5–Atg12 complexes in pairs with Atg16L dimers to form a multimeric Atg5–Atg12–Atg16L complex that associates with the extending phagophore. The association of Atg5–Atg12–Atg16L complexes is thought to induce curvature into the growing phagophore through asymmetric recruitment of processed microtubule-associated protein light chain 3 (LC3B-II). Atg5–Atg12 conjugation is not dependent on activation of autophagy and once the autophagosome is formed, Atg5–Atg12–Atg16L dissociates from the membrane, making conjugated Atg5–Atg12 a relatively poor marker of autophagy. The second ubiquitin-like system involved in autophagosome formation is the processing of LC3B. LC3B is expressed in most cell types as a full-length cytosolic protein that, upon induction of autophagy, is proteolytically cleaved by Atg4, a cysteine protease, to generate LC3B-I. The carboxyterminal glycine exposed by Atg4-dependent cleavage is then activated in an ATP-dependent manner by the E1-like Atg7 in a manner similar to that carried out by Atg7 on Atg12. Activated LC3B-I is then transferred to Atg3, a different E2-like carrier protein before phosphatidylethanolamine (PE) is conjugated to the carboxyl glycine to generate processed LC3B-II. Recruitment and integration of LC3B-II into the growing phagophore is dependent on Atg5–Atg12 and LC3B-II is found on both the internal and external surfaces of the autophagosome,

where it plays a role in both hemifusion of membranes and in selecting cargo for degradation. The synthesis and processing of LC3 is increased during autophagy, making it a key readout of levels of autophagy in cells. It is proposed that LC3B-II, acting as a 'receptor' at the phagophore, interacts with 'adaptor' molecules on the target (eg protein aggregates, mitochondria) to promote their selective uptake and degradation[6]. The best-characterized molecule in this regard is p62/SQSTM1, a multi-functional adaptor molecule that promotes turnover of polyubiquitinated protein aggregates.

Fusion

Newly synthesized autophagosomes then undergo extensive remodelling to acquire degradative capabilities. The remodelling process, also known as autophagosomal maturation, involves sequential fusion of autophagosomes with endocytic vesicles (early and late endosomes) and lysosomes, producing degradative autolysosomes. The sequestered material is then degraded into building blocks for synthesis of macromolecules and energy production.

A prerequisite for vesicle fusion is vesicle tethering. The tethering events at the lysosomes have been thoroughly studied and shown to require the class C vacuolar protein sorting (Vps) complex[16]. The core class C Vps complex (hereafter referred to as C-Vps), including Vps11, Vps16, Vps18 and Vps33 exists into two configurations: the HOPS complex (for homotypic vacuole fusion and protein sorting), which contains two additional subunits (Vps39 and Vps41), acts at the vacuole, whereas the class C core vacuole/endosome tethering (CORVET) complex has Vps3 and Vps8 instead, and functions at the endosome.

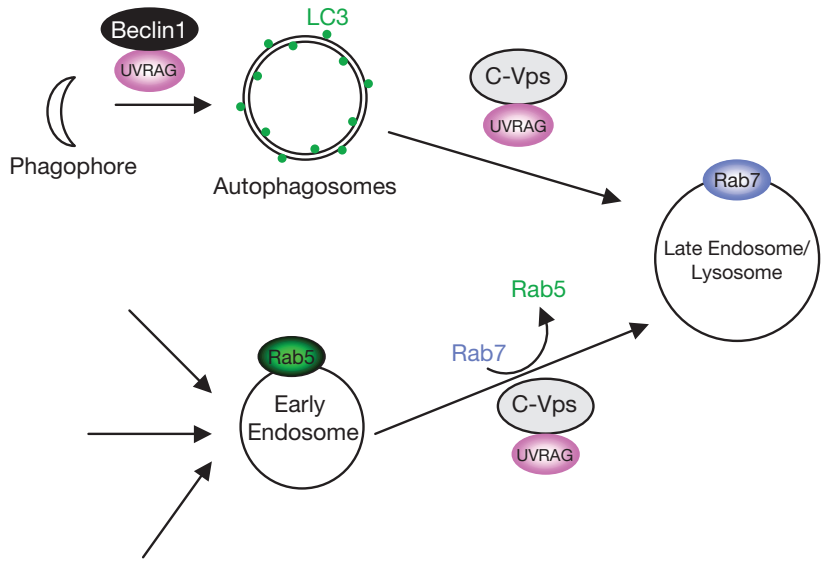

Figure 5. Model of the role of UVRAG as a coordinator of the autophagosomal and endosomal machineries.
At an early stage of autophagy, UVRAG targets Beclin1 to facilitate autophagosome formation, whereas at later stages, UVRAG interacts with C-Vps to promote autophagosome maturation. UVRAG–C-Vps is also involved in the endosome–lysosome transition by activation of Rab7 (adapted from[16]).

Has been demonstrated that mTORC1 regulates early stages as well as later stages of autophagy[17]. Independently of Beclin1, UVRAG interaction with C-Vps stimulates autophagosome maturation and endosomal fusion, thereby enhancing both autophagic and endocytic protein degradation (**Figure 5**). This interaction stimulates delivery and degradation of autophagic cargo through enhancing of Rab7 GTPase activity. The function of UVRAG to regulate the HOPS complex is antagonized by Rubicon [18].

Under nutrient-enriched conditions mTORC1 binds and phosphorylates UVRAG at Ser497. UVRAG phosphorylation has a positive effect on the interaction between UVRAG and Rubicon, whereas it has a negative effect on the kinase activity of Vps34 and the interaction between UVRAG and the HOPS complex (**Figure 6**). In addition, has been demonstrated that UVRAG-S497 phosphorylation suppresses the UVRAG-

mediated stimulation of the Vps34 kinase activity[17]. Consequently, it decreases the production of PI(3)P required for vesicles fusion and autophagosome maturation. Collectively, these findings define the mTORC1-UVRAG pathway as an important regulatory axis through which cells coordinate autophagy and the endosome-lysosomal degradation pathway. The coordinate regulation might be important to maintain normal cellular physiology under changing environments of growth factors and nutrients.

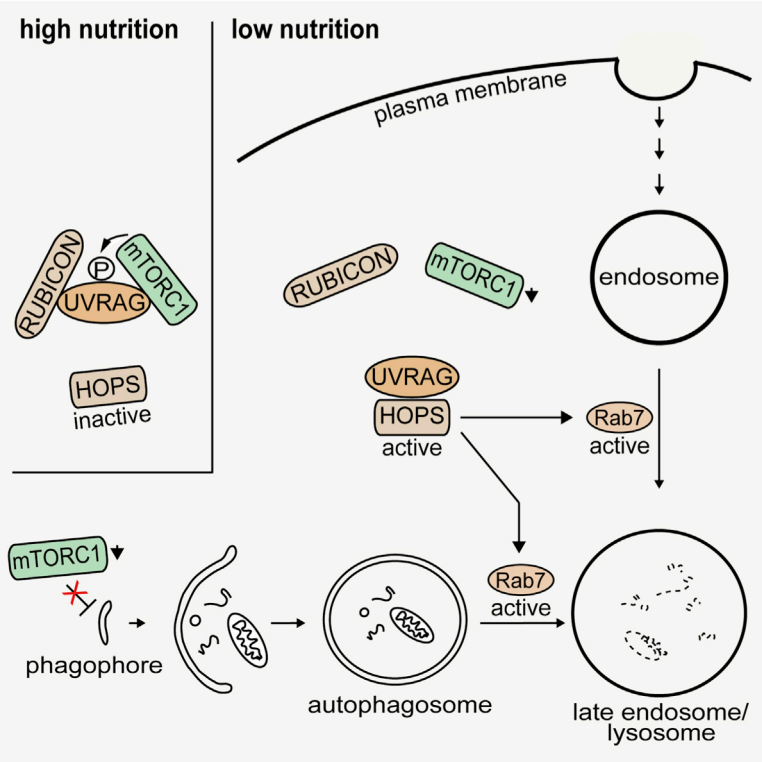

Figure 6. Model of mTORC1 regulation of UVRAG function.
In the absence of nutrients, UVRAG binding to the HOPS complex stimulates lysosomal fusion with autophagosome and endosome. Under nutrient-rich conditions mTORC1 binds and phosphorylates UVRAG. UVRAG phosphorylation has a positive effect on the interaction with its inhibitory partner Rubicon, and a negative effect on the kinase activity of Vps34 (adapted from [17]).

The available evidence indicates also that Rubicon acts at a later stage of the autophagic process. Because Rubicon contains a RUN domain, a conserved motif known to interact with and regulate small GTPases, one possibility is that Rubicon interacts with specific Rabs that were previously shown to regulate the autophagic process in the later stage of autophagosome-lysosome fusion, counteracting these step of the autophagic-lysosomal

pathway[18].

2.3 Signaling pathways that regulate autophagy.

Autophagy is active at basal levels in most cell types where it is postulated to play a housekeeping role in maintaining the integrity of intracellular organelles and proteins. However, autophagy is strongly induced by starvation and is a key component of the adaptive response of cells and organisms to nutrient deprivation that promotes survival until nutrients become available again[19]. In mammals, a major intracellular hub for integrating autophagy-related signals is the mTOR-TFEB axis.

mTOR is the catalytic subunit of two functionally and structurally distinct complexes called mTOR complex 1 (mTORC1) and mTORC2[8] (**Figure 7**).

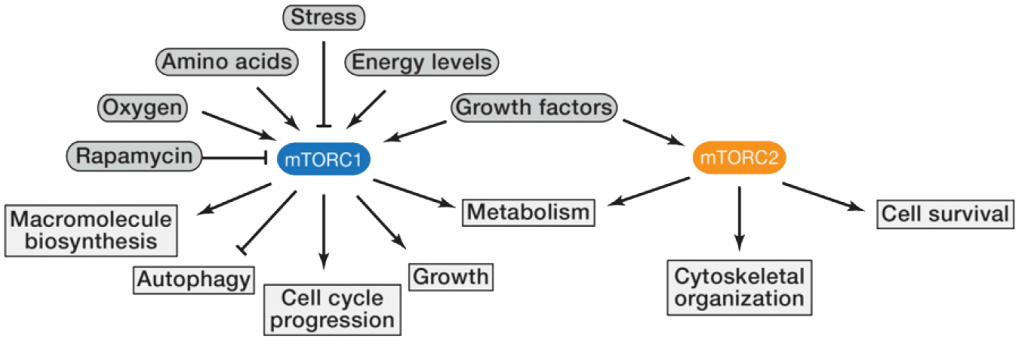

Figure 7. mTORC1 and mTORC2 complexes.
The mTOR kinase nucleates two distinct protein complexes termed mTORC1 and mTORC2. mTORC1 responds to amino acids, stress, oxygen, energy, and growth factors and is acutely sensitive to rapamycin. It promotes cell growth by inducing and inhibiting anabolic and catabolic processes, respectively, and also drives cell-cycle progression. mTORC2 responds to growth factors and regulates cell survival and metabolism, as well as the cytoskeleton (adapted from [8]).

Unique accessory proteins distinguish these complexes: regulatory-associated protein of

mTOR (Raptor) and rapamycin-insensitive companion of mTOR (Rictor) define mTORC1 and mTORC2, respectively. These companions function as scaffolds for assembling the complexes and for binding substrates and regulators.

2.4 mTOR complex 1 (mTORC1).

mTORC1 is activated by growth factors (for example, insulin), nutrients (amino acids) and the cellular energy status (high ATP/AMP ratio). Growth factors such as insulin stimulate mTORC1 through the PI3K–phosphoinositide-dependent kinase 1 (PDK1)–AKT pathway[20]. Activated AKT phosphorylates tuberous sclerosis complex 2 (TSC2) at multiple sites to inhibit the TSC complex (composed by several members) that acts as a GTPase-activating protein (GAP) for the small GTPase RAS homologue enriched in brain (Rheb). During inhibition of the TSC complex, GTP-loaded Rheb binds the mTOR catalytic domain to activate mTORC1 through an as yet unknown mechanism (**Figure 8**). Among regulators of mTORC1, amino acids contribution have until very recently been unclear. They represent the basic building blocks for protein synthesis, thus, both unicellular and multicellular organisms have evolved mechanisms to sense amino acids, import them into the cell when they are available, and synthesize new ones when they are lacking.

For a long time, the understanding of amino acid regulation of mTORC1 remained confined to a few circumstantial observations, above all the fact that amino acids acted independently of the insulin/PI3K pathway.

The nutrient signal to mTORC1 is transduced through the RAS-related GTP-binding protein (RAG) family of small GTPases [21], [22]. An active RAG heterodimer mediates the translocation of mTORC1 from the cytoplasm to the surface of the lysosome, where mTORC1 encounters and is activated by Rheb (**Figure 8**).

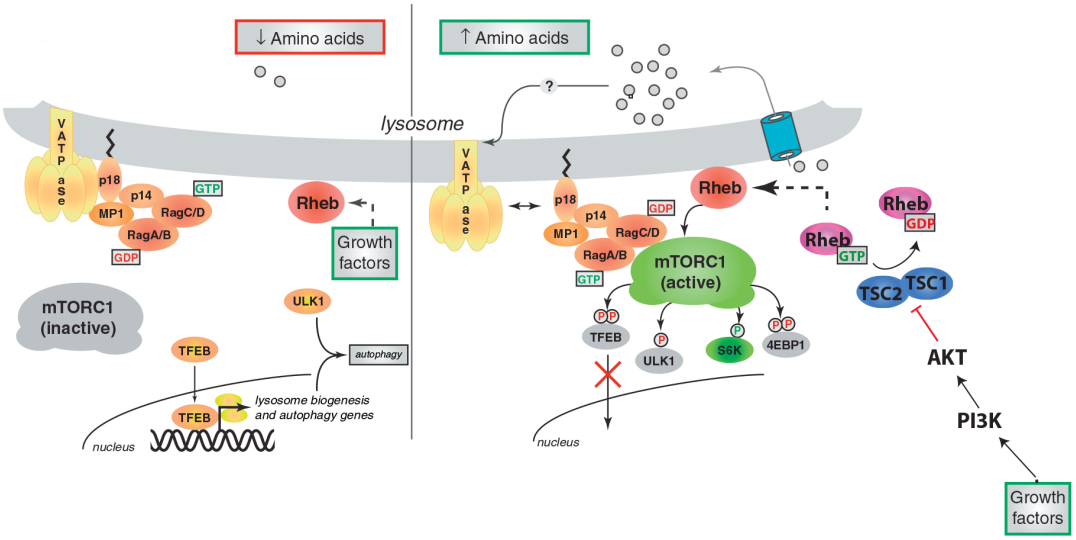

Figure 8. mTORC1 and the lysosomal surface.
Growth factors stimulate mTORC1 through the PDK1–AKT pathway. Activated AKT phosphorylates tuberous sclerosis complex 2 (TSC2) at multiple sites to inhibit the TSC complex (composed by several members) that acts as a GAP for Rheb. During inhibition of the TSC complex, GTP-loaded Rheb binds the mTOR catalytic domain to activate mTORC1. Amino acids regulate the recruitment of mTORC1 to the lysosomal surface, where mTORC1 is activated. Under low amino acids (left) the v-ATPase-Ragulator-Rag GTPase complex is in the inactive conformation and is unable to bind to mTORC1, resulting in its cytoplasmic localization. Amino acids (right) signal to the v-ATPase–Ragulator complex and through them to the Rag GTPases, which switch their nucleotide loading and become activated. In turn, active Rag GTPases recruit mTORC1 to the lysosomal surface, where the small GTPase Rheb turns on the kinase activity of mTORC1. Active mTORC1 phosphorylates several targets, including S6K, 4E-BP1, ULK1 and the transcription factor TFEB. Phosphorylated S6K and 4E-BP1 favor protein synthesis; phosphorylation of ULK1 blocks autophagosome formation, whereas phosphorylation of TFEB prevents it from entering the nucleus and activating a catabolic transcriptional program. Adapted from [20].

Following the discovery of mTORC1, it was observed that withdrawal of amino acids from the culture media potently suppressed mTORC1 signaling in mammalian cells and yeast alike; moreover, suppressing mTORC1 by starvation or using its chemical inhibitor rapamycin strongly induced autophagy[23]. Thus, a feedback loop began to emerge, connecting amino acids, mTORC1, and autophagy in a mechanism that drives growth under nutrient abundance and mediates growth arrest under starvation conditions, allowing amino acid stores to be replenished.

The Rag GTPases localize to lysosomal surface thanks to a platform composed by three

small proteins, LAMTOR1-3, collectively known as Ragulator, which reside on the lysosome [24]. Along with v-ATPase and other amino acid transporters they create the necessary and sufficient condition by which mTORC1 can sense nutrients and can be activated[25].

Independently of the stimuli that activate mTORC1, readout of its function is the phosphorylation of key substrates such as ribosomal protein S6 kinase (p70-S6K), 4eBP1 and ULK1. While the first two are directly implicated in the initiation of protein synthesis and translation, respectively, the latter, as described above, regulates autophagy initiation[8].

The presence of mTORC1 at the lysosome has important implications for its ability to control autophagy. In non-starving cells, mTORC1 suppresses the formation of the phagophore by phosphorylating and inhibiting the kinase ULK1 and its interacting partner, ATG13. These effects depend on the Rag GTPases; expression of the active Rags suppresses autophagy under starvation conditions, whereas expressing the inhibitory mutants results in constitutive autophagosome formation[21].

2.5 Transcription factor EB (TFEB).

Very recently, a novel paradigm has begun to emerge where the amino acid/mTORC1 pathway centered at the lysosome may be part of a novel signaling mechanism that controls lysosomal gene expression and, through this process, affects cellular clearance and metabolism. A bioinformatics search for consensus binding sites in the promoters of lysosomal genes identified the coordinated lysosomal expression and regulation (CLEAR) element, which is bound by the MiT/TFE subfamily of helix–loop–helix (bHLH) transcription factors[26]. One member of the MiT/TFE family, known as transcription factor EB (TFEB), physically binds the CLEAR motif in the promoter of

multiple lysosomal genes, including luminal hydrolases and membrane transporters, to upregulate their expression. Overexpressing TFEB in cells led to a striking expansion of the lysosomal compartment, both in terms of size and number. This, in turn, resulted in enhanced clearance capacity towards multiple lysosomal substrates.

Shuttling between the nucleus and the cytoplasm regulates the activity of TFEB. A key observation was that withdrawal of nutrients from the culture media induced the nuclear translocation of TFEB in cells. Among the transcriptional targets of TFEB are several autophagy-mediating genes and, accordingly, TFEB overexpression resulted in enhanced formation of LC3-positive autophagosomes. Conversely, siRNA-mediated TFEB depletion resulted in a defective autophagic response to nutrient starvation. These findings support a model where TFEB is a key component of a transcriptional starvation-response program. By expanding the lysosomal and autophagic compartments, this program increases the ability of cells to degrade and recycle their substrates, and thus to sustain adequate levels of energy and metabolites[27].

mTORC1 exerts a tight control over the subcellular localization of TFEB: when cells are replete with nutrients, mTORC1 phosphorylates TFEB at two critical serines, sequestering TFEB in the cytoplasm[28]. A series of observations strongly suggest that the amino acids/mTORC1 pathway is especially important in controlling TFEB nuclear localization[29]. Treatments that cause starvation or lysosomal stress, including amino acid withdrawal, v-ATPase inactivation, and overexpression of transporters that empty the lysosome of its amino acid content, caused a massive translocation of TFEB to the nucleus. TFEB phosphorylation occurs on the lysosomal membrane, where mTORC1 and TFEB physically bind to each other (**Figure 8**). Thus, the lysosome seems to operate as a ‘gate’ that controls the amount of TFEB allowed to reach the nucleus. In fully fed cells, active mTORC1 meets TFEB at the lysosome, phosphorylates it, and

releases it back into the cytoplasm. When mTORC1 is inactivated, it detaches from the lysosomal membrane, allowing TFEB to become unphosphorylated and move to the nucleus. This lysosome-to-nucleus signaling system may play a key role in coordinating cellular adaptation to growth-promoting, versus starvation, conditions[27].

In comparison to mTORC1 regulation, mTORC2 regulation is poorly understood. Only growth factors stimulate mTORC2 kinase activity, which is mediated through PI3K-dependent mTORC2–ribosome association[8]. The signaling steps beyond phosphatidylinositol-3,4,5-triphosphate ($PI(3,4,5)P_3$) in the activation of mTORC2 are unknown and distinct from those upstream of mTORC1. mTORC2 will not be further subject of study or discussion in this thesis work.

3. Autophagy in skeletal tissue.

Recently the work done by our lab clarified the role of autophagy during skeletal growth[30]. We showed that autophagy is induced in growth-plate chondrocytes during post-natal development and regulates the secretion of type II collagen (Col2), the major component of cartilage ECM. Mice lacking the autophagy related gene 7 (*Atg7*) in chondrocytes experience endoplasmic reticulum storage of type II procollagen (PC2) and defective formation of the Col2 fibrillary network in the ECM. We observed induction of autophagy in growth plate chondrocytes during post-natal development. Notably, collagen production by chondrocytes was also increased at these ages, suggesting that the two processes could be co-regulated. After a screening of chondrogenic molecules for their potential to induce autophagy *in vitro*, we identify Fibroblast growth factor 18 (FGF18) as the only molecule that significantly increased autophagy flux. FGF signaling is among the most studied pathways in bone due to its involvement in many forms of skeletal disorders [31]. FGF18 plays a key role in skeletal growth and development in mice, regulating multiple aspects of chondrogenesis in the growth plate, including ECM composition [32]. Mice lacking FGF18 exhibited very low levels of autophagy in chondrocytes compared to control mice, pointing to FGF18 as a physiological regulator of chondrocyte autophagy. Among the different FGF receptors, *in vitro* and *in vivo* data suggest that FGF18 acts mainly through FGF receptor 4 (FGFR4), and to a lesser extent through FGFR3, to regulate autophagy. $Fgf18^{+/-}$ and $Fgfr4^{-/-}$ mice failed to induce chondrocyte autophagy during post-natal bone development and as a consequence displayed PC2 storage in the ER of chondrocytes and decreased Col2 levels in the ECM. Biochemical studies suggested that FGF18 induces autophagosome biogenesis through the autophagy initiation complex Vps34-Beclin1. When active, this complex produces PI(3)P which is essential for autophagosome biogenesis. Consistent with this model, we rescued autophagy in the

growth plates of Fgf18$^{+/-}$ mice by using TAT-Beclin1, a peptide able to enhance the activity of endogenous Beclin1 protein[33]. Notably, TAT-Beclin1 restored ECM matrix defects in Fgf18$^{+/-}$ and Fgfr4$^{-/-}$ mice, indicating autophagy as a physiological regulator of FGF-mediated bone growth. Thus, this study has identified a novel mechanism by which FGF signaling regulates post-natal bone development and demonstrates that autophagy is a developmentally regulated process necessary for bone growth (**Figure 9**)[30].

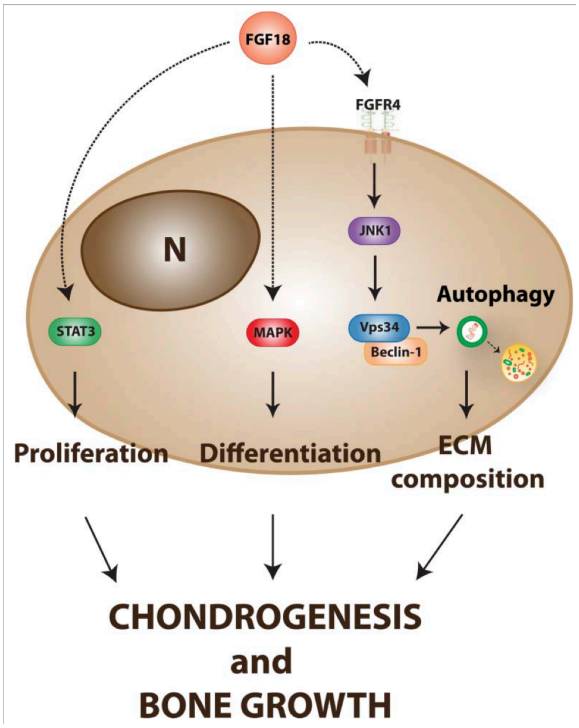

Figure 9. Proposed role of FGF-mediated induction of autophagy during bone growth.
FGF signaling modulates multiple aspects of chondrogenesis and bone growth through the regulation of different intracellular pathways. During post-natal bone development, FGF18 induces chondrocyte autophagy through the activation of the Beclin1-Vps34 complex via FGFR4 and c-Jun N-terminal kinases (JNK). The FGF-mediated induction of autophagy controls collagen homeostasis and ECM composition during postnatal bone growth. Adapted from [30].

3.1 mTORC1 in skeletal growth.

As described above, a major signaling hub for autophagy regulation is mTORC1. In the course of my PhD, experimental evidence were published showing that although mTORC1 activity is required for chondrocyte growth and proliferation, its inactivation is essential for proper chondrocyte differentiation[34]. In addition, it has been showed that inactivation of the gene encoding either mTOR or Raptor (a component of mTOR complex 1) in the entire limb clearly causes growth retardation[35]. Furthermore, rapamycin induces mild growth retardation when administrated either systemically or locally, an effect primarily linked to attenuation of chondrocyte hypertrophy and decreased production of extracellular matrix [35], [36]. Whether activation of autophagy or another mTORC1-mediated function(s) is involved remains to be elucidated. So far, a transcriptional hypothesis has been proposed[34]: Bo Yan et al. showed that mTORC1 activity is required for chondrocyte growth and proliferation, but declines during the process of differentiation *in vitro* and *in vivo*. Low mTORC1 activity is necessary for chondrocyte differentiation and maturation. Hyperactivation of mTORC1 in chondrocytes uncouples the normal proliferation and differentiation programme within the growth plate, leading to impairment of chondrocyte hypertrophic and terminal differentiation, chondrodysplasia and dwarfness in mice. Mechanistically, mTORC1 activation promotes the nuclear accumulation of a transcription factor (Gli1/2) required for the transcription of PTHrP; PTHrP is a key signaling molecule for bone growth by promoting chondrocyte proliferation and preventing chondrocyte hypertrophic and terminal differentiation.

Neither the role of mTORC1 as principal regulator of autophagy nor the autophagic

status of chondrocytes have been taken in consideration in this context; besides, given the fundamental role of autophagy during skeletal growth it is reasonable to expect finely tuning of these two pathways during bone development. Thus oscillations in mTORC1 activity, that have been described for the bone either in physiological and pathological conditions, suggest a consequent impact on autophagy that still needs to be elucidated.

Furthermore, even though the role of autophagy during bone growth has been successfully addressed, the lack of information about its regulation and contribution in pathological conditions prompted us to investigate in this direction.

4. Lysosome and Proteasome players of cellular metabolism.

Macromolecule biosynthesis and degradation must be coordinated to maintain cell and tissue homeostasis. The main degradation stations of the cells are lysosomes and proteasomes, organelles deputed to the digestion of cargoes into elementary units that can be either recycled or used to generate energy during period of nutrient shortage[37]. Moreover, protein degradation controls processes like the cell cycle, signaling, DNA transcription, repair and translation, by downregulating their critical regulatory elements. The two major pathways by which these organelles exert their function are:

- Lysosome: autophagy is responsible for degradation of most long-lived proteins, but also aggregated proteins as well as whole cellular organelles.

- Proteasome: the ubiquitin proteasome system (UPS) is responsible for degradation of most of the cellular proteins including the short-lived and the damaged ones.

Autophagy and UPS are two cornerstones of cellular catabolism that are involved in most aspects of normal physiology and development, and are also implicated in a broad array of pathological states[37]. Their critical role in the maintenance of cellular homeostasis, suggests that their activities need to be carefully orchestrated[38].

4.1 Lysosome.

In the mid-1950s, Christian de Duve discovered the lysosome as a vacuolar structure that contains various hydrolytic enzymes, which function optimally at an acidic pH. The definition of the lysosome has been broadened over the years. Lysosomes are organelles delimited by a single membrane and filled with digestive enzymes that are able to degrade molecules and structures into their elementary constituents[39]. Therefore they

represent the final destination for many endocytic and autophagic secretion molecules targeted for degradation or recycling. Furthermore lysosomes are involved in various specific cellular pathways such as autophagic degradation of molecules, matrix modelling, pathogen defence and plasma membrane repair via lysosomal exocytosis[27].

Lysosomes originate from the fusion between endosomes and the Golgi's hydrolytic vesicles. The Golgi's hydrolytic vesicles, also called primary lysosomes, already contain all necessary hydrolases, but their local pH is not sufficiently acidic for their activation. Therefore lysosomal enzymes are activated only after the primary lysosome fuses with endosomes, as the latter carries proton pumps necessary for the acidification of the lumen.

Lysosomes are involved in the degradation of a wide variety of structurally diverse substances into their basic building blocks, such as proteins, glycosaminoglycans (GAGs), sphingolipids, glycogen, nucleic acids, oligosaccharides and complex lipids. These are either recycled through biosynthetic pathways or further degraded to generate energy. Cellular and foreign material destined for degradation reach lysosomes via endocytosis, phagocytosis, autophagy, or direct transport.

4.2 Lysosomal storage disorders (LSDs).

Lysosomal storage disorders (LSDs) are characterized by progressive accumulation of undigested macromolecules within the cell due to lysosomal dysfunction[40].

So far, LSDs are recognized as a cohort of nearly 60 different inherited disorders, with each sharing a genetic defect that renders the lysosomal system dysfunctional and unable to degrade specific materials normally processed within the cell. As a consequence, many tissues and organ systems are affected, including brain, viscera,

bone and cartilage. Whereas clinical features of these disorders vary widely, most are fatal within the first two decades of life following many years of worsening disease. The progressive nature of phenotype development is one of the hallmarks of LSDs.

Lysosomal storage disorders (LSDs) affects many organs, included the skeleton[41]. The most prevalent LSD's with skeletal abnormalities are the mucopolysaccharidoses (MPSs)[42]. Mucopolysaccharidoses (MPSs) are caused by deficiency of a specific lysosomal enzyme, consisting of seven subtypes. In MPSs, the breakdown of the glycosaminoglycans (GAGs), chondroitin sulfate (CS), dermatan sulfate (DS), heparan sulfate (HS), keratan sulfate (KS) and/or hyaluronan is disrupted. Accumulation of undegraded GAG(s) is observed in multiple tissues, leading to broad clinical manifestations including mental retardation, skeletal dysplasia, corneal clouding, abnormal facies, coarse hair, hernia, hepatosplenomegaly, respiratory and heart valvular diseases, and abnormal joint mobility.

MPS varies from severe systemic bone dysplasia to a lesser form of the disease that includes mild bone involvement, depending upon MPS type and clinical phenotype[43]. MPS patients with skeletal dysplasia (dysostosis multiplex) have deformity of the spine (lumbar gibbus, kyphoscoliosis), deformity of the chest (pectus carinatum, flaring of the rib cage), abnormal joint mobility, abnormal gait, short trunked dwarfism, and/or genu valgum. Patients may require a series of orthopedic surgeries (cervical decompression and fusion, femoral or tibial osteotomy, hip reconstruction and replacement etc.) throughout all their life.

The pathophysiology is not completely understood, and likely involves a complicated interplay of storage, inflammation and epigenetic factors[40]. Better understanding of the etiology is of increasing importance, since recently developed treatments such as enzyme replacement therapy (ERT) for several of the MPS's and hematopoietic stem

cell transplantation (HSCT) for MPS I appear to have limited effect on skeletal disease[44]. ERT is approved for use in patients with MPS I, MPS II, MPS IVA, and MPS VI. Patients treated with ERT show clinical improvement of somatic manifestations and improved quality of life. However, there are several limitations with current ERT: i) limited effect on skeletal symptoms (one possibility is due to the limited penetration of enzyme into avascular cartilage), ii) rapid clearance from the circulation, and iii) immunological issues (antibody production leads to reduced therapeutic efficacy). To resolve the above issues, a long circulating or bone-targeting enzyme was devised to deliver the enzyme to bone [45]. The earlier that ERT is performed in animal models and human patients, the better the outcome.

On the other side, potential advantages of HSCT for treating MPSs are that marrow-derived donor cells could provide a continuous source of secreted enzyme, and also provide access of enzyme to bone and cartilage that is close to the bone marrow. However, has been proposed that secreted enzyme may not penetrate into the bone after HSCT [46]. Skeletal pathology from surgical remnants shows almost complete clearance of storage materials in chondrocytes with normal level of blood HS and DS. Thus, even though pathology in chondrocytes appeared to be normalized, there was incomplete correction of the skeletal phenotype by HSCT. The reasons for the continued skeletal phenotype are not known, but it is possible that irreversible bone abnormalities may have already occurred prior to transplantation or that the structure of the extracellular matrix remains abnormal [44].

4.3 Mucopolysaccharidosis and treatment options.

Mucopolysaccharidosis type VII (MPS VII)

In mucopolysaccharidosis type VII (MPS VII; Sly syndrome)[47] the GAGs, dermatan sulfate, heparan sulfate, chondroitin 4-sulfate, and chondroitin 6-sulfate, accumulate in lysosomes in the absence of the catabolic enzyme β-glucuronidase (GUSB). MPS VII is characterized by short stature, dysmorphic features, corneal clouding, hepatomegaly, skeletal abnormalities collectively referred to as dysostosis multiplex, and developmental delay. These clinical manifestations become progressively worse over time if left untreated. MPS VII patients with the most severe phenotype have hydrops fetalis prenatally and often are stillborn or survive only a few months. At the other extreme, patients with attenuated manifestations of MPS VII have survived into the fifth decade of life.

Murine models of MPS VII have characteristics similar to the human disease[47]. MPS VII mice show GAG storage in lysosomes of visceral organs, skeleton, and brain. They have facial dysmorphism, growth retardation, deafness, behavioral deficits, and a shortened lifespan.

Mucopolysaccharidosis type VI (MPS VI)

Mucopolysaccharidosis type VI[48] is caused by deficiency of the enzyme arylsulfatase B [ARSB] (N-acetylgalactosamine-4-sulfatase) which removes the C4 sulfate ester group from the N-acetylgalactosamine sugar residue at the nonreducing terminus of the glycosaminoglycans dermatan sulfate (DS) and chondroitin sulfate (CS). Deficiency of ARSB results in intralysosomal storage and urinary excretion of these partially degraded GAGs. MPSVI shows a wide spectrum of symptoms ranging from slowly to rapidly progressing forms. It is characterized by characteristic skeletal dysplasia

(including short stature, dysostosis multiplex and degenerative joint disease), cardiac valve disease, reduced pulmonary function, hepatosplenomegaly, sinusitis, otitis media, hearing loss, sleep apnea, corneal clouding, carpal tunnel disease, and inguinal or umbilical hernia. Although intellectual deficit is generally absent in MPS VI patients, central nervous system findings may include cervical cord compression caused by cervical spinal instability, meningeal thickening and/or bony stenosis, communicating hydrocephalus, optic nerve atrophy and blindness. Clinical presentation of MPSVI varies greatly with respect to age of onset and rate of disease progression. Rapidly, intermediate and slowly progressing forms have been described, varying both in the severity and timing of symptoms development. Rapidly progressing forms may be evident since birth with elevated urinary GAGs, severe dysostosis multiplex, short stature, and death before the 2nd or 3rd decades. A slowly progressing form has been described as having later onset, mildly elevated urinary GAGs, mild dysostosis multiplex, with death in the 4th or 5th decades.

Mucopolysaccharidosis type I (MPS I)

Mucopolysaccharidosis-I (MPS I)[49] is a prototypical LSD caused by deficiency of a single lysosomal enzyme and occurs at a frequency in the range of 1:100.000. The disease is caused by homozygous inactivating mutations of the IDUA gene, encoding α-l-iduronidase, an enzyme required for degradation of heparan and dermatan sulfate, representing two highly abundant GAGs. Depending on the type of mutation, there is a wide range of disease severity. The most severe forms of MPS-I (commonly termed Hurler syndrome) are characterized by mental retardation, hepatosplenomegaly, dysostosis multiplex, corneal clouding, cardiac dysfunction and death within the first decade of life. The mildest forms (commonly termed Scheie syndrome) are characterized by normal intelligence and life expectancy, yet corneal clouding, dysostosis multiplex and mild visceral storage are still causing serious problems in the

affected patients.

Therapies for LSDs.

Few therapies are available for LSDs, and treatments are mostly symptomatic as they are not able to completely revert the pathologic phenotype. There are different clinical trials mainly based on enzyme replacement therapy, bone marrow transplantation, ex-vivo and *in-vivo* gene therapy, enzyme enhancement therapy and substrate reduction[50].

However the lack of complete knowledge of the pathogenic mechanisms behind the disease is still problematic when developing new therapeutic approaches for the treatment of LSDs.

In recent years biochemical and cell biology studies of LSDs have revealed an ample spectrum of abnormalities in a variety of cellular functions. These include defects in signaling pathways, calcium homeostasis, lipid biosynthesis and degradation and intracellular trafficking[51]. Therefore, an emerging view to explain the disease cascade is now focused on the importance of the multiple endosomal and autophagosomal streams flowing into the lysosomal system for processing. Failure to degrade and recycle sequestered materials in lysosomal disease may also lead to deficiency states in which precursors for metabolic pathways in the cell are diminished, followed by altered synthetic pathways and an increased metabolic demand on affected cells. The lysosomal system has thus emerged from being considered only an end-organelle, to being at the very hub of metabolic regulatory control. Perhaps the best example of the interconnection of the lysosome with other cellular systems is autophagy[52].

Considering the highly integrated function of lysosomes and autophagosomes it was reasonable to expect that lysosomal storage in LSDs would have an impact upon

autophagy [53].

In the last years, genome-wide association study (GWAS) has demonstrated that defects in the autophagy-lysosomal pathway are associated with bone size and stature in humans[54], [55], suggesting that the autophagic-lysosomal pathway plays an important role in bone homeostasis and development. The understanding of the biological and molecular system that links autophagy dysfunction and bone growth impairment has to be elucidated and it can further expand the possibility to treat bone defects in lysosomal-autophagy related disorders. Also, since the available therapies seem to have limited effects on bone defects in LSDs, it's clear how important is to develop new therapeutic pharmacological tools to treat bone diseases.

4.4 Proteasome.

The 26S proteasome, often called "the proteasome", is a multicatalytic enzyme complex expressed in the nucleus and cytoplasm of all eukaryotic cells[37]. The primary function of the proteasome is to degrade proteins. Proteasome substrates include signaling molecules, tumor suppressors, cell-cycle regulators, transcription factors and inhibitory molecules, among others. For a protein to be recognized by the proteasome, a small peptide (ubiquitin; Ub) must first be attached to the target protein. This process is carried out by a cascade of enzymes that activate free ubiquitin and carry it to the target protein[56].

The pathway by which proteins are ubiquitinated and degraded by the proteasome is termed the ubiquitin–proteasome pathway (UPS). The proteasome is a complex of ~33 different proteins that are arranged in an elongated particle composed of a central core with cap structures at one or both ends. It is a multicatalytic protease complex consisting of the 20S core particle (CP) and the 19S regulatory particles (RPs). The 20S

CP is composed of several subunits with distinct peptidase activities. The 19S is responsible for the recognition, unfolding, and subsequent translocation of ubiquitinated substrates into the 20S CP. This process is accompanied by enzymatic removal of Ub moieties, which are recycled. The proteasome is widely distributed in the cell, is localized to the cytosol and nucleus, and is also found tethered to several subcellular organelles. It is highly abundant, composing ~1% of the total protein mass of cells[57].

Recently, a new cross talk connecting mTORC1 and proteasome has emerged[58]. Manning et al described a mechanism by which through the involvement of the proteasome, mTORC1 exerts a coordinated regulation of protein synthesis and degradation. They show that as well as increasing protein synthesis, mTORC1 activation in mouse and human cells also promotes an increased capacity for protein degradation. Cells with activated mTORC1 exhibited elevated levels of intact and active proteasomes through a global increase in the expression of genes encoding proteasome subunits. They hypothesized that, in addition to serving as a quality control mechanism for newly translated proteins, the enhanced proteasome activity upon mTORC1 activation could serve to maintain adequate pools of amino acids to sustain new protein synthesis.

Given the tight regulation of mTORC1 on autophagy it is reasonable to expect a fine interplay that involves lysosome and proteasome in orchestrating cellular energy demand[38].

Aim of the thesis

The observation that mutations in more than 20 genes encoding for lysosomal proteins causes defects in skeletal development suggests that the lysosome may be involved in the regulation of intracellular signaling during skeletogenesis.

When I started working on my PhD project little if anything was know about this regulation. Thus I started my work on LSD mouse models, which were previously shown to be characterized by severe skeletal abnormalities similar to those found in human patients.

The main goals of this thesis project were to identify the mechanism(s) that underlie the skeletal manifestations of LSDs and to develop a therapeutic treatment.

In the course of my PhD, our lab published a work showing that autophagy is a developmentally regulated process required for bone growth. My work started with the aim to extend these findings; exploring the possibility that autophagy dysfunction may be implicated in the pathogenesis of skeletal disorders.

Defective autophagy is a generalized phenomenon occurring in many LSDs, although the pathogenic mechanisms are still unclear. By combining the knowledge of signaling that conveys on lysosome (the mTORC1-autophagy axis), I focused on the impaired lysosomal function to unravel the contribution of mTORC1 in bone growth.

The thesis will cover two main topics:

1) To characterize the contribution of mTORC1 signaling in the autophagy dysfunction found in LSD chondrocytes, thereby drawing a potential pathogenic mechanism.

2) To apply the deriving knowledge towards genetic and pharmacological approaches to rescue impaired mTORC1 signaling and consequently bone growth in LSDs mouse models.

Material and Methods

1. In vivo

Animals.

The *Gusb*$^{-/-}$ line carrying the missense E536Q mutation was kindly shared by W. Sly (St Louis University). The *Raptor*$^{flox/flox}$ line was purchased from Jackson Laboratories (stock no. 013188). The CMV-Cre line was from A. Ballabio (TIGEM, Pozzuoli). Raptor $^{flox/flox}$ were mated with CMV-Cre to obtain heterozygous mice that were subsequently mated with *Gusb*$^{+/-}$ mice. Double heterozygous *Gusb*$^{+/-}$*;Raptor*$^{+/-}$ mice were then mated with *Gusb*$^{+/-}$ in order to obtain *Gusb*$^{-/-}$*;Raptor*$^{+/-}$. *Arsb*$^{-/-}$ line was kindly shared by A. Auricchio (TIGEM, Pozzuoli). All mice used were maintained in a C57BL/6 strain background. The number of mice used in each experiment is specified in figure legends. Sex of the mice was not taken into account until post-natal day 15. Mice were randomly assigned to treatment groups. The investigators were not blinded to allocation during experiments and outcome assessment. Experiments were conducted in accordance with the guidelines of the Animal Care and Use Committee of Cardarelli Hospital in Naples and authorized by the Italian Ministry of Health.

Skeletal staining.

Skeletons were fixed in 95% ethanol overnight and stained with alcian blue and alizarin red (Sigma Aldrich) according to standardized protocols (http://empress.har.mrc.ac.uk/browser/). Alizarin red stains calcium and calcified structures, whereas alcian blue stains acetic mucins enriched in cartilage, thus the resulting colored skeleton will be red in bony parts and blue in cartilaginous parts. Measurement of bone length was performed using the Leica M205 A stereo microscope equipped with LAS X Software.

Tissue histology, immunohistochemistry and immunofluorescence.

Histology was performed according to standardized procedures (http://empress.har.mrc.ac.uk/browser/). Briefly, femurs were fixed overnight in 4% (wt/vol) paraformaldehyde (PFA) and then demineralized in 10% EDTA (pH 7.4) for 48 h. Specimens were then dehydrated, embedded in paraffin and sectioned at 7 μm, and stained with haematoxylin and eosin.

*Collagen type II, type X and phospho-S6 ribosomal protein***.** PIER (proteolytic induced epitope retrieval) was performed as antigen retrieval method. Deparaffinised sections were treated with 1mg/ml pepsin at 37 °C for 20 minutes then with testicular hyaluronidase (2 mg/ml, Sigma Aldrich) at 37 °C for 60 min for Collagen type X or with chondroitinase ABC (Sigma) for 2 hours at 37°C for Collagen type II, washed in PBS and incubated in 3% H_2O_2 in methanol. Sections were incubated with diluted normal blocking serum for 20 minutes and overnight at 4°C with monoclonal antibody to collagen X (clone X53, Quartett, Berlin, Germany*)*, collagen II (II-II6B3) (Hybridoma Bank) or Phospho-S6 Ribosomal Protein (Ser240/244) (Cell Signaling). *P62-SQSTM1*. For immunofluorescence, femurs were dissected from euthanized mice and fixed with buffered 4% PFA overnight at 4 °C, then washed with PBS and cryo-protected in successive sucrose solutions diluted with PBS (10% for 2 h, 20% for several hours and 30% overnight at 4 °C; all wt/vol), and finally embedded in OCT (Sakura). Cryostat sections were cut at 10μm. Sections were blocked and permeabilized in 3% (wt/vol) BSA, 5% fetal bovine serum (FBS) in PBS plus 0.3% Triton X-100 for 3 h and then incubated with the primary antibody (p62-SQSTM1, Progen) overnight. Sections were washed three times with 3% BSA in PBS plus 0.3% Triton X-100 and then incubated for 3 h with secondary antibodies conjugated with Alexa Fluor 568.

Growth Plate measurement. Individual zonal heights were measured for the

morphologically defined proliferative and hypertrophic zones of the growth plate. The proliferative zone (PZ) is defined as the region of chondrocyte displaying flattened-disc morphology. The hypertrophic zone (HZ) is defined as the region beginning with the consistent cylindrical cellular profile and extending to the metaphyseal chondro-osseous junction. We have estimated PZ and HZ heights measuring the length between the initial and final proliferating and hypertrophic chondrocytes respectively, by CellSens software (Olympus Life Science; manual measurement).

Collagen quantification and analysis.

Colorimetric assay. This was performed using the Sircol soluble collagen assay (Biocolor) following the manufacturer's protocol. Briefly, femoral cartilages were isolated from two/three mice with the same genotype, pooled and homogenized in 0.5 ml of 1 mg/ml cold (4 °C) pepsin in 0.2M NaCl, 0.5M acetic acid to pH 2.1 with HCl and then digested at 4 °C for 24 h, twice. The pellet was discarded and an equal volume (1 ml) of 4 M NaCl in 1M acetic acid was added to precipitate collagen. The pellet was then resuspended in 0.8 ml of 0.2M NaCl in 0.5M acetic acid and was precipitated again two times. After the last precipitation the pellet was washed twice with 70% EtOH to remove residual NaCl. The pellet was then complexed with Sircol dye (the dye reagent contains Sirius Red in picric acid and has been formulated for specific binding to collagen). Absorbance was measured at 555nm and concentration was calculated using a standard curve. Values were normalized to DNA levels calculated measuring the absorbance at 260 nm.

2. In vitro

Transmission electron microscopy.

For EM analysis, growth plates were fixed in 1% glutaraldehyde in 0.2M HEPES

buffer. Small blocks of growth plates were then post-fixed in uranyl acetate and in OsO_4. After dehydration through a graded series of ethanol, tissue samples were cleared in propylene oxide, embedded in Epoxy resin (Epon 812) and polymerized at 60 °C for 72 h. For pre-embedding immuno-EM RCS cells were fixed, permeabilised and labelled as described previously[59]. Anti-human LAMP-1 antibody was purchased by Sigma (Cat N-L1418). From each sample, thin sections were cut with a Leica EM UC6 ultramicrotome and images were acquired using a FEI Tecnai-12 electron microscope (FEI, Eindhoven, Netherlands) equipped with a VELETTA CCD digital camera (Soft Imaging Systems GmbH, Munster, Germany). EM analysis was performed by Elena Polishchuk in the "Advance Microscopy and Imaging core" at TIGEM, Pozzuoli.

Cell culture, transfections and plasmids.

Primary cultured chondrocytes were prepared from rib cartilage of P5 mice. Rib cages were first incubated in DMEM (Euroclone) using 0.2% collagenase D (Roche) and after adherent connective tissue had been removed (1.5 h) the specimens were washed and incubated in fresh collagenase D solution (3mg/ml) for a further 4.5 h. Isolated chondrocytes were maintained in DMEM supplemented with 10% FBS, 1% penicillin/streptomycin (Invitrogen). Adult fibroblasts were prepared from skin of P5 mice. Samples, cut in small pieces using a razor blade, were first incubated with collagenase (30 min) and then were washed and incubated in trypsin for 20 min. After centrifuging, cell pellet was resuspended in complete medium. MPSI mesenchymal-derived chondrocytes were provided by M. Serafini (University of Milano-Bicocca). *ArsbKO* HeLa cell line was provided by J. Monfregola (TIGEM, Pozzuoli). For amino acid starvation and stimulation experiments the cell culture medium was amino acid free RPMI 1640 (US Biological) supplemented with 10% dialyzed FBS (Invitrogen). Cells were rinsed twice with starvation medium then kept in a full volume of starvation

medium for 50 min. At 50 min time point a standard amino acids mixture comprising MEM non-essential amino acids solution, MEM essential amino acids solution and L-Glutamine (Invitrogen) was added back to a final concentration of 3X for the indicated time points. Unless otherwise specified, to synchronize mTORC1 signaling before performing the experiments, primary chondrocytes and RCS cells were stimulated with A.A. for 24h and 6h, respectively. Cells were transfected with Lipofectamine LTX and Plus reagent (Invitrogen) following a reverse transfection protocol. The tandem mRFP–GFP–LC3 plasmid was from T. Yoshimori (Osaka University, Japan). The myc-UVRAG plasmid was from DH. Kim (University of Minnesota, USA). The GFP-2xFYVE plasmid was from S. Tooze (Francis Crick Institute, London)

Cell immunofluorescence.

Chondrocytes were fixed for 10 min in 4% PFA in PBS and permeabilized for 30 min in 0.05% (w/v) saponin, 0.5% (w/v) BSA, 50mM NH_4Cl and 0.02% NaN_3 in PBS (blocking buffer). For the detection of endogenous LC3 cells were methanol-fixed. The cells were incubated for 1h with the primary antibodies against Lamp-1 (Santacruz biotechnology), SQSTM1-p62 (Progen), mTOR (Cell Signaling), LC3 (Novus Biologicals) and WIPI-2 (Abcam) washed three times in PBS, incubated for 1 h with the secondary (Alexa Fluor-labelled) antibody, washed three times in PBS, incubated for 20 min with 1 μg/ml Hoechst 33342 and finally mounted in Mowiol. For the detection of TFEB and TFE3 cells were permeabilized for 30 min in 0.2% Triton X-100 in PBS and blocked for 1 h with 0.1% Triton X-100, 10% goat serum in PBS. The cells were incubated overnight with primary antibodies against TFEB (MyBioSource) and TFE3 (Bethyl). All confocal experiments showing co-localization were acquired using slice thickness of 0.5μm using the LSM 710 confocal microscope equipped with a 63 × 1.4 numerical aperture oil objective. Co-localization analysis was performed using the

ImageJ software (JaCoP plug-in).

Western blotting.

Cells were washed twice with PBS and then scraped in lysis buffer (RIPA lysis buffer [20 mM Tris (pH 8.0), 150 mM NaCl, 0.1% SDS, 1% NP-40, 0.5% sodium deoxycholate] in the presence of PhosSTOP and EDTA-free protease inhibitor tablets; Roche). Cell lysates were incubated on ice for 30 min and then the soluble fraction was isolated by centrifugation at 14,000 r.p.m. for 20 min at 4 °C. Total protein concentration in cellular extracts was measured using the colorimetric BCA protein assay kit (Pierce Chemical). Protein extracts, separated by SDS–PAGE and transferred onto membranes, were probed with antibodies against phospho (p)-p70S6K (T389), p70S6K, (p)-ULK1 (S757; S555; S317), ULK1, raptor (Cell Signaling), LAMP-1 (Abcam), LC3B, β-actin (Novus Biologicals), P62/SQSTM1 (Abnova). Proteins of interest were detected with horseradish peroxidase (HRP)-conjugated goat anti-mouse or anti-rabbit IgG antibody (Vector Laboratories) and visualized with the Super Signal West Dura substrate (Thermo Scientific), according to the manufacturer's protocol. The western blotting images were acquired using the Chemidoc-lt imaging system (UVP) and band intensity was calculated using ImageJ software using the 'Gels and Plot lanes' plug-in.

Generation of *Gusb*$^{-/-}$ RCS cell line.

To create Gusb gene disruption an RCS chondrocyte cell line was used. $1x10^6$ cells were transfected with an all-in-one vector contains the sgRNA of interest (target site sequence: CACCTTGAGTTCCCGCGAAG with predicted no off-targets), which expression was driven by the U6 promoter, a recombinant form of Cas9 protein under the control of the CMV promoter and a mCherry reporter gene under the control of the

SV40 promoter (Genecopoeia). Cells were transfected with Lipofectamine LTX and Plus reagent (Invitrogen) following a reverse transfection protocol. 48h after transfection, putative positive clones were FACS sorted for the mCherry expression using the BD FACSAria. Sorted cells were kept in culture until confluence and then subjected to PCR analysis followed by Sanger sequencing to identify mutations. Positive clones were screened for β-gluronidase activity. Briefly, cell pellets were lysed in extraction buffer [50 mM $NaHPO_4$, pH 7.0, 10 mM 2-mercaptoethanol, 10 mM Na_2EDTA, 0.1% sodium lauryl sarcosine, 0.1% Triton X-100(100 ml)] and protein concentration was measured using the colorimetric BCA protein assay kit (Pierce Chemical). 200 and 400 μg of proteins were incubated with 200μl of the fluorogenic substrate, 4-methylumbelliferyl-β-D-glucuronide (2mM, Sigma-Aldrich, Milan, Italy), for 0.5 and 1 h at 37 °C. The reaction was stopped by adding 200μl of the carbonate stop buffer (0.5 M NaHCO3/0.5 M Na2CO3, pH 10.7), and the fluorescence of the 4-methylumbelliferone liberated was measured in a fluorimeter (GloMax-Multi Detection System; Promega) using 365nm excitation and 460nm emission. Absolute fluorescence of wild-type RCS was used as control. *GusbKO* clones as well as WT RCS cells were kept in medium containing 2mg/ml chondroitin sulphate (Sigma Aldrich) for 48h before any experiment.

Co-Immunoprecipitation experiment.

For co-immunoprecipitation experiments, whole-cell extracts were prepared in 0.3% Chaps-containing lysis buffer (40 mM HEPES, pH 7.4, 120 mM NaCl, 1 mM EDTA, 50 mM NaF, 1.5 mM Na_3VO_4, 10 mM β-glycerophosphate, 0.3% Chaps, and EDTA-free protease inhibitors) as described in a previous report (Kim et al., 2002), and immunoprecipitated with anti-UVRAG antibody (MBL). Precipitated proteins were washed five times with 0.3% Chaps lysis buffer, separated by SDS–PAGE and

transferred onto membranes, were probed with antibodies against P-Uvrag S498 (gift from DH. Kim), Beclin-1 (CST), UVRAG (MBL), Rubicon (CST), Vps16 (SantaCruz).

Procollagen secretion assay.

Synchronized procollagen type II (PC2) secretion was obtained after incubating chondrocytes for 3 h at 40 °C to block PC2 in the ER, and then shifting the temperature to 32 °C (ER block release) for 15 min. Cells were then fixed in 4%PFA for 10' at room temperature and then processed for immunofluorescence. Cells were incubated 1h with primary antibodies against PC2 (Ibridoma Bank) and Giantin (Abcam).

Proteasome assay.

RCS cells were amino acid starved for 50 minutes then stimulated for 6h with 3X amino acid mix. Proteasome activity was measured in 10µg of cell lysates with a Proteasome Activity Assay Kit (Abcam). The fluorogenic substrate Succ-LLVY-AMC was used to measure the chymotrypsin-like proteasome activity. Assays were carried out in a 100µl reaction volume according to the manufacturer's instructions. Fluorescence was measured with a microtiter plate reader (GloMax-Multi Detection System; Promega) in the presence/absence of MG-132 after 20 min at 37°C for 30 min. The MG132-sensitive increase of fluorescence at 350/440 nm was considered as proteasomal activity and was expressed as relative fluorescence units (RFU).

Long-lived protein degradation assay.

RCS cells were seeded in 6 well/plate at $2.5x10^5$ cells/well. Intracellular proteins were labeled for 18 h at 37°C with 5 µCi/ml of L-[^{3}H]serine (Perkin Elmer) in complete medium. Any unincorporated radioactivity was eliminated by rinsing the cells 3 times

with PBS. The cells were then incubated with fresh complete medium, and 2 mM serine for 2h to degrade short-lived proteins. Next, the medium was removed by aspiration and replaced. This first time point (Time 0h) was harvested: the cells were washed twice with cold 10% TCA (w/v), plus 2 mM serine, to make sure that no radioactivity has remained adsorbed to the denatured proteins. The cell pellet was then dissolved at 37°C in 0.2 M NaOH for 2 h. The remaining wells were then incubated in fresh complete medium supplemented with 2 mM serine and 100nM MG-132 or DMSO, and incubated for 48h. The rate of degradation of long-lived proteins was calculated from the ratio 48h/0h of the acid-precipitable cell fraction. Plotting these values versus time gave the total rates of proteolysis.

Tat–beclin-1 peptide treatment.

In vivo. Newborn mice were intraperitoneally injected daily with Tat–beclin-1 peptide at 2 mg/kg resuspended in PBS. Control mice were injected with vehicle only. Mice were killed after 6 or 15 days, as specified in figure legends. *In vitro.* For peptide treatment, cells were washed with PBS(−) and treated with peptides (20μM, 2h) dissolved in OPTI-MEM (Gibco) acidified with 0.15% (v/v) 6N HCl.

Chemicals.

Tat-beclin-1 peptide (20μM) (Beclin-1 Activator II, retro-inverso Tat-beclin-1, Millipore). Tat-beclin-1-mutated (L17S) (20μM) was a gift from B. Levine. BafilomycinA_1 (200nM) (Sigma), Torin-1 (1μM) (CST), MG132 (10μM) (Sigma), SAR405 (10μM) (Sigma). Protein G Sepharose (GE Healthcare).

Statistics.

Paired Student's *t*-test was performed when comparing the same cell population with two different treatments. Unpaired Student's *t*-test was performed when comparing two groups of mice or different primary chondrocyte preparations. One-way ANOVA and Tukey's post-hoc tests were performed when comparing more than two groups relative to a single factor (treatment or genotype).

Results

1. Pathogenic mechanism for dysfunctional autophagy in LSD cells.

1.1 *Defective autophagosome-lysosome fusion and collagen trafficking in MPS chondrocytes.*

To investigate if autophagy dysfunction in MPSs chondrocytes plays a role in the pathogenesis of bone growth retardation we analyzed autophagy in primary chondrocytes isolated from a mouse model of Mucopolysaccharidosis type VII (MPSVII)[47], which is caused by mutations in the *b-glucuronidase* gene (referred as *Gusb*$^{-/-}$ chondrocytes). In addition a cellular model of Rat Chondrosarcoma cell line (RCS)[60] knock-out for Gusb (referred as *GusbKO*) was created using Crispr/Cas9 genome editing (**Figure 10**).

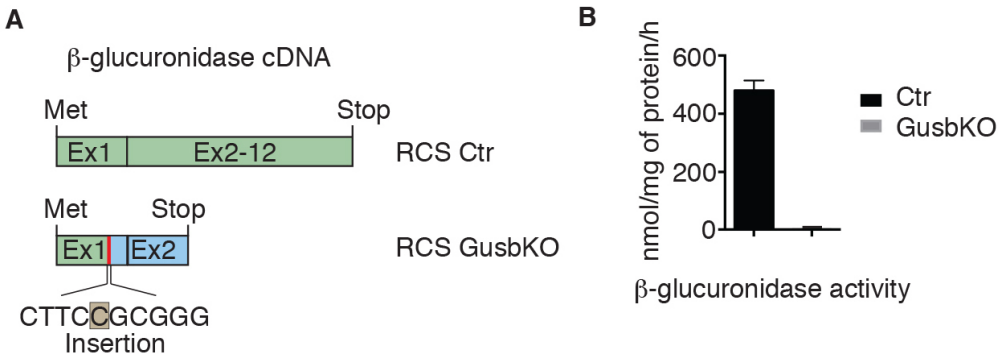

Figure 10. Characterization of Crispr/Cas9 GusbKO RCS clones.
A, schematic representation of the genetic mutation found in the *Gusb*KO clone: a single base insertion within the first exon causes a frameshift and a premature stop codon within the second exon of the protein. **B**, the resulted truncated protein lacks enzymatic activity. Bar graph displaying β-glucuronidase enzymatic activity.

Gusb$^{-/-}$ chondrocytes showed swollen lysosomes (Lys), monitored by electron microscopy and accumulation of the lysosomal marker LAMP-1 (**Figure 11A**).

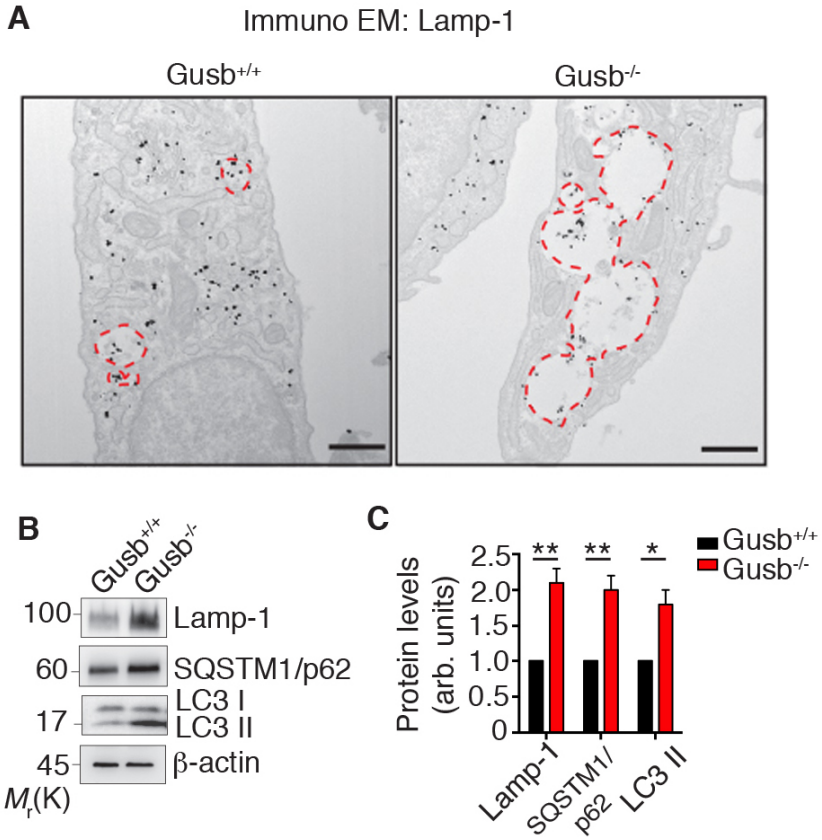

Figure 11. A block of autophagy in MPS cells.
A, Lamp-1 Immuno-EM from primary cultured chondrocytes isolated from Gusb$^{+/+}$ and Gusb$^{-/-}$ mice. Scale bar, 500nm. Red line indicates lysosomes. **B**, Western blot analysis of Lamp-1, SQSTM1/p62 and LC3 II accumulation in primary cultured chondrocytes with the indicated genotypes. β-Actin was used as a loading control. Blot is representative of 3 independent experiments. **C**, Bar graphs show protein levels of the indicated protein (normalized to β-Actin) in Gusb$^{-/-}$ chondrocytes and expressed as fold increase compared to control (Gusb$^{+/+}$). Values are expressed as mean (±s.e.m.) of $n = 3$ independent chondrocyte preparations (Student's t-test, * $p \leq 0.05$, ** $p \leq 0.005$).

Damaged organelles result to be filled with undigested substrates, as demonstrated by SQSTM1/p62 receptor accumulation (**Figure 11B-C**). *Gusb*$^{-/-}$ cells had higher number of autophagosomes (AVs) compared to their correspondent control, as monitored by quantifying the conversion of LC3I to the autophagosome–associated lipidated form (LC3II) (**Figure 11B-C**) and by MAP1LC3 immunofluorescence analysis (**Figure 12A-B**).

To test if the accumulation of AVs was due to an enhanced rate of AV biogenesis we performed two assays: an immunofluorescence to detect WIPI-2 puncta formation (**Figure 12A-B**) and a time course analysis of LC3-I to -II lipidation in presence of the lysosomal inhibitor Bafilomycin A_1 (Baf.A_1) (**Figure 12C-D**). WIPI-2 is an early autophagosomal marker: it is recruited to form autophagosomes before and during LC3 lipidation and it disassociates before the autophagosome matures[61]. Baf.A_1 is a lysosomal inhibitor used to measure autophagic flux by preventing AV degradation within the Lys[62]. The rate of AV formation during the time course of inhibition is calculated using the ratio of AV accumulation between 3h and 1h of treatment.

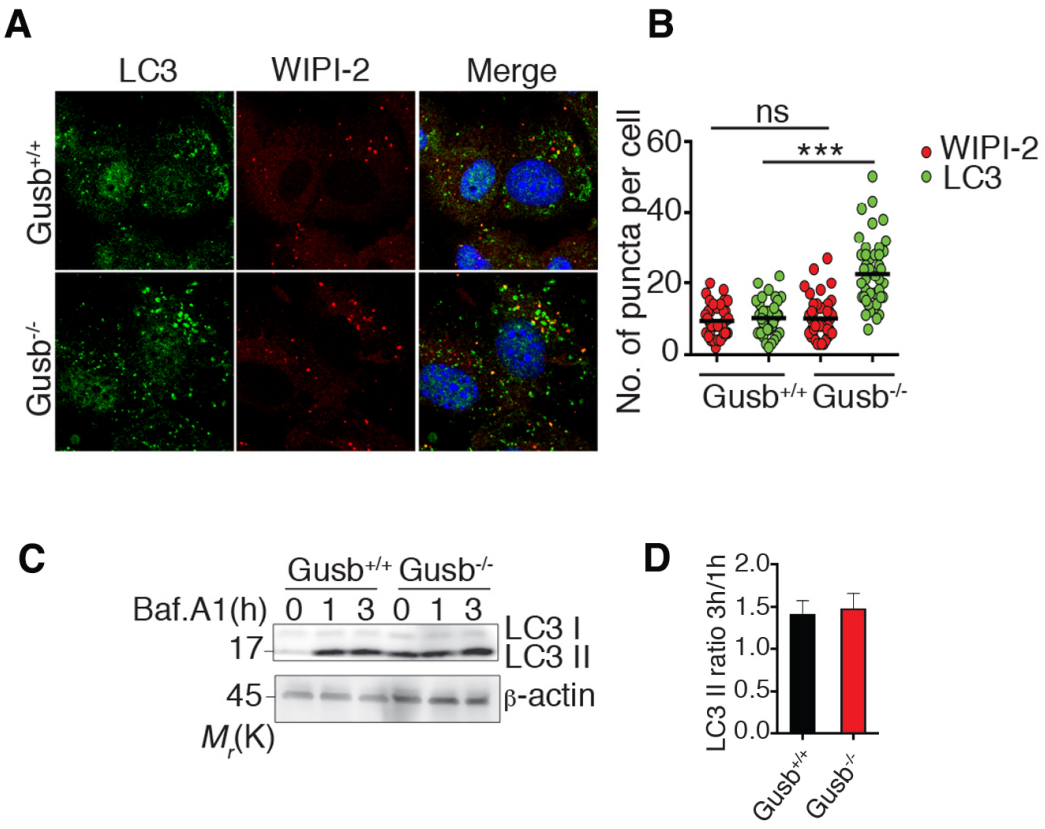

Figure 12. Normal autophagosome biogenesis in Gusb$^{-/-}$ primary chondrocytes.
A, Immunofluorescence of WIPI-2 and LC3 in primary chondrocytes with the indicated genotypes, after 24h amino acid treatment. **B**, bar graph displaying quantization of WIPI-2 and LC3 puncta per cell (Student's *t*-test, *** $p \leq 0.0005$). $N \geq 40$. **C**, Western blot analysis of LC3II accumulation in the presence of the lysosomal inhibitor Bafilomycin A1 (200nm) for the indicated time points. **D**, bar graph displaying the rate of autophagosome formation in the presence of Baf. A1 (the rate is calculated using the ratio of accumulated LC3 II between 3h and 1h of treatment). N = 3 independent experiments.

As shown in Figure 12, both of these assays display normal AV biogenesis in Gusb$^{-/-}$ when compared to control cells.

The accumulation of AV was rather the consequence of a failure to properly complete the late stage of the autophagic process that is a defective AV digestion by Lys[53]. By performing a triple immunofluorescence for Lamp-1, LC3 and SQSTM1/p62 in primary chondrocytes, we observed a defective AV-Lys co-localization and accumulation of the SQSTM1/p62 autophagy substrate in MPS compared to control chondrocytes (**Figure 13A-C**).

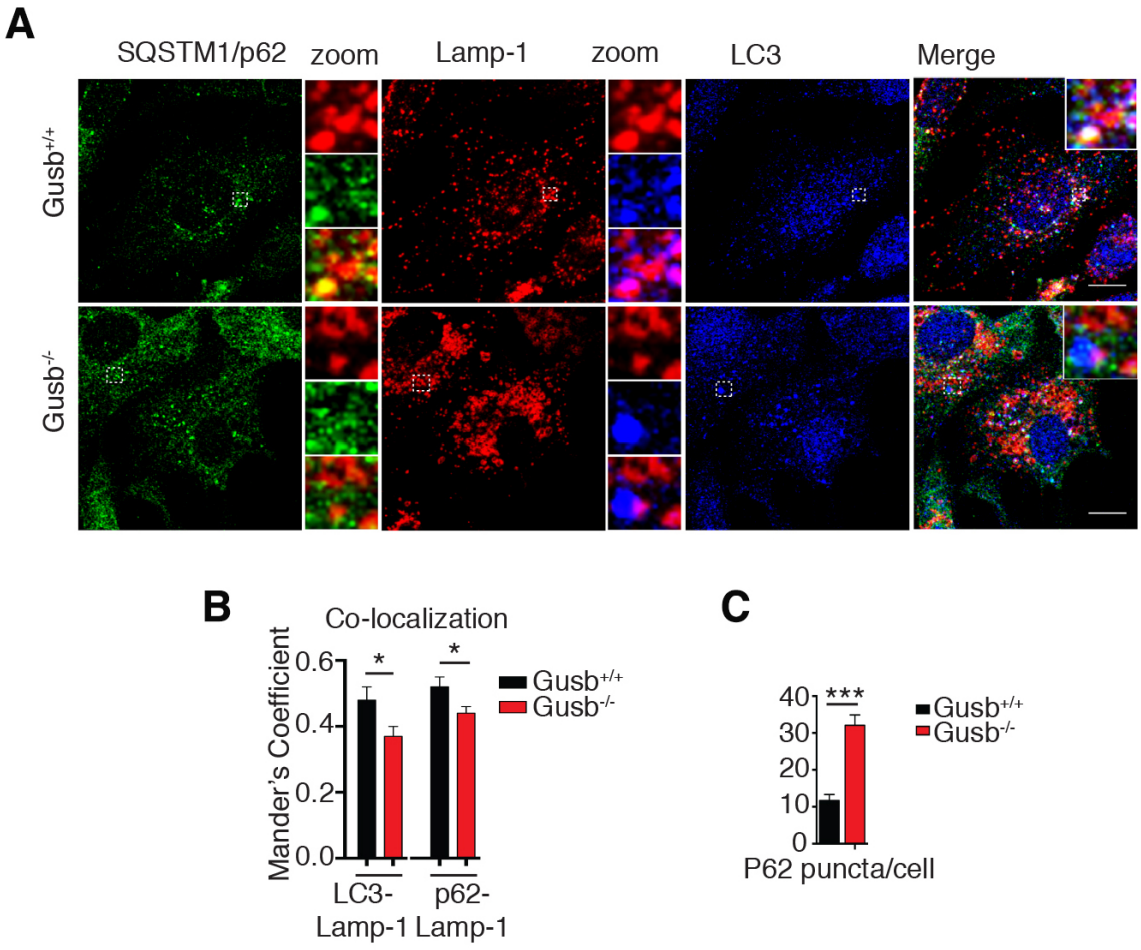

Figure 13. See page 57 for figure legend.

Figure 13. Impaired autophagosome-lysosome fusion in MPS cells.
A, Immunofluorescence of Lamp-1, SQSTM1/p62 and LC3 in primary chondrocytes isolated from mice with the indicated genotypes. The insets show higher magnification, single color channels, Lamp-1-p62 and Lamp-1-LC3 co-localization of the boxed area. Scale bar, 10µm. **B**, Bar graph displays quantification of Lamp-1 co-localization with LC3 and p62. Data are Mander's coefficient means (±s.e.m.) of 3 independent experiments (Student's *t*-test *p<0.05). **C**, Bar graph displays quantification of SQSTM1/p62 puncta per cell. Data are means (±s.e.m.) of 3 independent experiments (Student's *t*-test ***p<0.0005).

In addition, the co-localization between SQSTM1/p62 and lysosomes was found impaired, suggesting an improper cargo delivery to lysosomes (**Figure 13A-B**). As shown in Figure 14, these finding were extended to the *GusbKO* cells for which we found the same results.

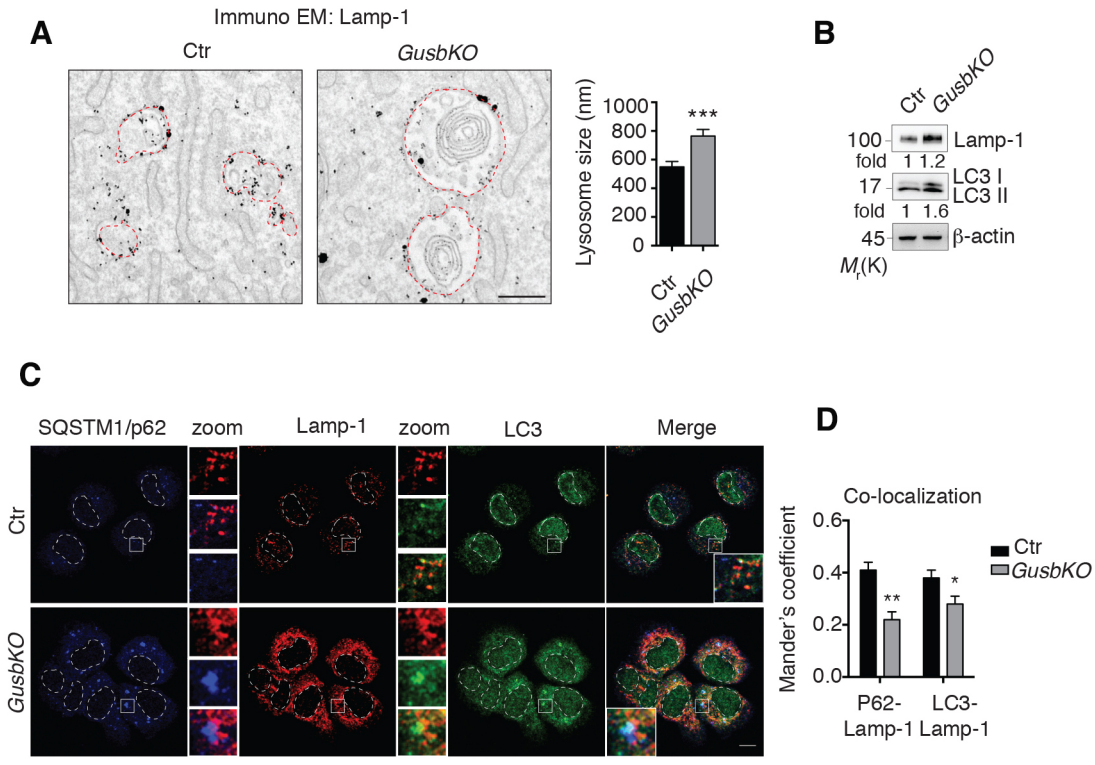

Figure 14. Block of autophagy in GusbKO RCS cell line.
A, Lamp-1 Immuno-EM from control (Ctr) and *GusbKO* RCS cells. Scale bar, 500nm. Bar graph displays the lysosome size (Student's *t*-test, *** p<0.0005). **B**, Western blot analysis of Lamp-1 and LC3 II accumulation in control and *GusbKO* RCS cells. β-Actin was used as a loading control. Blot is representative of 3 independent experiments. **C**, immunofluorescence of Lamp-1, SQSTM1/p62 and LC3 in control and *GusbKO* RCS cells. Scale bar, 10µm. **D**, Bar graph displays quantification of Lamp-1 co-localization with LC3 and p62. Data are Mander's coefficient means (±s.e.m.) of 3 independent experiments (Student's *t*-test **p<0.005, *p<0.05).

We also analyzed the rate of fusion between lysosomes and autophagosomes using a tandem fluorescent-tagged autophagosomal marker in which LC3 was engineered with both monomeric red fluorescent protein (mRFP) and GFP. In this assay the GFP fluorescence loss is a direct measurement of autophagosome fusion because of GFP quenching by lysosomal acidic pH[63]. The validity of this analysis is not affected by the decreased degradation capability of lysosomes in the LSD models analyzed, as the green fluorescence is rapidly quenched by protonation occurring in the acidic lysosomal lumen. Specifically, control and *GusbKO* cells were transfected with the mRFP-GFP-LC3 construct, and the autophagosome maturation was followed over a 48h period. The rate of autophagosome maturation, measured with the number of RFP-only puncta/autolysosomes, was markedly lower in *GusbKO* cells compared to that of control cells (**Figure 15A-B and later on Figure 30 for primary *Gusb*$^{-/-}$ chondrocytes**).

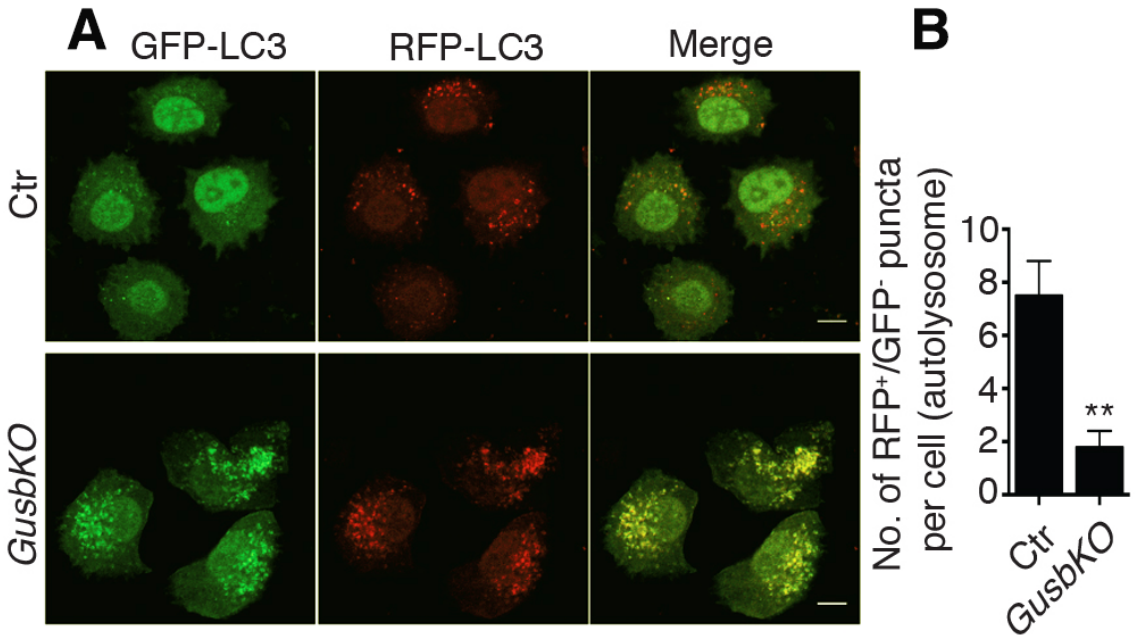

Figure 15. Impaired autolysosome formation in GusbKO cells.
A, RFP-GFP-LC3 was transiently expressed in control and *GusbKO* RCS cells. LC3 was monitored by fluorescence microscope two days post transfection. Scale bar, 10μm. **B**, bar graph displays quantitative analysis of RFP-only puncta (autolysosome) per cell (Student's *t*-test **p<0.005).

Previous work from our lab demonstrates that during bone growth autophagy plays a pivotal role in collagen trafficking and secretion[30]. In particular, has been shown that autophagy is induced in growth-plate chondrocytes during post-natal development and regulates the secretion of type II collagen (Col2), the major component of cartilage ECM. Mice lacking autophagy in chondrocytes experience endoplasmic reticulum (ER) storage of type II procollagen (PC2) and defective formation of the Col2 fibrillary network in the ECM. To investigate whether the autophagy dysfunction found in our cell models affects procollagen homeostasis in chondrocytes, we performed a procollagen trafficking assay in primary chondrocytes derived from *Gusb*$^{+/+}$ and *Gusb*$^{-/-}$ mice. The trafficking test is achieved by exposing cells to shift temperature experiments. The incubation at 40°C blocks the procollagen in the ER and the subsequent shift at 32°C for 15 min allows the secretion wave to move towards the Golgi. Consistent with an impaired autophagy, we observed defective type II procollagen (PC2) trafficking in *Gusb*$^{-/-}$ chondrocytes compared to control cells (**Figure 16A-B**). In particular, the trafficking was not abolished but significantly delayed.

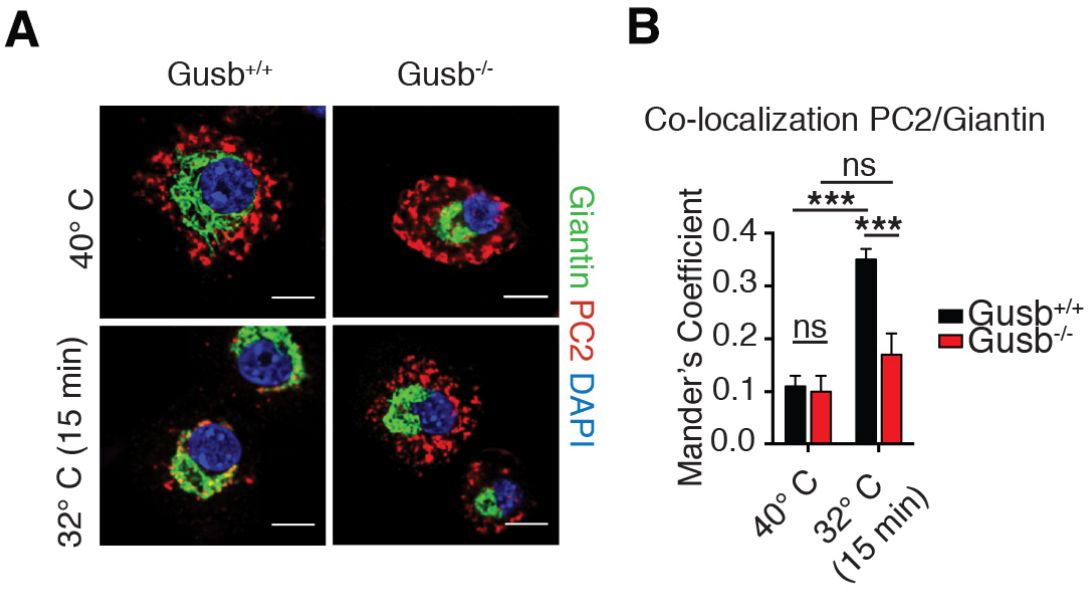

Figure 16. See page 60 for figure legend.

Figure 16. Delayed procollagen type 2 (PC2) trafficking in Gusb$^{-/-}$ chondrocytes.
A, Giantin and PC2 immunostaining in Gusb$^{+/+}$ and Gusb$^{-/-}$ chondrocytes. Synchronized PC2 secretion was obtained after incubating chondrocytes for 3 h at 40 °C to block PC2 in the ER, and then shifting the temperature to 32 °C (ER block release) for 15 min. **B**, Bar graph displaying quantification of Giantin-PC2 co-localization. The data are Mander's Coefficient means (±s.e.m.) representative of 2 independent experiments, n > 90 cells were analyzed for each experiment and time point. Scale bar, 10μm (Student's *t*-test, *** p<0.0005).

1.2 Enhanced mTORC1 signaling in LSD chondrocytes.

Lysosome is emerging as critical regulator of mTORC1 signaling. Pharmacological inhibition of lysosome impairs mTORC1 activation in response to amino acids in different cell types[25]. However, a similar inhibition in chondrocytes has been recently reported to have an opposite effects on mTORC1 signaling, suggesting that chondrocytes may respond differently than other cells to the lysosomal impairment[64]. To assess the status of mTORC1 activity in case of LSD we took advantage of different cellular models: primary chondrocytes isolated from mouse models of MPSVII (*Gusb*$^{-/-}$) and MPSVI (*Arsb*$^{-/-}$)[48], mesenchymal-derived chondrocytes isolated from three MPSI human patients[65] and *GusbKO* RCS cells.

As discussed in the introduction, the mTORC1 kinase is known to be responsive to most of the stimuli a cell can encounter. The pathway that connects growth factors to mTORC1 has been extensively characterized and is activated when insulin and other ligands/growth factors bind their tyrosine kinase receptors at the plasma membrane. This initiates a series of intracellular phosphorylation-cascades that ultimately lead to the inactivation of the multiple mTORC1 inhibitors (see introduction), thus enhancing the activity of the complex.

To measure the activity of the mTORC1 complex in our cell lines we performed a stimulation with a cocktail of growth factors. Cells were starved for fetal bovine serum

(FBS) for 50 minutes and then stimulated for different time points with 10% FBS. mTORC1 activation was monitored by analyzing the phosphorylation of two known substrates: S6K on threonine 389 (T-389) and ULK1 on serine 757 (S-757). As shown in Figure 17, both *Gusb*$^{-/-}$ and control cells display the same activation kinetics during the time course stimulation.

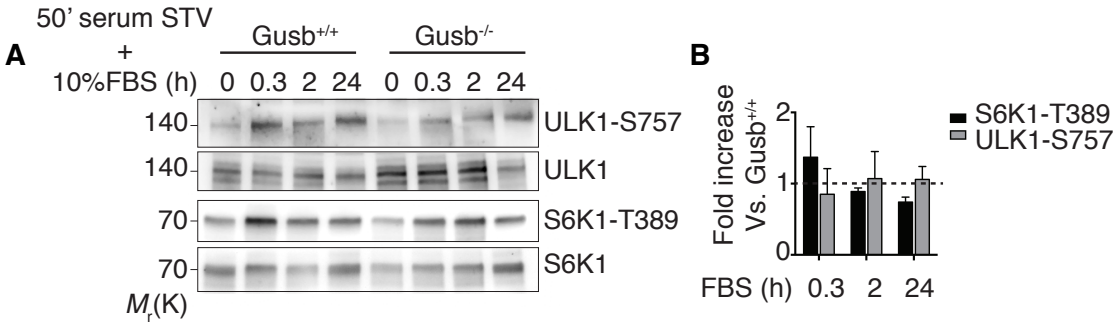

Figure 17. Normal mTORC1 response after growth factors stimulation.
A, Western blot analysis of mTORC1 signaling in primary chondrocytes isolated from mice with the indicated genotype and stimulated with 10% Fetal Bovine Serum (FBS) for the indicated hours (h). (**B**) Bar graphs showing phosphorylation levels of the indicated protein (normalized to their total levels) in *Gusb*$^{-/-}$ chondrocytes and expressed as fold increase compared to control (Gusb$^{+/+}$; dotted line). Values are expressed as mean (±s.e.m.) of n = 2 independent chondrocyte preparations.

Given the peculiar contribution of amino acids to the regulation of mTORC1 (see introduction) and since they act independently of the insulin/PI3K pathway, relying most on nutrients derived from functional lysosome and proteasome activities, we plan to analyze the response of cells with impaired lysosomal function to this particular source of energy.

MPS cells were kept in culture with normal growth medium until they where subjected to an amino acids deprivation/stimulation time course. Cells were starved for 50 minutes in a medium containing everything but amino acids, then were subjected to refeeding with an excess of amino acids for different time points. As shown in Figure 18, *Gusb*$^{-/-}$ primary chondrocytes showed enhanced and sustained mTORC1 signaling

both at steady state (**Figure 18A**) and in response to amino acid stimulation (**Figure 18B-C**) compared to their correspondent controls.

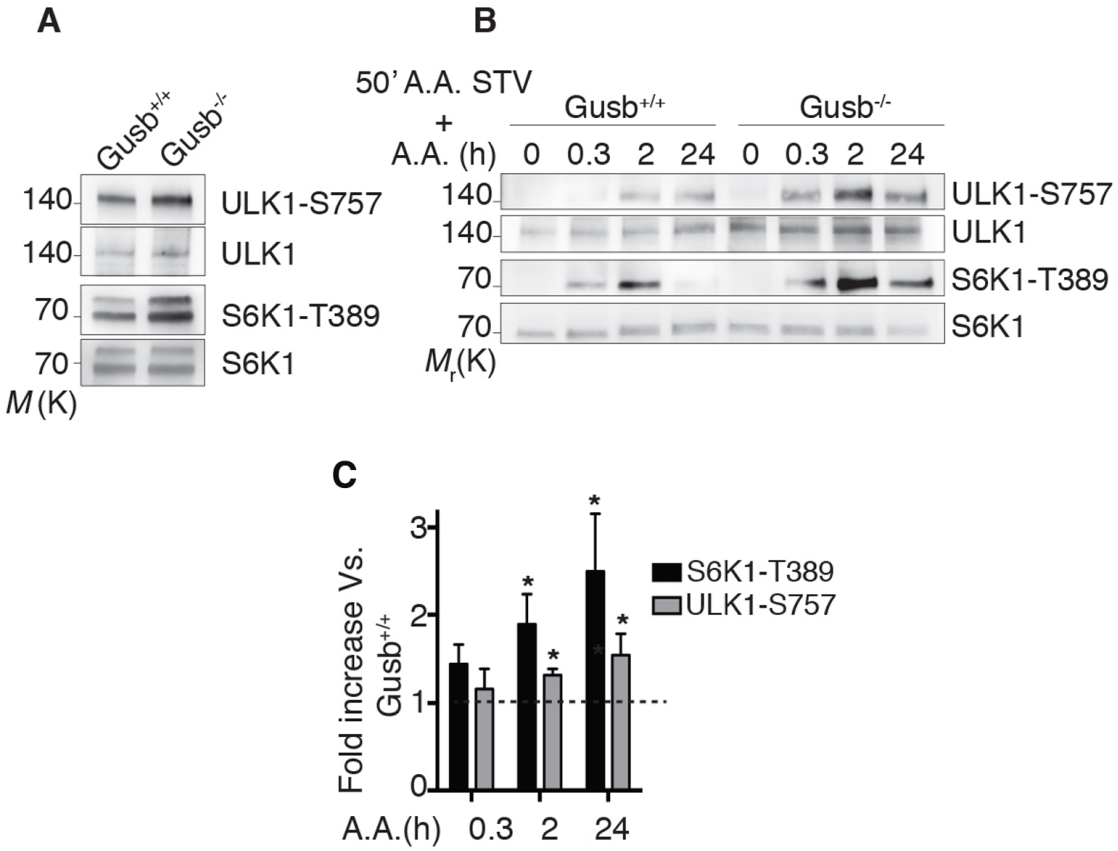

Figure 18. Enhanced mTORC1 signaling in Gusb-/- chondrocytes.
A-C, Phosphorylation levels of mTORC1 substrates (ULK and S6K1) in primary chondrocytes isolated from *Gusb*$^{+/+}$ and *Gusb*$^{-/-}$ mice (**A**) at steady state and (**B**) stimulated with amino acid (A.A) for the indicated time (h=hour). **C**, Bar graphs show phosphorylation levels of the indicated protein (normalized to their total levels) in *Gusb*$^{-/-}$ chondrocytes and expressed as fold increase compared to control (Gusb$^{+/+}$; dotted line). Values are expressed as mean (±s.e.m.) of *n* = 4 independent chondrocyte preparations (Student's *t*-test, * p≤ 0.05).

These abnormal responses to amino acid stimulation were further confirmed in the other LSD cell lines analyzed, as shown in Figure 19.

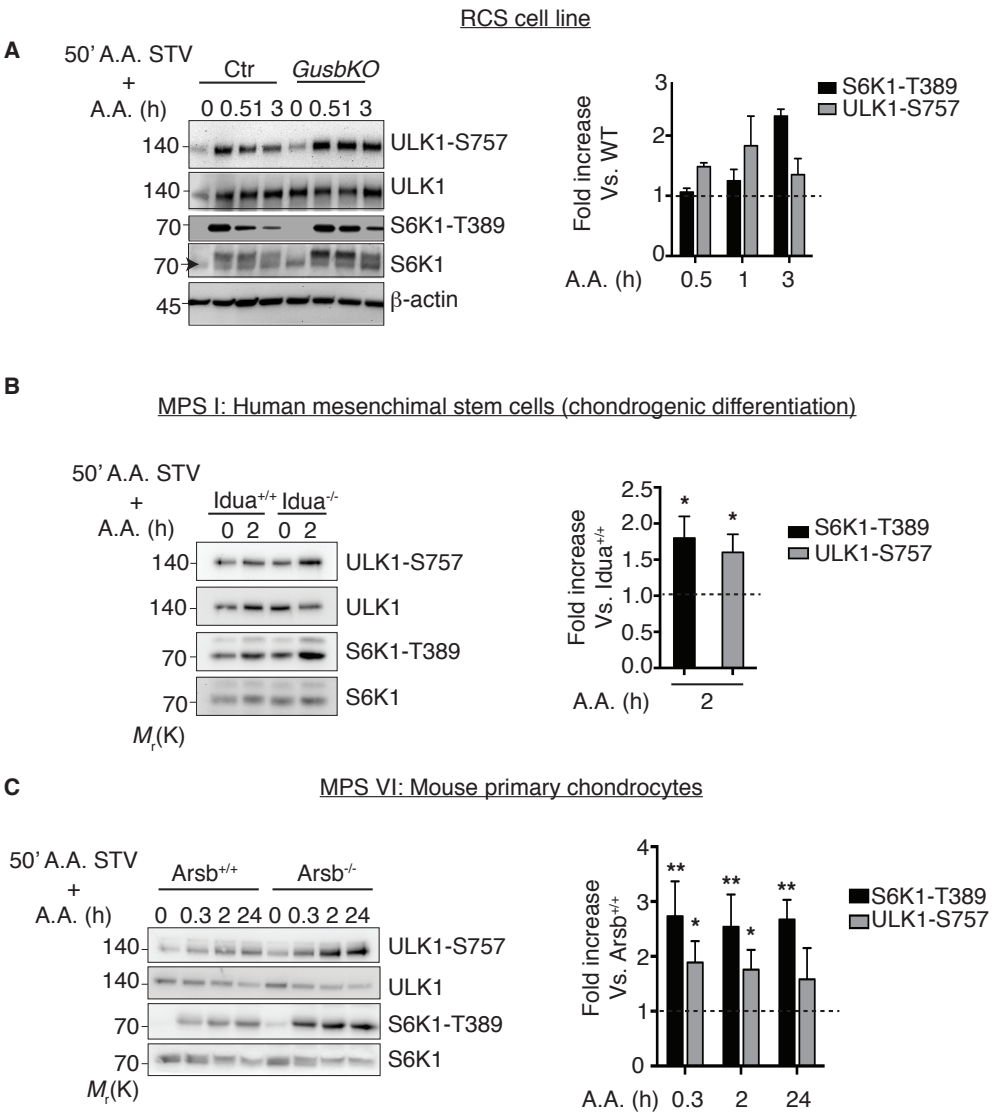

Figure 19. Enhanced mTORC1 signaling in LSD cells.
A-C, Western blot analysis of mTORC1 signaling upon a time course of amino acid stimulation. Bar graphs display phosphorylation levels of the indicated protein (normalized to their total levels and expressed as fold increase vs each relative control) in (**A**) *GusbKO* RCS cells, (**B**) *Idua*$^{-/-}$ differentiated human mesenchimal stem cells and (**C**) *Arsb*$^{-/-}$ mouse primary chondrocytes expressed as fold increase compared to their corresponding control. N = 3 independent experiments (Student's *t*-test *p<0.05, **p<0.005). Arrow head in **A** indicates the specific band for S6K.

Amino acids activate mTORC1 by inducing its association to the lysosomal membrane, where the main mTORC1 activator Rheb resides[21]. To further analyze this phenomenon and to verify that the enhanced activity was coupled with a higher association to lysosomes, a co-immunofluorescence was performed. Consistently, the association of mTOR to lysosomes (revealed by the co-localization between mTOR and

the lysosomal marker Lamp-1) was found significantly increased in *Gusb*$^{-/-}$ (**Figure 20A-B**) and *Arsb*$^{-/-}$ (**Figure 21A-B**) chondrocytes compared to controls when subjected to the same starvation/stimulation experiments as in Figures 18 and 19.

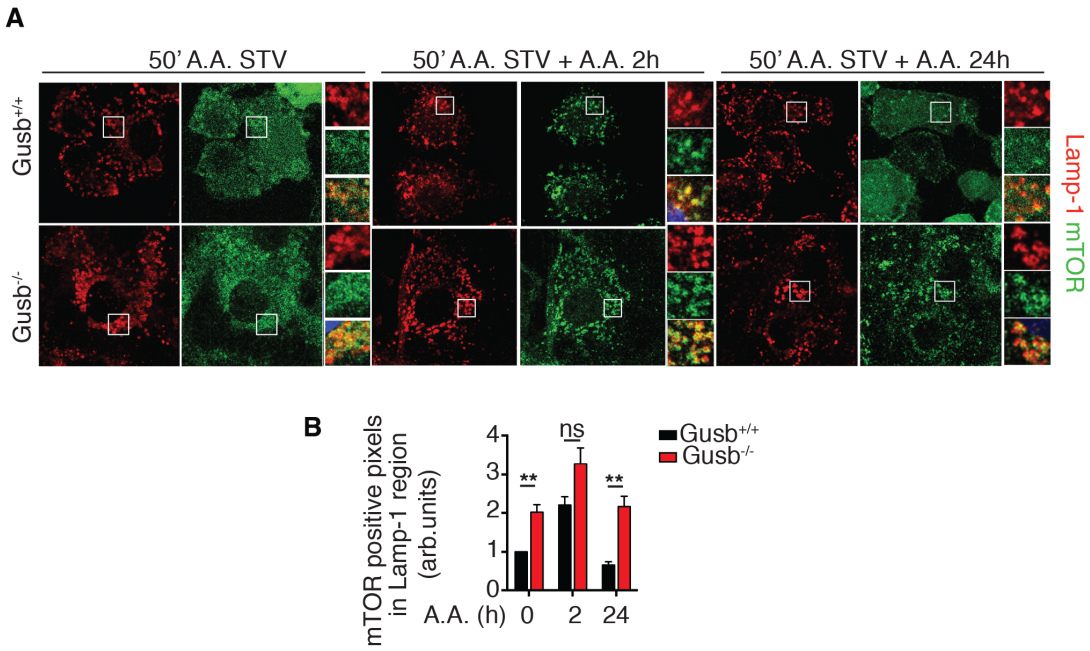

Figure 20. Enhanced mTORC1 association to lysosome in Gusb$^{-/-}$ primary chondrocytes.
A, Primary chondrocytes were starved for amino acids for 50 min and then amino acids were added for the indicated time points. Cells were then processed in an immunofluorescence assay to detect mTOR (green)-Lamp-1 (red) colocalization. Cell were co-stained with 4′,6′-diamidino-2- phenylindole (DAPI) for DNA content (blue), and imaged. The insets show higher magnification and single color channels of the boxed area. Scale bar, 10 μm. **B**, Bar graph displays co-localization analysis (mTOR positive pixels in Lamp-1 regions) in Gusb$^{-/-}$ expressed as fold increase compared to control (Gusb$^{+/+}$). Data are expressed as mean (±s.e.m) of n=3 independent experiments (Student's *t*-test, ** p≤ 0.005).

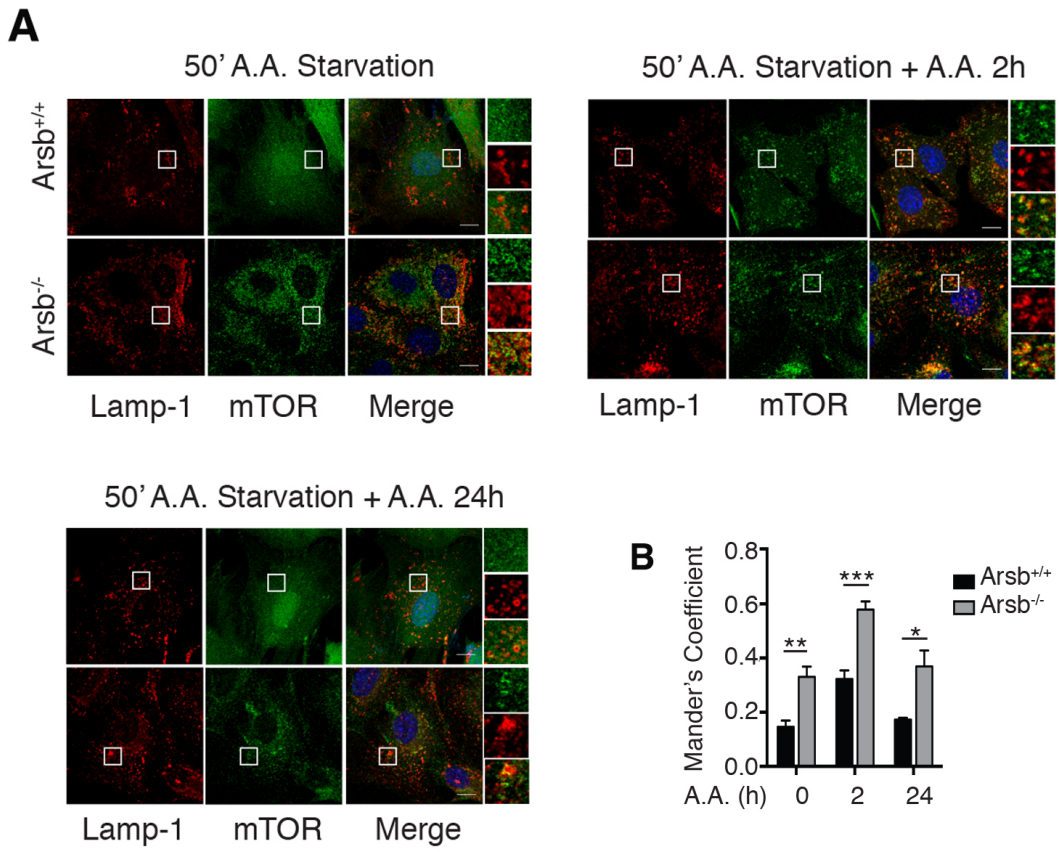

Figure 21. Enhanced mTORC1 association to lysosome in Arsb$^{-/-}$ primary chondrocytes.
A, *Arsb*$^{-/-}$ chondrocytes were starved for amino acids for 50 min or starved and then re-stimulated with amino acids for the indicated times. Cells were then processed in an immunofluorescence assay to detect mTOR, Lamp-1, co-stained with DAPI for DNA content, and imaged. The insets show higher magnification and single color channels of the boxed area. Scale bar, 10µm. **B**, Bar graphs display quantitative analysis of co-localization, data are expressed as mean (±s.e.m) of n=3 independent experiments (Student's *t*-test, * $p<0.05$, ** $p<0.005$, *** $p<0.0005$).

This suggests that an altered insulin/growth factor signaling pathway was not the main cause of mTORC1 hyperactivity in MPS cells and that in particular the signaling arising from amino acids (lysosomal and/or proteasomal) was the major cause of the observed phenotype.

Literature data so far suggests that an impaired lysosomal function would impair the mTORC1 signaling, probably because it hampers the capability to pump amino acids to the complex. We hypothesized that this phenomenon might be true if restricted to the acute inhibition (hours) of lysosomal function achieved by drugs, since our data were

suggesting that the chronic inhibition of lysosomal function enhances rather than inhibits mTORC1 signaling in MPS chondrocytes.

Surprisingly, mTORC1 signaling was not enhanced in fibroblasts isolated from MPSVII mice (**Figure 22**) and in MPSVI HeLa cell line (*ArsbKO*)(**Figure 23**), generated by Crisp/Cas9 mediated genome editing, compared to their respective control cells.

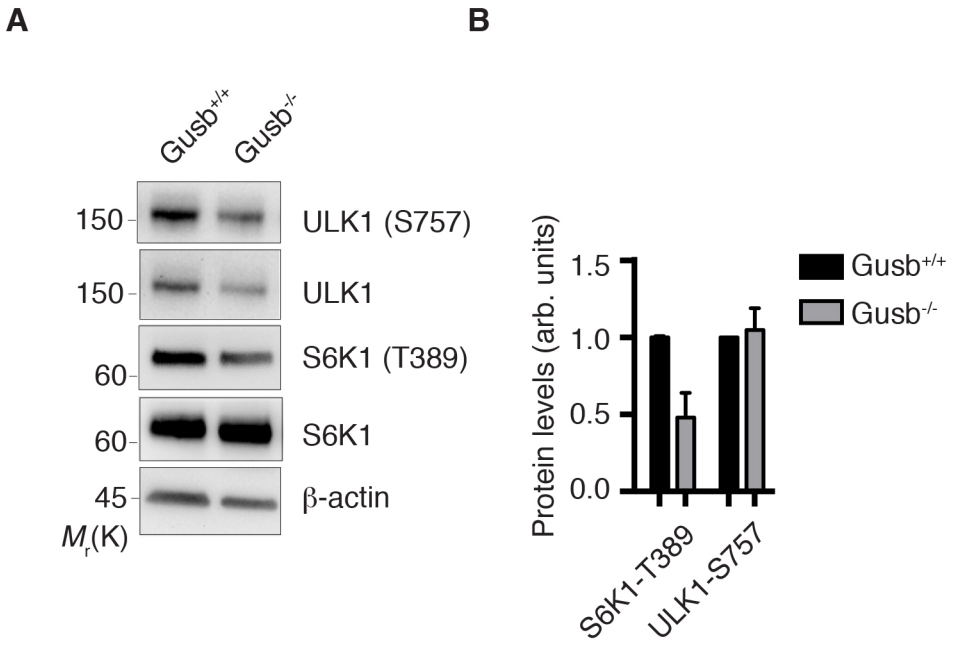

Figure 22. mTORC1 signaling in MPS fibroblast.
A, Phosphorylation levels of mTORC1 substrates (ULK1 and S6K1) in primary fibroblasts isolated from *Gusb*$^{+/+}$ and *Gusb*$^{-/-}$ mice upon 2h A.A. stimulation. **B**, Bar graphs display phosphorylation levels of the indicated protein (normalized to their total levels). The data are representative of 2 independent experiments.

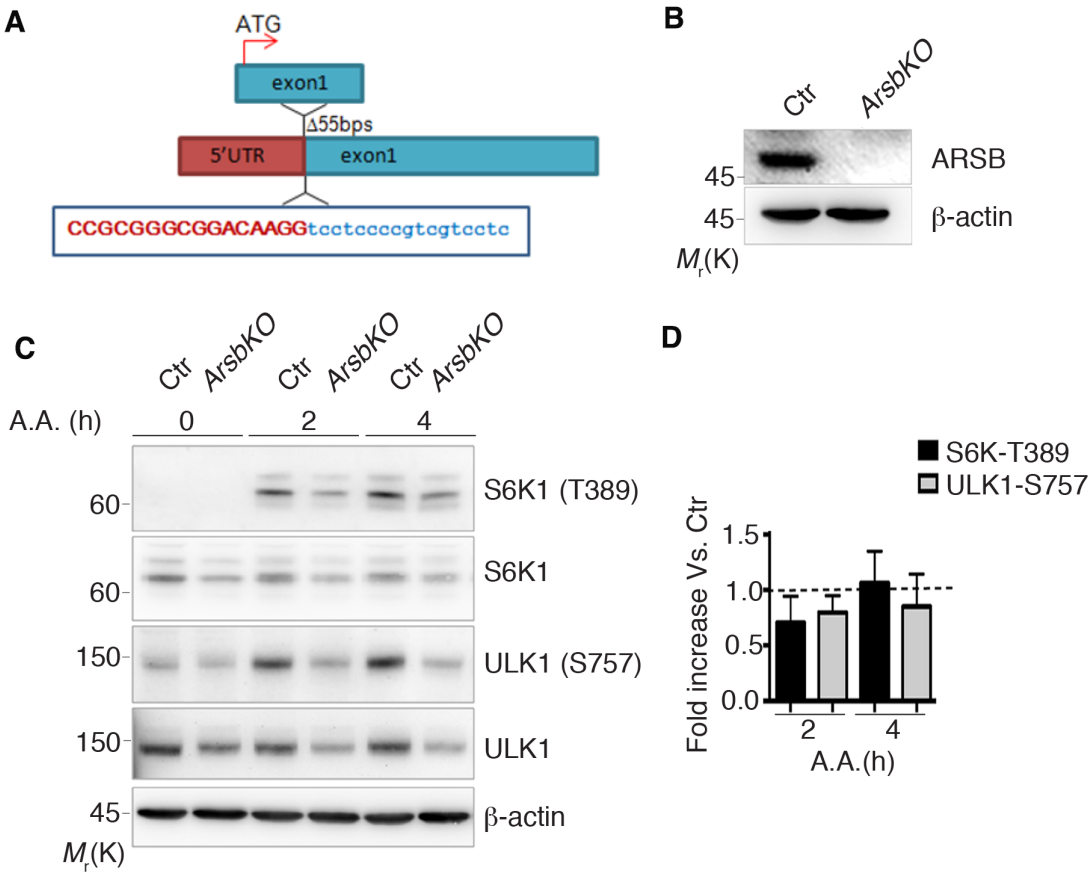

Figure 23. mTORC1 signaling in ArsbKO HeLa cell line.
A, schematic representation of genetic mutation found in the *ArsbKO* Hela clone: a deletion of 55 base pairs within the first exon causes a frameshift and a premature stop codon. **B**, Western blot displaying absence of the Arsb protein. β-Actin was used as a loading control. **C**, Phosphorylation levels of mTORC1 substrates (ULK and S6K1) in *ArsbKO* and Ctr stimulated with amino acid (A.A) for the indicated time points. **D**, Bar graphs show phosphorylation levels of the indicated protein (normalized to their total levels) in *ArsbKO* and expressed as fold increase compared to controls. Values are expressed as mean (±s.e.m.) of n = 3 independent experiments

1.3 Proteasomal regulation of mTORC1

We hypothesized that lysosomal storage triggers a chondrocyte-specific response that enhances mTORC1 signaling. A cross talk between lysosomes and proteasomes, the two main degradative station of the cell, exists. Furthermore, the amino acids derived from proteasome-mediated proteolysis can induce mTORC1 signaling. To assess the contribution of proteasome to the increased mTORC1 signaling a series of experiments were performed. By using a luminescent Suc-LLVY peptide, susceptible to the

chymotrypsin-like activity of the proteasome, we measured the luminescent signal resulting from its cleavage in control and *GusbKO* RCS cells. We observed a significantly higher proteasome activity in *GusbKO* compared to control chondrocytes (**Figure 24A**).

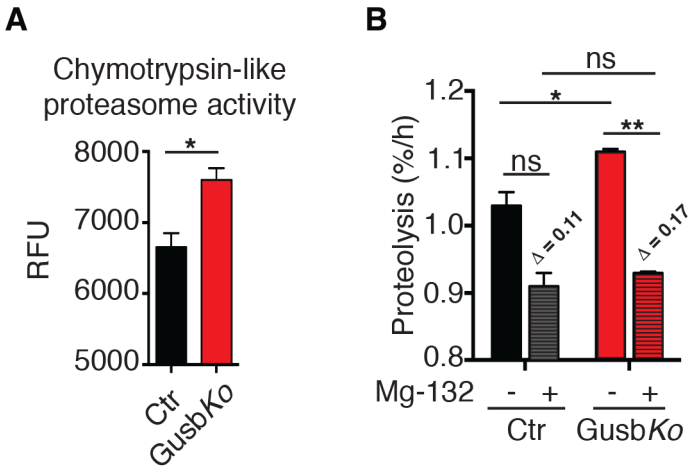

Figure 24. Enhanced proteasome activity in MPS cells.
A, Luminescent signal resulting from the cleavage of a luminescent Suc-LLVY peptide by the chymotrypsin-like activity of the proteasome was measured in control and *GusbKO* RCS cells. Data are representative of 3 independent experiments and are graphed as relative fluorescence units (RFU) (Student's *t*-test, * $p \leq 0.05$). **B**, Control and *GusbKO* RCS cells were pulse labeled for 18h with ^{3}H-Ser and chased for 48h in medium containing vehicle or 100nM Mg-132. The rate of protein degradation was measured as the difference of initially incorporated radioactivity relative to that remaining at the end of the chase period. Values are expressed as mean (±s.e.m.) of $n = 3$ independent experiments (Student's *t*-test, * $p \leq 0.05$, ** $p \leq 0.005$).

Then, we decided to measure the overall rate of protein degradation. Control and *GusbKO* RCS cells were pulse labeled for 18h with ^{3}H-Ser, in order to labeled long-lived proteins, and chased for 48h in cold medium. The rate of protein degradation was measured as the difference of initially incorporated radioactivity relative to that remaining at the end of the chase period. In spite of a lysosomal damage, proteolysis rate was found significantly increased in *GusbKO* compared to controls (**Figure 24B**). To determine to what extent proteasome contributes to this increased proteolysis, the chased period was performed in the presence of the proteasome inhibitor MG-132. As

shown in Figure 24B, the fraction of amino acids generated by the proteasome (MG132-sensitive) was increased in *GusbKO* chondrocytes compared to controls. We reasoned that the higher proteasomal proteolysis, by generating an excess of amino acids, was the driving force for the increased mTORC1 signaling found in our cellular models. In this scenario, a similar MG132-sensitive mTORC1 signaling would be expected. We observed that treatment with MG132 (**Figure 25A-B**), but not with lysosomal inhibitors (E64-d) (**Figure 25C-D**), normalized mTORC1 signaling in *GusbKO* chondrocytes.

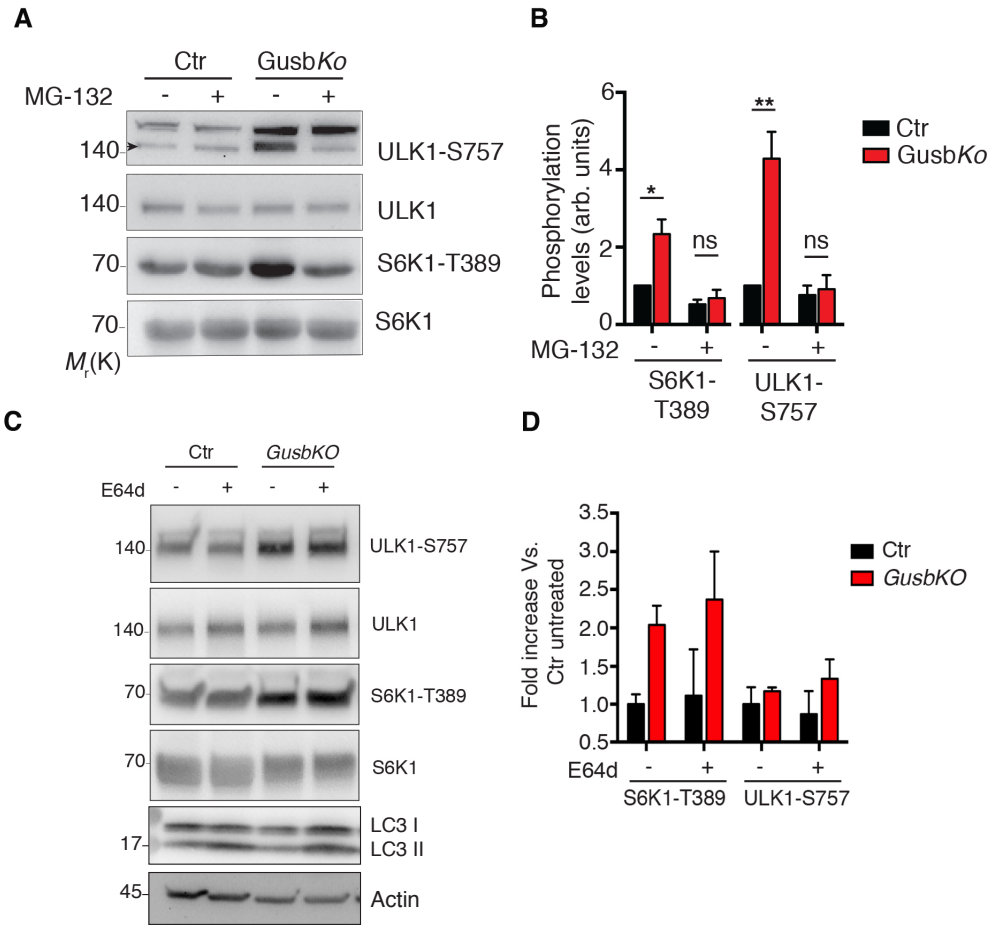

Figure 25. mTORC1 signaling is proteasome-sensitive in MPS cells.
A, Western blot analysis of mTORC1 signaling in control (Ctr) and *GusbKO* RCS cells treated with Mg-132 (10μM) or DMSO (-) in the presence of A.A. for 6h. Arrowhead indicate specific band. **B**, Bar graphs show phosphorylation levels of the indicated protein (normalized to their total levels) in *GusbKO* chondrocytes expressed as fold increase compared to control cells. Values are expressed as mean (±s.e.m.) of $n = 3$ independent experiments (Student's t-test, * $p \leq 0.05$, ** $p \leq 0.005$). **C**, Western blot analysis of mTORC1 signaling in control (Ctr) and *GusbKO* RCS cells pre-treated for 16h with E64-d (20μg/ml) or vehicle (-) and then stimulated with A.A. for 6h. **D**, Bar graphs show phosphorylation levels of the indicated protein (normalized to their total levels) in *GusbKO* chondrocytes expressed as fold increase compared to control cells. Values are expressed as mean (±s.e.m.) of $n = 2$ independent experiments.

These data confirm that an enhanced mTORC1 signaling in MPS chondrocytes is mediated by an increased proteasomal proteolysis. Notably, proteasome activity was not enhanced in MPSVII fibroblasts and in *ArsbKO* cell compared to their respective control cells (**Figure 26**) and consistently in these cells mTORC1 signaling was not induced compared to controls (**See Figures 22 and 23**).

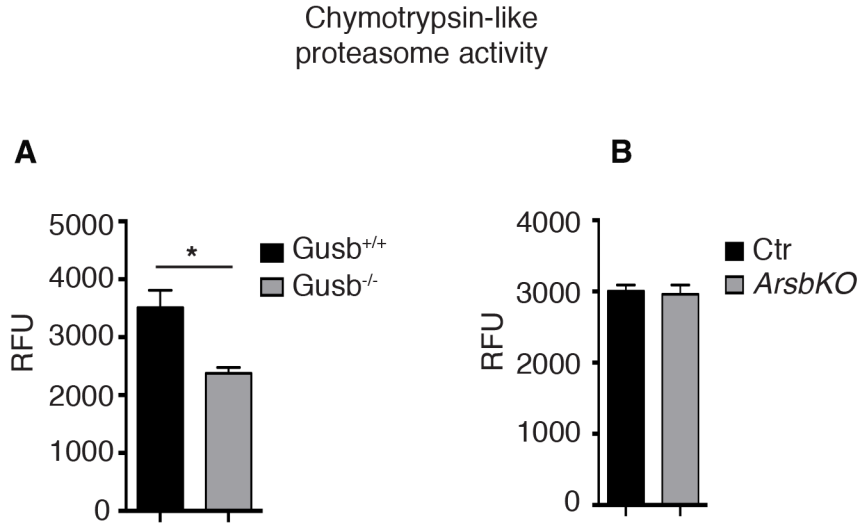

Figure 26. Proteasome activity in non-chondrocyte MPS cells.
A-B, Luminescent signal resulting from the cleavage of a luminescent Suc-LLVY peptide by the chymotrypsin-like activity of the proteasome was measured in control and *GusbKO* RCS cells (**A**), or control and *ArsbKO* Hela cells (**B**). Data are representative of 3 independent experiments and are graphed as relative fluorescence units (RFU) (Student's *t*-test, * $p \leq 0.05$).

This phenotype seems to be the consequence of an enhanced proteasome activity that, by increasing cellular amino acid levels, sustains mTORC1 signaling. The mechanism by which lysosome inhibition led to the increased proteasome activity is currently unclear and it is beyond the aim of this thesis. Recent data indicated that proteasome turnover is mediated by lysosomes[66]. One possibility could be that lysosome dysfunction by impairing proteasome turnover raises its intracellular level and in turn enhances its total activity [67]. In any case, these observations suggest the existence of

additional, still uncharacterized, pathways through which the lysosome may indirectly regulate mTORC1 signaling.

1.4 *mTORC1 inhibits autophagosome-lysosome fusion in MPS chondrocytes via UVRAG.*

To verify whether the enhanced mTORC1 signaling contributed to the inhibition of autophagy in MPS chondrocytes, we genetically reduced the amount of mTOR by generating a mouse line lacking one allele of the mTORC1 scaffold subunit Raptor[68]. Heterozygous *Raptor* (*Rpt*) mice[69] were then backcrossed with heterozygous *Gusb* mice in order to obtain double *Gusb*$^{-/-}$;*Rpt*$^{+/-}$ mice. As expected, primary chondrocytes isolated from these mice showed almost 50% reduction in the amount of Raptor protein (**Figure 27**).

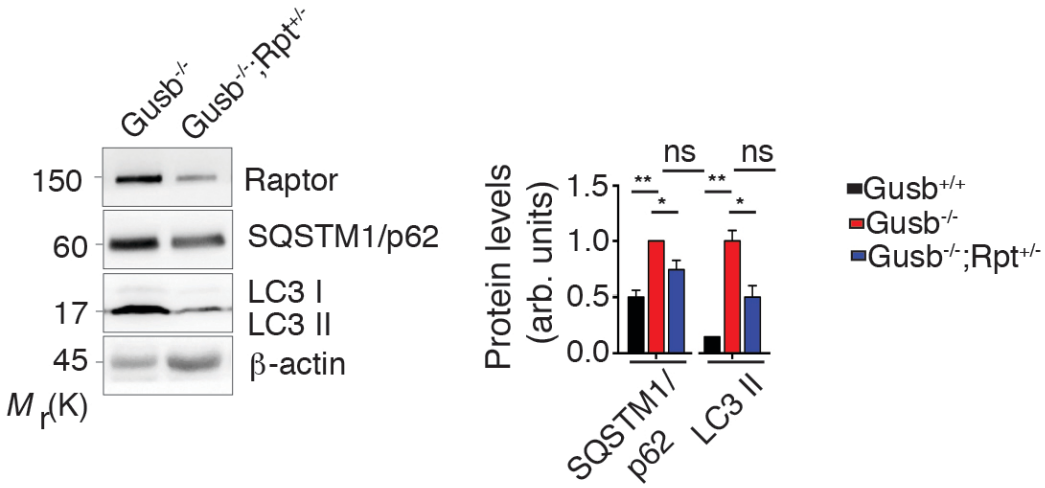

Figure 27. Normalization of mTORC1 signaling restores autophagy flux in MPS chondrocytes.
A, Western blot analysis of LC3I/II, SQSTM1/p62 and Raptor in chondrocytes isolated from mice with the indicated genotypes. β-Actin was used as a loading control. Blot is representative of 3 independent experiments. **B**, Bar graph shows quantification of protein amount normalized to β-actin and relative to Gusb$^{-/-}$ (ANOVA, P=0.0064 ; Tukey's post-hoc test, ** p≤0.005, * p≤0.05).

Strikingly, *Gusb*$^{-/-}$;*Rpt*$^{+/-}$ primary chondrocytes showed reduced accumulation of LC3II and of SQSTM1/p62 compared to *Gusb*$^{-/-}$ chondrocytes (**Figure 27**).

The subsequent reduction in mTORC1 signaling was tested by subjecting cells to amino acids starvation/stimulation time course. Figure 28 shows normalization of mTORC1 signaling in Gusb$^{-/-}$;Rpt$^{+/-}$ cells.

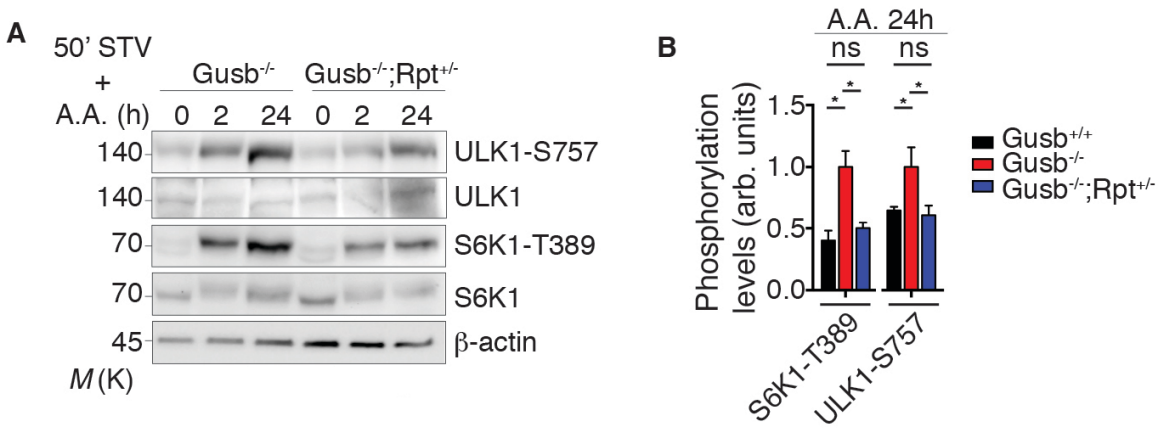

Figure 28. ***Normalization of mTORC1 signaling in MPS chondrocytes.***
A, Western blot analysis of mTORC1 signaling in primary cultured chondrocytes isolated from *Gusb*$^{-/-}$ and *Gusb*$^{-/-}$;*Rpt*$^{+/-}$ mice upon a time course of amino acid stimulation. **B**, Bar graphs show phosphorylation levels of indicated proteins (normalized to their total levels) after 24h of amino acids (A.A.) stimulation. Values were expressed as fold increase compared to *Gusb*$^{-/-}$ (ANOVA, P=0.009; Tukey's post-hoc test, *p<0.05).

The rescue found in autophagy substrates was most likely the consequence of a restoration of the autophagy flux, as demonstrated by enhanced AV-Lys co-localization and increased SQSTM1/p62 delivery to lysosomes in *Gusb*$^{-/-}$;*Rpt*$^{+/-}$ compared to *Gusb*$^{-/-}$ chondrocytes (**Figure 29**).

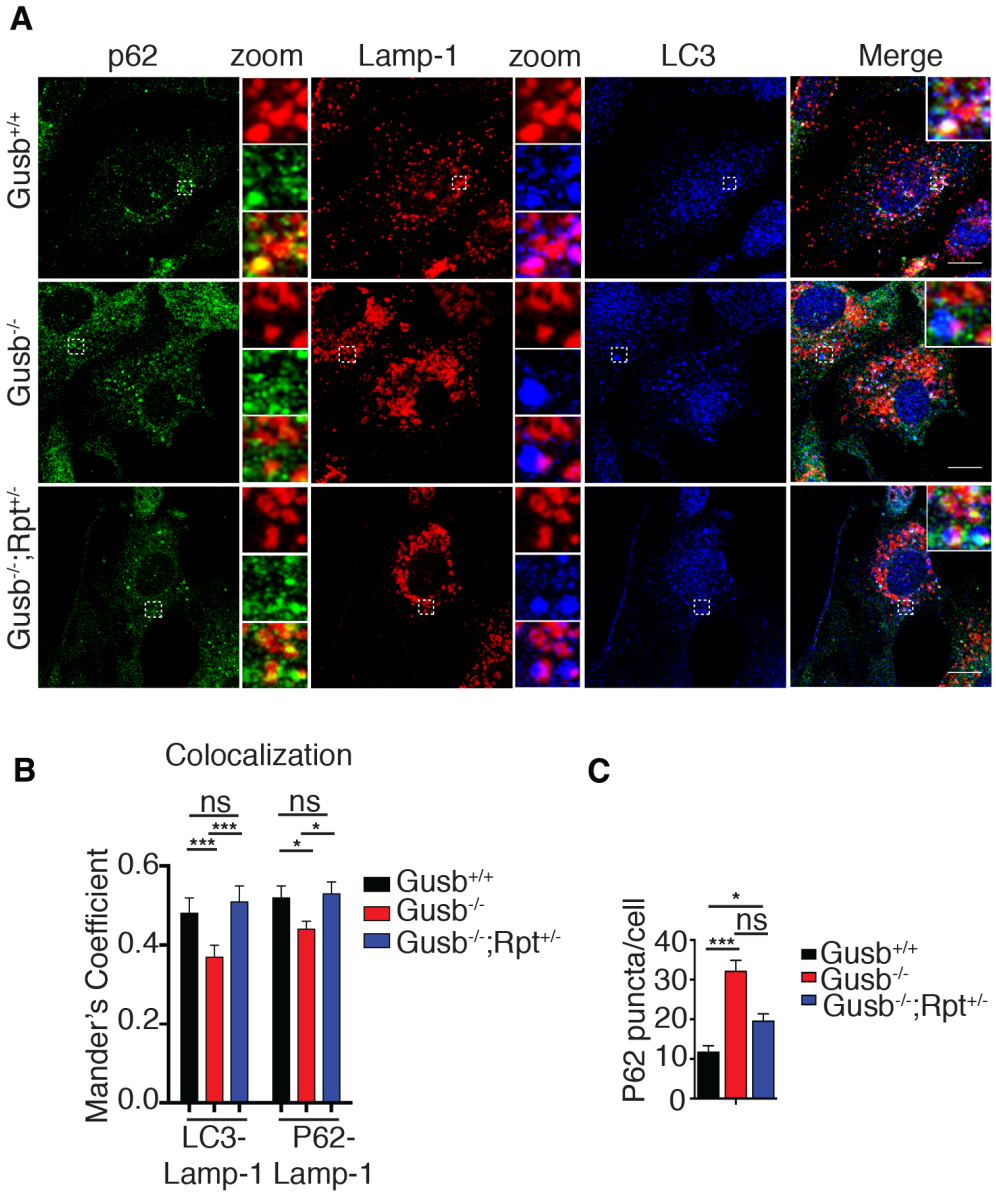

Figure 29. Normalization of mTORC1 signaling restores autophagosome-lysosome fusion in MPS chondrocytes.

A, Immunofluorescence of Lamp-1, p62 and LC3 in primary chondrocytes isolated from mice with the indicated genotypes. The insets show higher magnification, single color channels, Lamp-1-p62 and Lamp-1-LC3 co-localization of the boxed area. Scale bar, 10 μm. **B**, quantification of Lamp-1 co-localization with LC3 and p62. Data are Mander's coefficient means (±s.e.m.)(ImageJ plug-in). ANOVA Lamp-1-LC3 P=7.39E-06, Lamp1-p62 P=0.008; Tukey's post-hoc test, *p≤0.05; *** p≤0.0005. **C**, quantification of p62 puncta of cells shown in A (ANOVA P=4.67E-05; Tukey's post-hoc test *** p≤0.005, *p≤0.05).

Restoration of proper AV-Lys was also demonstrated by transiently transfecting the tandem GFP-RFP-LC3 in primary chondrocytes from *Gusb*$^{-/-}$, *Gusb*$^{-/-}$;*Rpt*$^{+/-}$ and controls (**Figure 30**).

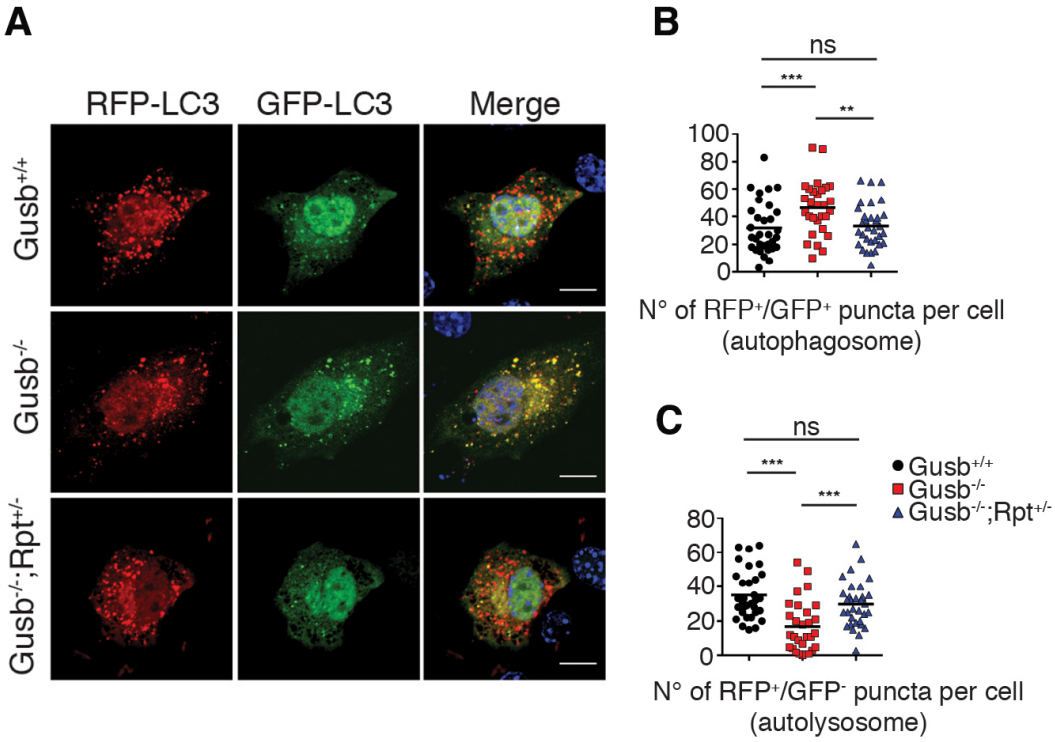

Figure 30. Autolysosome formation assay.
A, Tandem RFP-GFP-LC3 protein was transiently expressed in primary chondrocytes with the indicated genotypes. LC3 was monitored by fluorescence microscope two days post-transfection and after 24h amino acid treatment. Scale bar, 10µm. **B-C**, Quantitative analysis of GFP^{+}/RFP^{+} puncta (autophagosome, yellow) (**B**) and GFP^{-}/RFP^{+} puncta (autolysosome, red) (**C**). Mean value of 3 independent experiments is shown as a horizontal bar (ANOVA, GFP puncta P=0.002, RFP puncta P=1.63E-06; Tukey's post-hoc test, **p≤0.0005, ***p≤0.0005).

As expected, the lysosome phenotype was not rescued in *Gusb*$^{-/-}$*;Rpt*$^{+/-}$ compared to *Gusb*$^{-/-}$ chondrocytes (**Figure 31**).

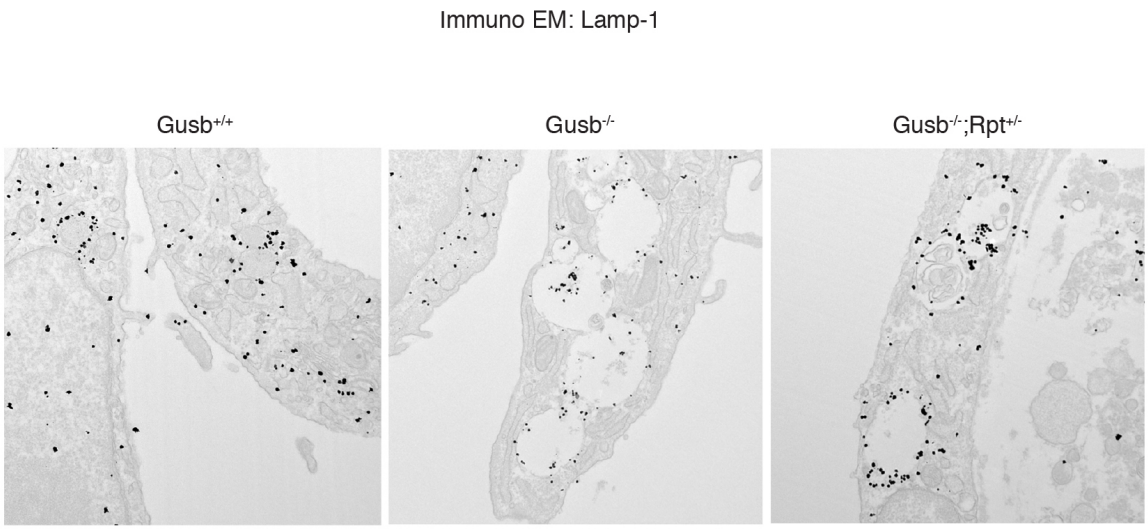

Figure 31. Lysosomal phenotype in MPS cells.
Lamp-1 Immuno-EM from primary chondrocytes isolated from mice with the indicated genotype. Scale bar, 500nm.

Notably, restoring mTORC1 signaling to normal levels did not alter AV biogenesis as measured by time course analysis of LC3-I to -II lipidation in the presence of the lysosomal inhibitor Bafilomycin A_1 (**Figure 32A-B**), suggesting that an enhanced mTORC1 signaling directly impact the rate of AV-Lys fusion. Moreover, the nuclear translocation of the pro-autophagy transcription factors TFEB and TFE3 was similar between *Gusb*$^{-/-}$*;Rpt*$^{+/-}$ and *Gusb*$^{-/-}$ chondrocytes (**Figure 32C-D**), suggesting that the normalization of mTORC1 signaling did not restore autophagy flux in MPS chondrocytes via TFEB/TFE3 nuclear translocation.

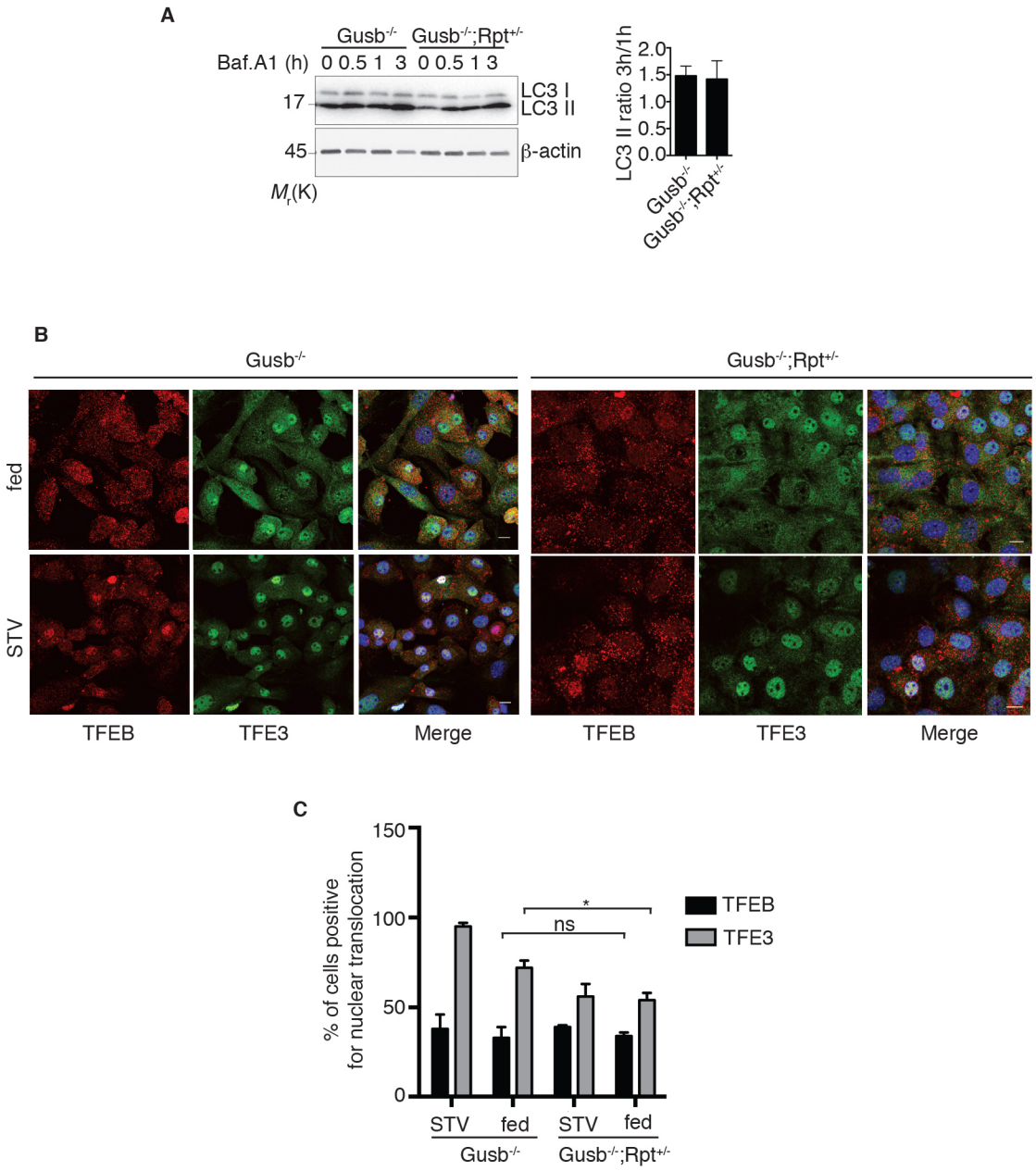

Figure 32. Normal autophagosome biogenesis in Gusb$^{-/-}$;Rpt$^{+/-}$ primary chondrocytes.
A, Western blot analysis of LC3II accumulation in the presence of the lysosomal inhibitor Bafilomycin A1 (200nm) for the indicated time points. Bar graphs display the rate of autophagosome formation calculated using the ratio of accumulated LC3 II between 3h and 1h of treatment. **B**, Immunofluorescence analysis of TFEB and TFE3 nuclear localization in primary chondrocytes with the indicated genotype after 50 minutes of amino acid starvation (STV) and upon 24h of amino acid stimulation (fed). Cells were co-stained with DAPI to define nuclear region. **C**, bar graphs display quantification of the percentage of cells positive for nuclear translocation. The data are representative of 3 independent experiments, n > 90 cells were analyzed for each time point. Scale bar, 10 μm (Student's *t*-test, * p≤0.05).

Until two years ago it was described that the major mechanism by which mTORC1 inhibits autophagy is by phosphorylating ULK1. It was shown that mTORC1 also

targets proteins other than ULK1, such as Atg13, Atg14L and AMBRA1. These mTORC1 targets are mainly known to function at early stages of autophagosome formation. Whether mTORC1 regulates autophagy at later stages, such as autophagosome maturation, remained unknown until it was demonstrated that, through phosphorylating UVRAG, mTORC1 was engaged in late stages of autophagy and endosome maturation, defining a broader range of mTORC1 functions in the membrane-associated processes[17]. Since we couldn't detect any obvious effect of mTORC1 on early autophagy stages (**see Figure 12**), we hypothesized a contribution in the late stages, according to the overt fusion defect that has been observed. It is known that once mTORC1 phosphorylates UVRAG its affinity for the inhibitor partner Rubicon is enhanced. Thus, to analyze the status of this protein complex in *GusbKO* cells, we performed co-IP experiments. Figure 33A shows that *GusbKO* cells had higher levels of UVRAG S497 phosphorylation compared to control cells, and this phosphorylation was mTORC1-dependent since it was blunted by Torin-1 treatment.

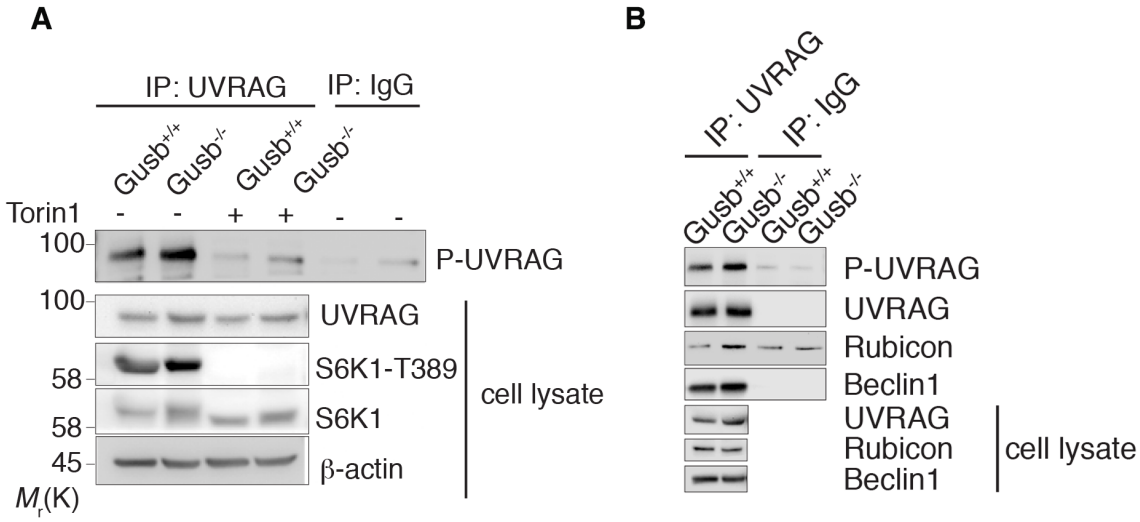

Figure 33. Enhanced UVRAG phosphorylation and Rubicon binding in MPS cells.
A-B, UVRAG immunoprecipitation (IP) assay testing endogenous UVRAG phosphorylation **(A)** and interaction with Rubicon and Beclin1 (**B)** in control and *GusbKO* RCS chondrocytes. The increased UVRAG phosphorylation is blunted after treatment with the mTORC1 inhibitor Torin-1 (1μM; 6h). IgG: negative IP control.

Furthermore, we found an increased interaction between UVRAG and Rubicon in *GusbKO* compared to control cells (**Figure 33B**). However, we observed no differences in the interaction between UVRAG and Vps16 (a member of the HOPS complex) (**Figure 34**) between *GusbKO* and control chondrocytes, suggesting that the activity of the UVRAG/HOPS complex was not altered in LSD chondrocytes.

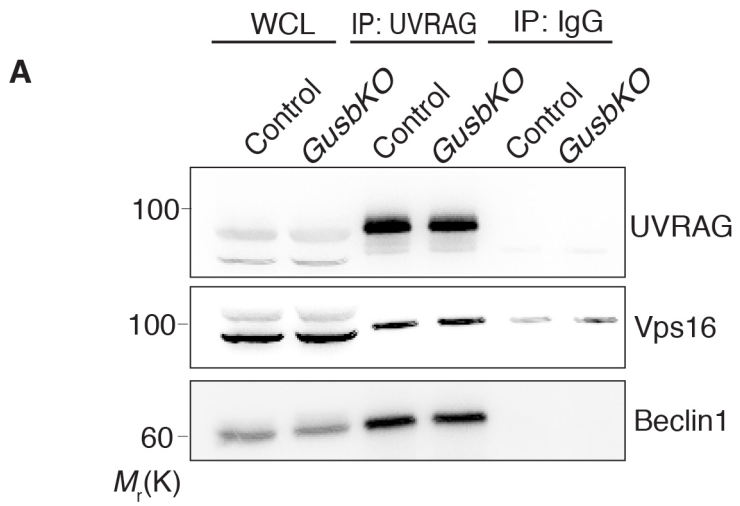

Figure 34. UVRAG/HOPS complex in MPS chondrocytes.
UVRAG immunoprecipitation assay testing endogenous UVRAG interaction with Vps16 and Beclin1 in control and *GusbKO* RCS chondrocytes. IgG: negative control.

UVRAG is also part of the Vps34/Beclin1 complex, which produces a pool of PI(3)P on endo-lysosome membrane that promotes AV-Lys fusion[10]. It has been demonstrated that UVRAG phosphorylation suppresses the UVRAG-mediated stimulation of Vps34 kinase activity, downregulating the amount of PI(3)P. As expected following a higher UVRAG phosphorylation, we observed a significant lower level of PI(3)P in *GusbKO* compared to control chondrocytes (**Figure 35**).

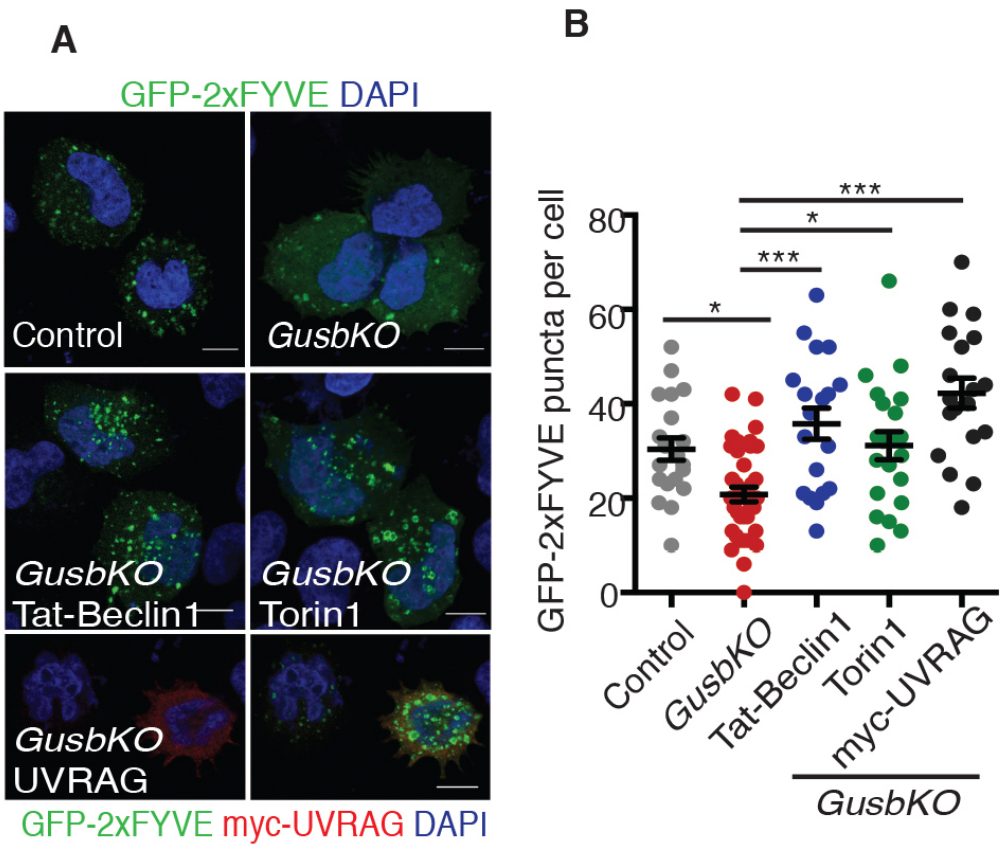

Figure 35. Impaired Vps34 kinase activity in MPS cells.
A, Representative images of membrane-associated PtdIns(3)K assay *in situ*. RCS chondrocytes were transfected with GFP-2xFYVE and treated with or without Tat-Beclin1 (10μM), Torin1 (1μM) or co-transfected with myc-UVRAG, in the presence of A.A. for 6h. **B**, graph shows quantitative analysis of PI3P puncta formation. Mean value is shown as a horizontal bar. The error bars represent means (±s.e.m.) (ANOVA $P<0.0001$; Tukey's post-hoc test, * $p\leq0.05$, *** $p\leq0.0005$; $n > 20$) Scale bar, 10 μm.

The identification of this pathological mechanism allowed us to develop several therapeutic options. We were able to demonstrate that (i) mTORC1 inhibition with Torin-1 treatment (**Figures 35-36**), (ii) forced overexpression of UVRAG (**Figures 35 and 37**) and (iii) enhancing Beclin-1 activity with Tat-Beclin-1 peptide (**Figures 35 and 38**) restored PI(3)P levels and in turn restored autophagy in *GusbKO* and *Gusb*$^{-/-}$ chondrocytes, as demonstrated by enhanced AV-Lys fusion, decreased LC3II and SQSTM1/p62 protein accumulation (**Figures 35-38**).

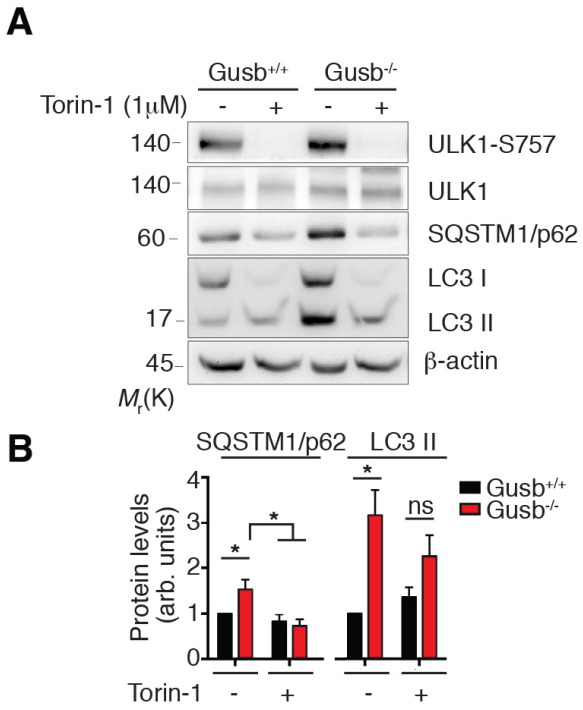

Figure 36. Torin-1 treatment rescues the autophagy flux in MPS cells.
A, Western blot analysis of P-ULK1, SQSTM1/p62 and LC3 in *Gusb*$^{+/+}$ and *Gusb*$^{-/-}$ primary chondrocytes treated for 24h with Torin-1 (1μM) or vehicle alone (DMSO). β-Actin was used as a loading control. The blot is representative of 3 independent experiments. **B**, Bar graph displaying the reduction of SQSTM1/p62 and LC3 II levels after Torin-1 treatment. Data are means (±s.e.m.) of protein levels (normalized to β-actin) and expressed as fold increase relative to untreated *Gusb*$^{+/+}$ (Student's *t*-test * $p<0.05$).

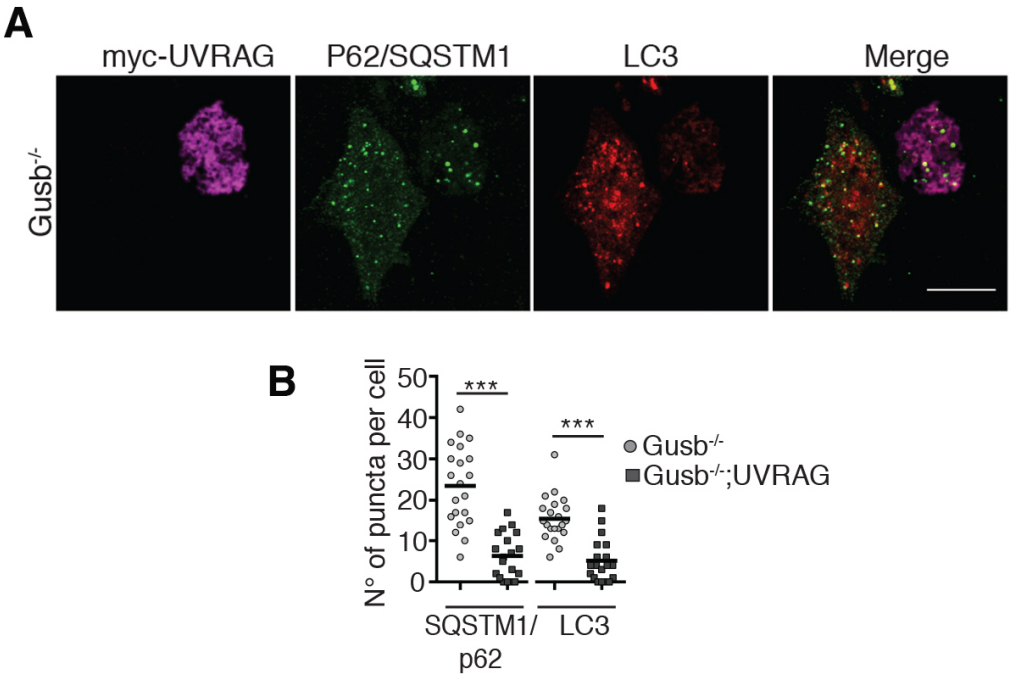

Figure 37. See page 81 for figure legend

Figure 37. UVRAG over-expression rescues autophagy flux in MPS cells.
A, myc-UVRAG was transiently expressed in Gusb$^{-/-}$ primary chondrocytes. Myc expression, LC3 and SQSTM1/p62 were monitored by fluorescence microscope two days post-transfection. Scale bar, 10µm . **B**, Bar graph displaying quantitative analysis of SQSTM1/p62 and LC3 puncta per cell. Mean value is shown as a horizontal bar. (Student's *t*-test, *** p≤ 0.0005, n ≥ 20).

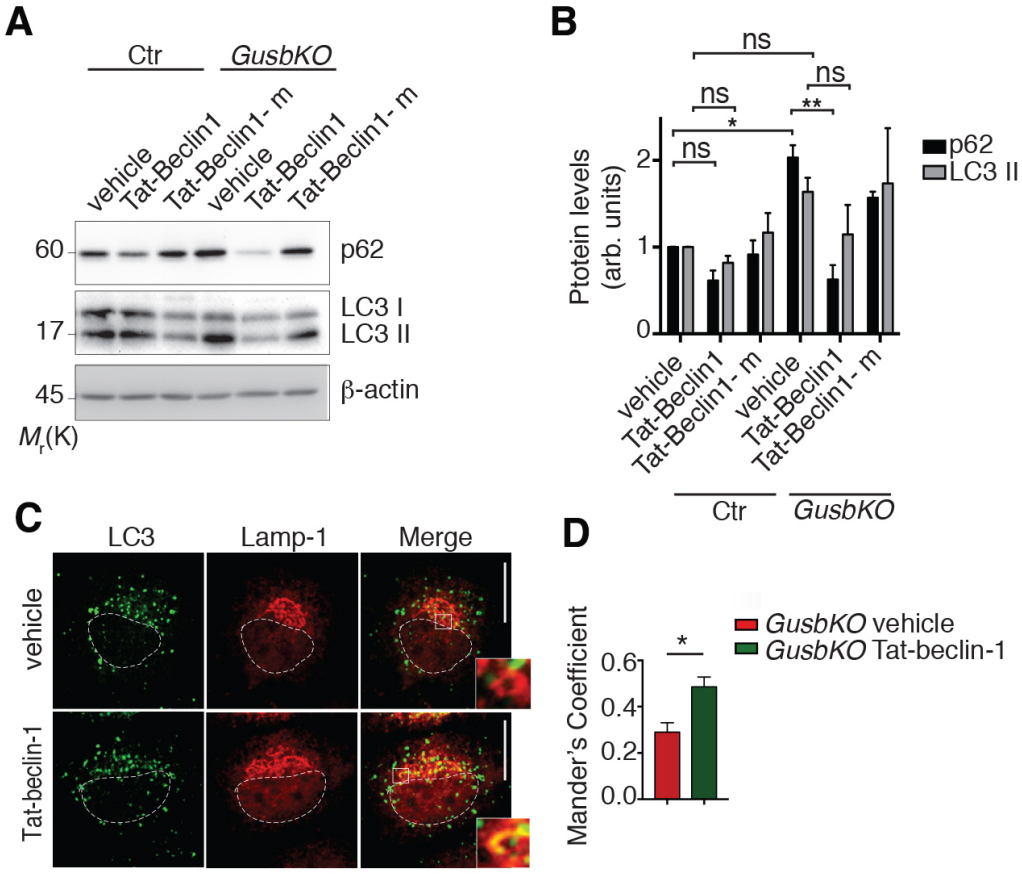

Figure 38. Tat-Beclin-1 treatment rescues autophagy flux in MPS cells
A, Western blot analysis of LC3I/II and SQSTM1/p62 in control and *GusbKO* RCS cells treated with Tat-Beclin-1 (10µM; 2h) and an inactive form of Tat-Beclin-1 (Tat-Beclin-1-m). β-Actin was used as a loading control. The blot is representative of 3 independent experiments. **B**, Bar graphs display quantification of protein amount normalized to β-actin and relative to control (vehicle treated) cells (ANOVA, P62 P<0.0001, Tukey's post-hoc test, ***p<0.0005, **p<0.005, *p<0.05). **C**, Immunofluorescence of Lamp-1 and LC3 in *GusbKO* cells treated with Tat-Beclin-1 peptide (10µM; 2h). The insets show a higher magnification of co-localization in selected areas. Scale bar, 10µm **D**, Quantification of Lamp-1-LC3 co-localization is shown as mean (±s.e.m.) of Mander's Coefficients resulting from three independent experiments (Student's *t*-test, *p<0.05).

Notably, the pharmacological inhibition of Vps34 with SAR405[70] in chondrocytes induced a LSD-like phenotype (accumulation of SQSTM1/p62 and of LC3II) (**Figure 39**). All together these data suggest that mTORC1 inhibits AV-Lys fusion in MPS chondrocytes at least in part through the inhibition of UVRAG-Vps34-Beclin1 complex activity.

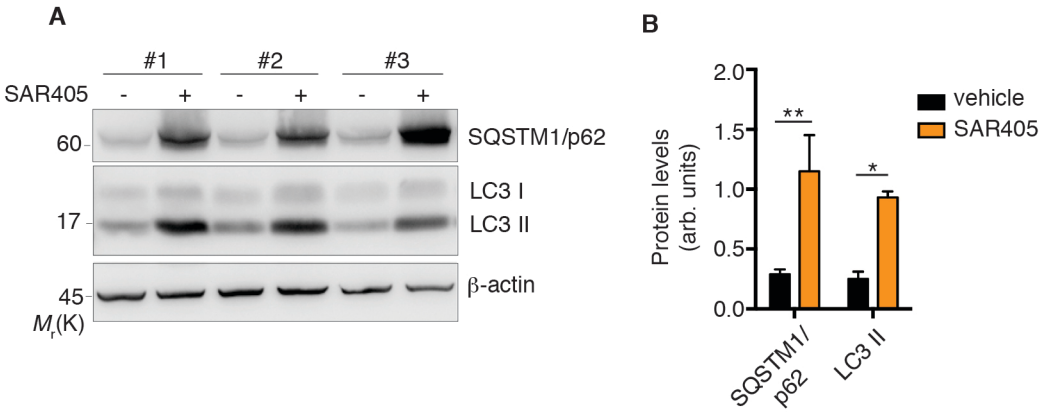

Figure 39. SAR405 treatment in chondrocytes induced a LSD-like phenotype.
A, western blot analysis of SQSTM1/p62 and LC3 in RCS cells treated with PIK3C3/Vps34 inhibitor (SAR405, 10μM, 24h). Blot shows three independent replicates. β-Actin was used as a loading control. **B**, bar graphs displaying proteins levels normalized to β-Actin. Values are expressed as mean (±s.e.m.) (Student's *t*-test, * $p<0.05$; ** $p<0.005$)

2. Genetic and pharmacological approaches to rescue mTORC1 signaling in the skeleton of LSD mouse models.

2.1 Genetic modulation of mTORC1 signaling.

As reported in the introduction, linear growth is largely a function of endochondral bone elongation, a process that occurs mainly in the cartilaginous growth plate. The growth plate is divided into several distinct regions, each populated with chondrocytes displaying characteristic behaviors. For instance, the hypertrophic chondrocyte, simply through its size, is the principal engine of bone growth. Thus the morphological analysis of the growth plate gives key information about the healthiness of long bones.

To analyze the long bone growth in LSD mice we performed both immunohystochemical analysis on growth plates and morphometric analysis of femur and tibia length. We performed immunohistochemistry of paraffin sections from *Gusb*$^{+/+}$ and *Gusb*$^{-/-}$ mice at post-natal day 15. As shown in Figure 40A (panels i-ii) the normal architecture of the growth plate was affected in *Gusb*$^{-/-}$ compared to control.

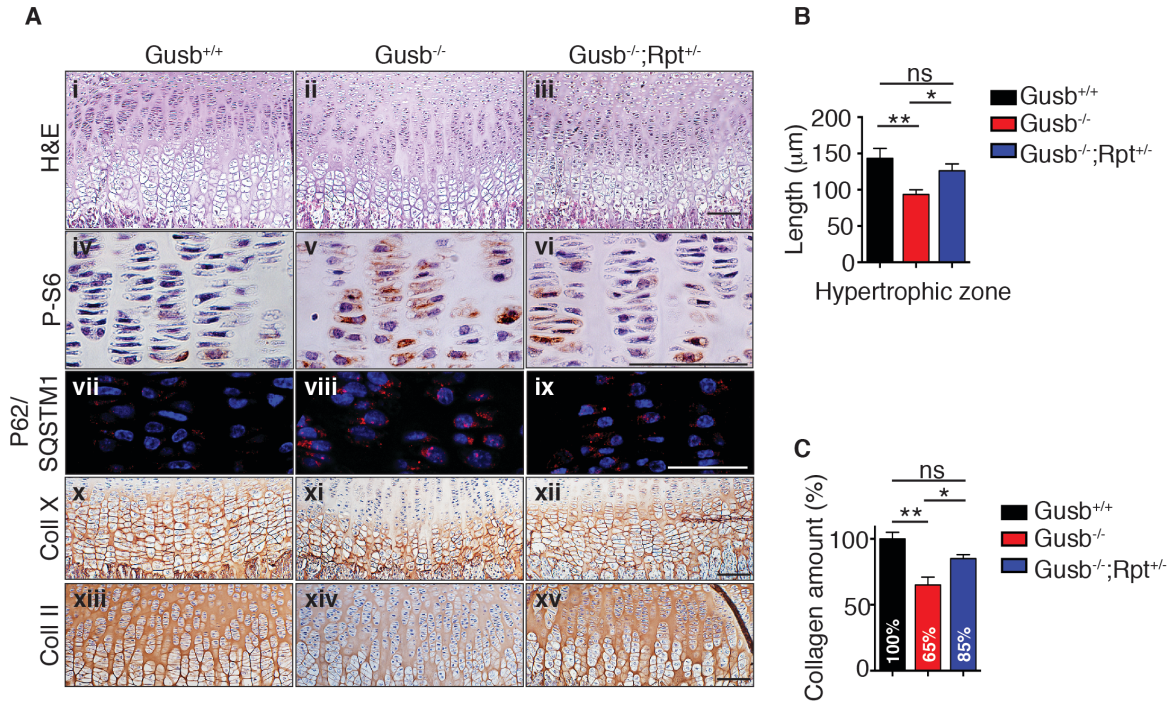

Figure 40. Limitation of mTORC1 improved bone phenotype in MPSVII mice.
A, Representative images of P15 femoral growth plates sections from *Gusb*$^{+/+}$, *Gusb*$^{-/-}$ and *Gusb*$^{-/-}$*; Raptor*$^{+/-}$ mice. Panels i-iii, staining with hematoxylin & eosin (H&E) shows the regions chosen for the analysis. Panels iv-xv, immunostaining with P-S6 (iv-vi), p62 (vii-ix), Coll X (x-xii) and Coll II (xiii-xv). Nuclei were counterstained with hematoxylin or DAPI (p62). n=5 mice per genotype. Scale bar (100 µm). **B-C**, Bar graphs displaying the length of hypertrophic zone measured according to Coll X staining (**B**; ANOVA, P=0.003; Tukey's post-hoc test, * $p \leq 0.05$, ** $p \leq 0.005$) and the amount of collagen (% of Gusb$^{+/+}$) in the growth plate homogenates (**C**; ANOVA, P=0.003; Tukey's post-hoc test, * $p \leq 0.05$, ** $p \leq 0.005$).

Ematoxilin and Eosin staining allows easy distinction between resting, proliferating and hypertrophic chondrocytes. Moreover *Gusb*$^{-/-}$ growth plates displayed accumulation of SQSTM1/p62 (**Figure 40A; panels vii-viii**) and significantly lower collagen type II and type X levels compared to the ones from littermate control mice (**Figure 40A; panels x-xii;xiii-xiv and Figure 40C**), suggesting that the mTORC1 signaling and autophagy were altered in the cartilage of *Gusb*$^{-/-}$ mice and this in turn results in improper collagen secretion, confirming the pathogenic mechanism obtained by analyzing primary chondrocytes *in vitro*.

Alteration of autophagy and reduction in collagen levels matched with an altered growth, thus *Gusb*$^{-/-}$ mice displayed shorter bones both at post-natal day 15 (P15) and

P30, as measured by morphometric analysis on alcian blue/alizarin red colored bones (**Figure 41A-D**).

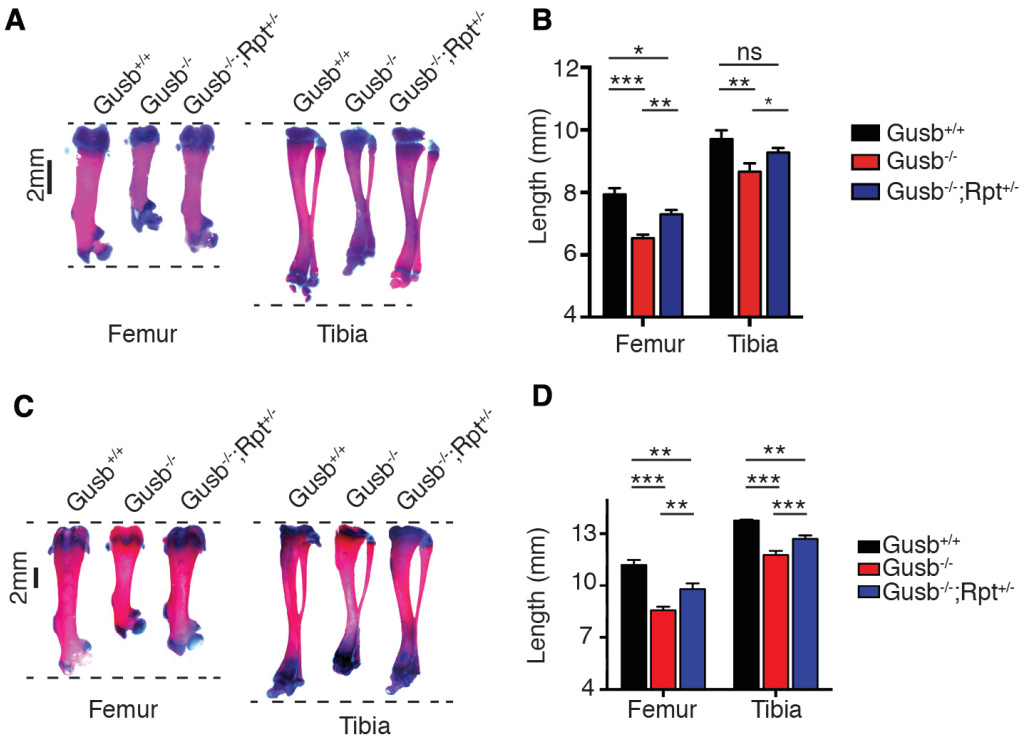

Figure 41. Limitation of mTORC1 improved bone growth in MPSVII mice
A, Representative images of alcian blue/alizared red staining of femurs and tibia from P15 *Gusb*$^{+/+}$, *Gusb*$^{-/-}$ and *Gusb*$^{-/-}$*; Raptor*$^{+/-}$ mice (n ≥ 6 mice per genotype). **B**, Bar graphs displaying femur and tibia lengths from mice with the indicated genotype, data are expressed as mean (±s.e.m) of n ≥ 6 mice per genotype (ANOVA, femur P=1.26E-05, tibia P=0.005; *p<0.05, **p<0.005, ***p<0.0005). **C,** Representative images of alcian blue/alizared red staining of femurs and tibias from P30 *Gusb*$^{+/+}$, *Gusb*$^{-/-}$ and *Gusb*$^{-/-}$*; Raptor*$^{+/-}$ mice (n ≥ 6 mice per genotype). **D,** Bar graphs displaying femur and tibia lengths from mice with the indicated genotype, data are expressed as mean (±s.e.m) of n ≥ 6 mice per genotype (ANOVA, femur P=8.44E-07, tibia P=1.79E-07; **p<0.005, ***p<0.0005).

Next we asked whether mTORC1 dysfunction played any role in the observed bone growth retardation. Limitation of mTORC1 signaling *in vivo* (*Gusb*$^{-/-}$*;Rpt*$^{+/-}$) reduced S6 phosphorylation (**Figure 40A, panels iv-vi**), restored autophagy flux, as measured by reduced SQSTM1/p62 levels (**Figure 40A, panels vii-ix**) and thus significantly improved collagen levels in the growth plates of *Gusb*$^{-/-}$*;Rpt*$^{+/-}$ compared to *Gusb*$^{-/-}$ mice (**Figure 40A-B; panels x-xv**). The improvement in collagen amount and ECM proper composition was further analyzed biochemically by analyzing the amount of collagen in

growth plate homogenates (**Figure 40C**), supporting the non-quantitative immunohystochemical technique.

Most importantly, femurs and tibia isolated from *Gusb*$^{-/-}$;*Rpt*$^{+/-}$ showed an almost complete rescued bone growth retardation when measured at both P15 and P30 (**Figure 41A-D**). These data clearly demonstrate that mTORC1 dysfunction plays an important role in the pathogenesis of the skeletal phenotype in MPSVII mice.

2.2 Pharmacological modulation of autophagy.

Next we tested whether enhancing autophagy would also have beneficial effects for the MPS bone phenotype. The activity of Beclin 1, a key pro-autophagy protein, can be pharmacologically enhanced using the TAT-Beclin1 peptide. When administered *in vivo*, Tat-Beclin1 is able to activate autophagy in growth plate chondrocytes without showing any side effects. *In vivo,* daily injection of Tat-Beclin1 peptide enhanced AV-Lys fusion and SQSTM1/p62 degradation in the growth plate of control (*Gusb*$^{+/+}$;GFP-LC3$^{tg/+}$) mice expressing the fluorescent autophagy reporter GFP-LC3 protein (**Figure 42A-B**).

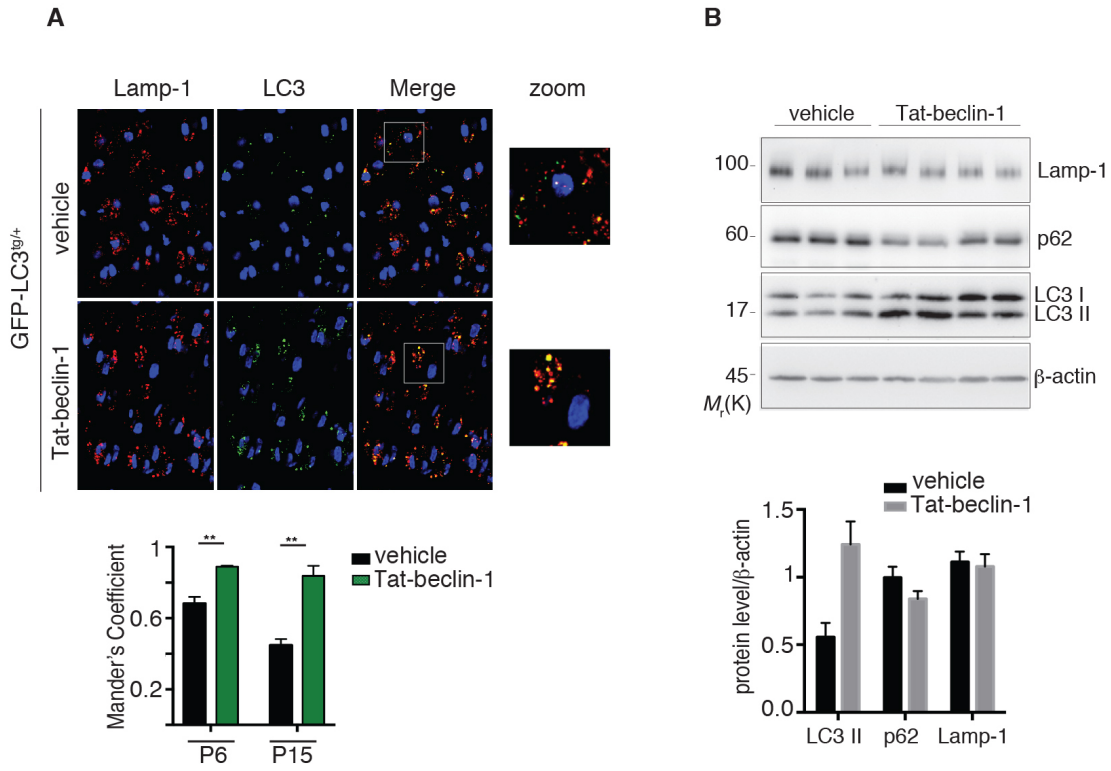

Figure 42. Tat-Beclin-1 peptide promotes Av-Lys fusion in the growth plate of wild type mice. **A**, Representative images of GFP–LC3 puncta (autophagosomes) and Lamp-1 immunostaining in femoral growth plates from GFP–LC3$^{tg/+}$ mice at P6 and P15. Tat–beclin-1 peptide was administered where indicated (2 mg kg^{-1}, daily for 6 and 15 days). The insets show a higher magnification of co-localization in selected areas. Scale bar, 10µm. Bar graphs display quantification of Lamp-1-LC3 co-localization. Values are Mander's coefficients means (±s.e.m.) of n = 3 mice per group (Student's t-test, **p<0.005). **B**, Western blot analysis of Lamp-1, SQSTM1/p62 and LC3 in femoral growth plates homogenates. Tat–beclin-1 peptide was administered where indicated (2 mg kg^{-1}, daily for 6 days). Bar graph displays amount of proteins relative to β-Actin. N=3 vehicle and n=4 Tat-Beclin-1 injected mice.

This beneficial effect was retained when Tat-Beclin1 was injected in *Gusb*$^{-/-}$ mice bearing the reporter GFP-LC3 protein (*Gusb*$^{-/-}$;GFP-LC3$^{tg/+}$) (**Figure 43A-B**).

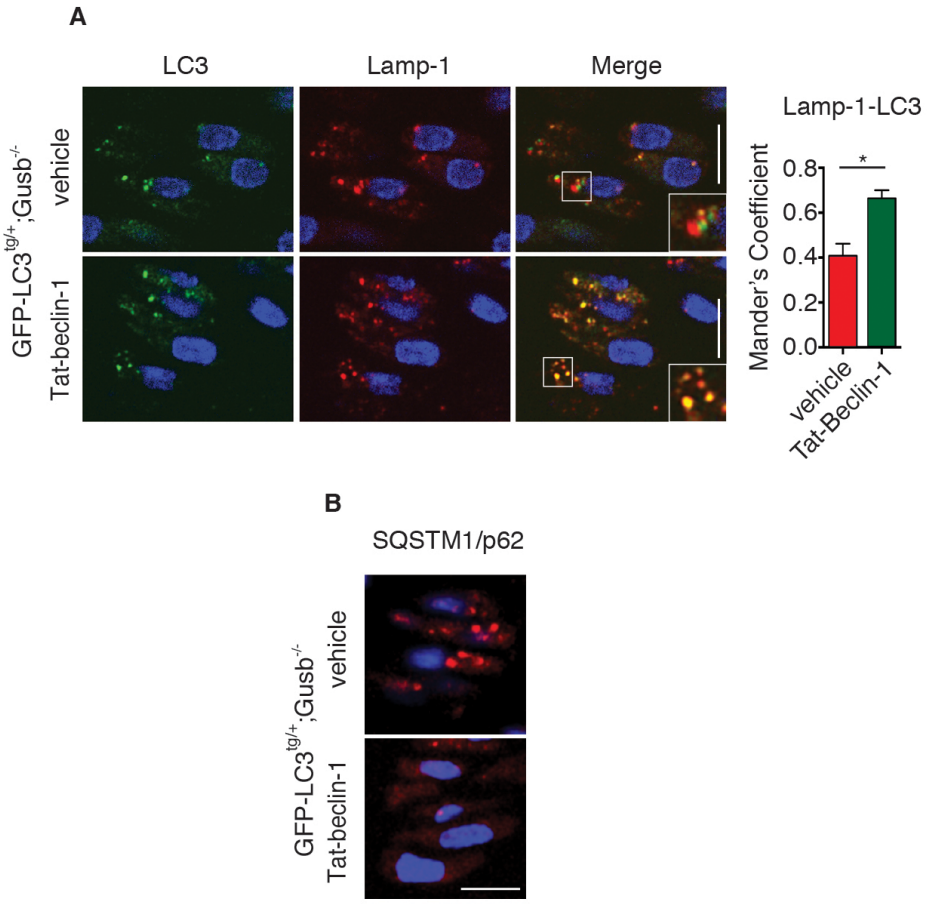

Figure 43. Enhanced autophagy improves bone phenotype in MPS mice.
A-B, Representative images of (**A**) GFP–LC3 puncta (autophagosomes), Lamp-1 and (**B**) SQSTM1/p62 immunostaining in femoral growth plates from *Gusb*$^{-/-}$;GFP–LC3$^{tg/+}$ mice at P6. Tat–beclin-1 peptide was administered where indicated (2 mg kg^{-1}, daily for 6 days). The insets show a higher magnification of co-localization in selected areas. Scale bar, 10µm. Bar graph displays quantification of Lamp-1-LC3 co-localization. Values are Mander's coefficients means (±s.e.m.) (ImageJ plug-in) of n = 3 mice per group (Student's t-test, *p<0.05).

Strikingly, *Gusb*$^{-/-}$ mice treated daily with Tat-Beclin1 showed increased collagen levels in femoral and tibia cartilages (**Figure 44A-C**) and increased femur and tibia length compared to untreated *Gusb*$^{-/-}$ mice at P15 (**Figure 44D-E**).

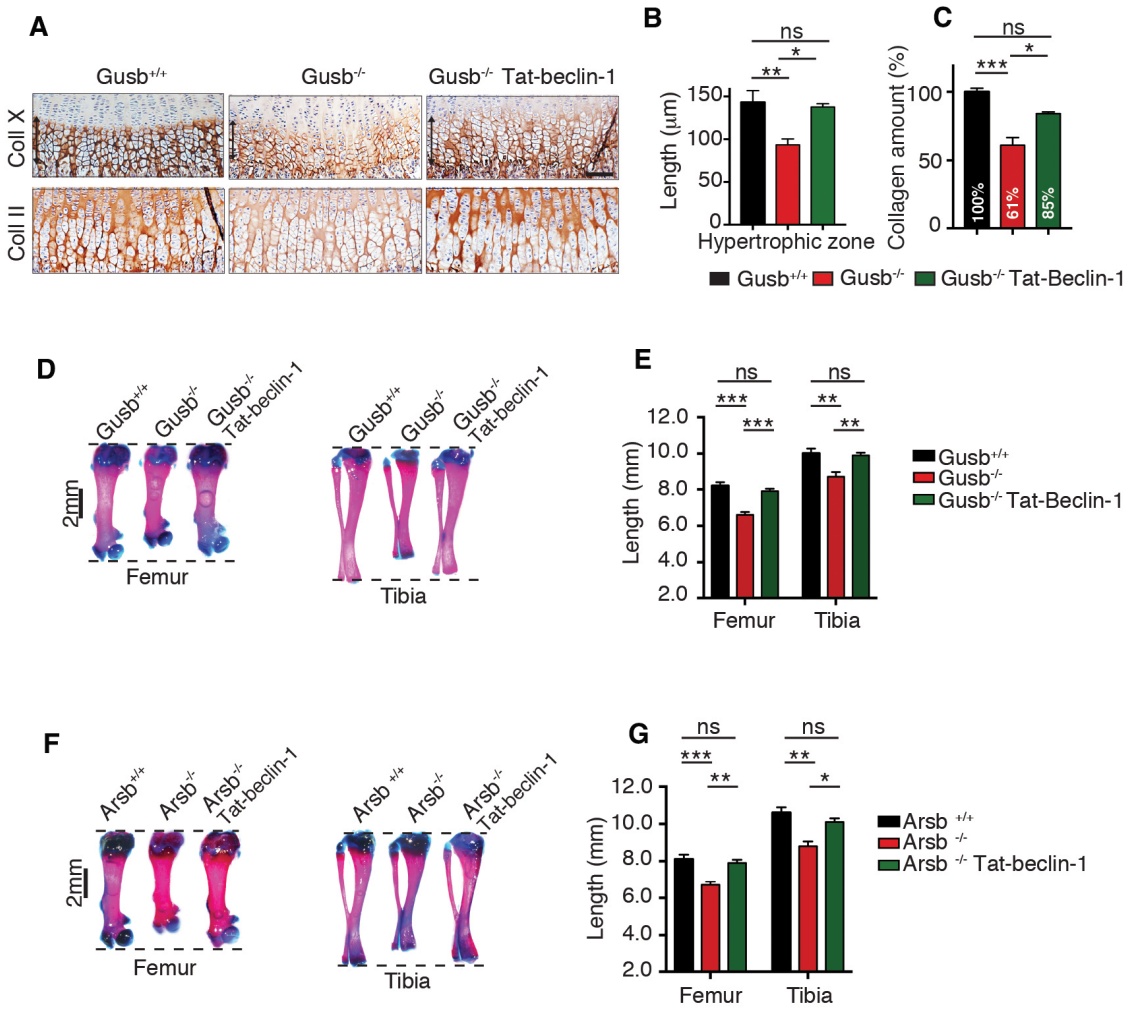

Figure 44. ***Enhanced autophagy improves bone growth in MPS mice.***
A, Representative images of P15 femoral growth plates sections from *Gusb*$^{+/+}$, *Gusb*$^{-/-}$ and *Gusb*$^{-/-}$ Tat-Beclin-1 treated mice immunostained with Coll X and Coll II. Nuclei were counterstained with hematoxylin. N=3 mice per group. Scale bar (100µm). **B,** Bar graphs displaying the length of hypertrophic zone measured according to Coll X staining (ANOVA, P=0.002; Tukey's post-hoc test, * $p \leq 0.05$, ** $p \leq 0.005$). **C,** Quantitative measure of collagen levels in the growth plate homogenates isolated from mice with indicated genotypes. Values are expressed as % relative to Gusb$^{+/+}$ mice. (ANOVA, P=9.52E-05; Tukey's post-hoc test, *p≤0.05, ***p<0.0005). **D**, Representative images of alcian blue/alizared red staining of femurs and tibias from P15 *Gusb*$^{+/+}$, *Gusb*$^{-/-}$ and *Gusb*$^{-/-}$ Tat-Beclin-1 treated (2mg/kg daily for 15 days) mice ($n \geq 8$ mice per group). **E**, Bar graphs displaying femur and tibia lengths from mice with the indicated genotype, data are expressed as mean (±s.e.m) (ANOVA, femur P=2.22E-06, tibia P=0.0006; ***p<0.0005). **F**, Representative images of alcian blue/alizared red staining of femurs and tibias from P15 *Arsb*$^{+/+}$, *Arsb*$^{-/-}$ and *Arsb*$^{-/-}$ Tat-Beclin-1 treated (2mg/kg daily for 15 days) mice ($n \geq 6$ mice per group). **G**, Bar graphs displaying femur and tibia lengths from mice with the indicated genotype, data are expressed as mean (±s.e.m) (ANOVA, femur P=0.0008, tibia P=0.001; * $p \leq 0.05$, ** $p \leq 0.005$, ***p<0.0005).

Similar results were obtained in a different LSD mouse model (MPSVI; *Arsb*$^{-/-}$) (**Figure 44F-G**), indicating that our findings may be also extended to other LSDs.

These data clearly point to autophagy dysfunction as a major contributor of the bone growth retardation in LSD mice.

Discussion

In the first part of my PhD I contributed to the identification of a novel pathogenic mechanism responsible for dysfunctional autophagy in lysosomal storage disorders, while in the second part of my PhD I used the knowledge derived from the previous work to develop therapeutic approaches for the treatment of bone growth retardation in LSDs mouse models.

Lysosomal storage disorders are inherited diseases characterized by progressive intracellular accumulation of undigested macromolecules due to lysosomal dysfunction. This results in a complex phenotype with broad pathological manifestations. Most of LSDs are characterized by defective skeletal growth[71]. Despite this, the mechanism by which lysosomal storage affects the function of bone cells is still unknown and the efficacy of current therapies on the skeletal system is very limited[44]. In this work we have identified a novel pathway that contributes to the bone growth retardation in LSDs. Autophagy dysfunction is a general phenomenon occurring in many LSDs although the pathogenic mechanisms are still unclear[72]. To date, the driving hypothesis is that the impairment of lysosomal degradation would impair the subsequent degradation of autophagosome, thus delaying the autophagic flux. However, our data point to mTORC1 and autophagy as main downstream effectors through which lysosomal storage affects chondrocyte functions. mTORC1 is a protein-signaling complex at the fulcrum of anabolic and catabolic processes, which acts depending on wide-ranging environmental cues[8]. It is generally accepted that lysosomes facilitate mTORC1 activation by generating an internal pool of amino acids. Amino acids activate mTORC1 by stimulating its translocation to the lysosomal membrane where it forms a super-complex involving several lysosomal resident proteins and where it can encounter its activator Rheb. The physical interaction between lysosome and mTORC1 suggests a

mechanistic co-regulation, indeed several studies have demonstrated that the translocation and mTORC1 activation require functional lysosomes[73][25]. Here we found that, in contrast to this well-accepted concept, in LSD chondrocytes inhibition of lysosomal activity potently activated mTORC1 signaling. Others have obtained similar results recently[64]: in 2015, Newton et al. found that the inhibition of v-ATPase proton pump by Bafylomycin A_1 treatment enhanced mTORC1 in chondrocytes. Their data point to an autophagy-independent mechanism and the authors do not provide sufficient explanation to this phenomenon. It is believed that in some terminally differentiated cell types the mechanism of lysosome-dependent mTORC1 activation might be different. Strikingly, our work shows that the mTORC1 over-activation can be blunted by pharmacological inhibition of the proteasome. Since we cannot extend our findings to other LSD cellular models, such as fibroblast or HeLa cell line knockout for a lysosomal gene, we hypothesized that lysosomal storage triggers a chondrocyte-specific response that enhances mTORC1 signaling.

A cross talk between lysosomes and proteasomes, the two main degradative station of the cell, exists. Thus, the autophagy and UPS are two cornerstones of cellular catabolism that are involved in most aspects of normal physiology and development, and are also implicated in a broad array of pathological states. Their critical role in the maintenance of cellular homeostasis, suggests that their activities need to be carefully orchestrated. Furthermore, the amino acids derived from proteasome-mediated proteolysis can induce mTORC1 signaling[58], [74]. Recently, a new mechanism has been described by which through the involvement of the proteasome, mTORC1 exerts a coordinated regulation of protein synthesis and degradation. Indeed, as well as increasing protein synthesis, mTORC1 activation also promotes an increased capacity for protein degradation. Cells with activated mTORC1 exhibit elevated levels of intact and active proteasomes through a global increase in the expression of genes encoding

proteasome subunits. Thus, in addition to serving as a quality control mechanism for newly translated proteins, the enhanced proteasome activity upon mTORC1 activation could serve to maintain adequate pools of amino acids to sustain new protein synthesis.

In our cellular model (**Figure 45**), the phenotype we described seems to be the consequence of an enhanced proteasome activity that, by increasing cellular amino acid levels, sustains mTORC1 signaling. The mechanism by which lysosome inhibition led to the increased proteasome activity is currently unclear. Recent data indicated that proteasome turnover is mediated by lysosome[66], [75]. One possibility could be that lysosome dysfunction by impairing proteasome turnover raises its intracellular level and in turn enhances its total activity. Our observations suggest the existence of additional, still uncharacterized, pathway through which the lysosome may indirectly regulate mTORC1 signaling in chondrocytes. The fine-tuning of the lysosome-proteasome cross talk may be of fundamental importance for chondrocytes and can be explained as an environmental adaptation that permits them to survive in the restricted vascular supply of cartilage. Similar findings have recently been reported to occur in denervated muscle fibers, suggesting that proteasome can sustain mTORC1 signaling during pathological conditions[76].

Surprisingly, we found that an enhanced mTORC1 signaling does not significantly impact AVs biogenesis but rather inhibits autophagy flux at level of autophagosome-lysosome fusion. Similarly, neurons in which mTORC1 is chronically active due to the lack of tuberous sclerosis complex activity showed inhibition of autophagy at the level of autophagosome-lysosome fusion[77]. These observations suggest that the activation of mTORC1 above physiological levels does not inhibit autophagy by further suppressing AV biogenesis, but rather acting on maturation steps.

Consistent with previous observations, we found that mTORC1 can inhibit autophagosome-lysosome fusion through the modulation of UVRAG activity[17]. In

particular, we found that in MPS chondrocytes the hyper-phosphorylation of UVRAG strengthens its association with the inhibitory partner Rubicon, while having no effect on the interaction with members of the HOPS tethering complex. Our data suggest that at least in chondrocytes UVRAG modulates autophagosome-lysosome fusion as part of the Beclin1/Vps34 complex, further reinforcing the observation that the production of PI3P by Vps34 complexes regulates autophagy at multiple levels[10] (**Figure 45**).

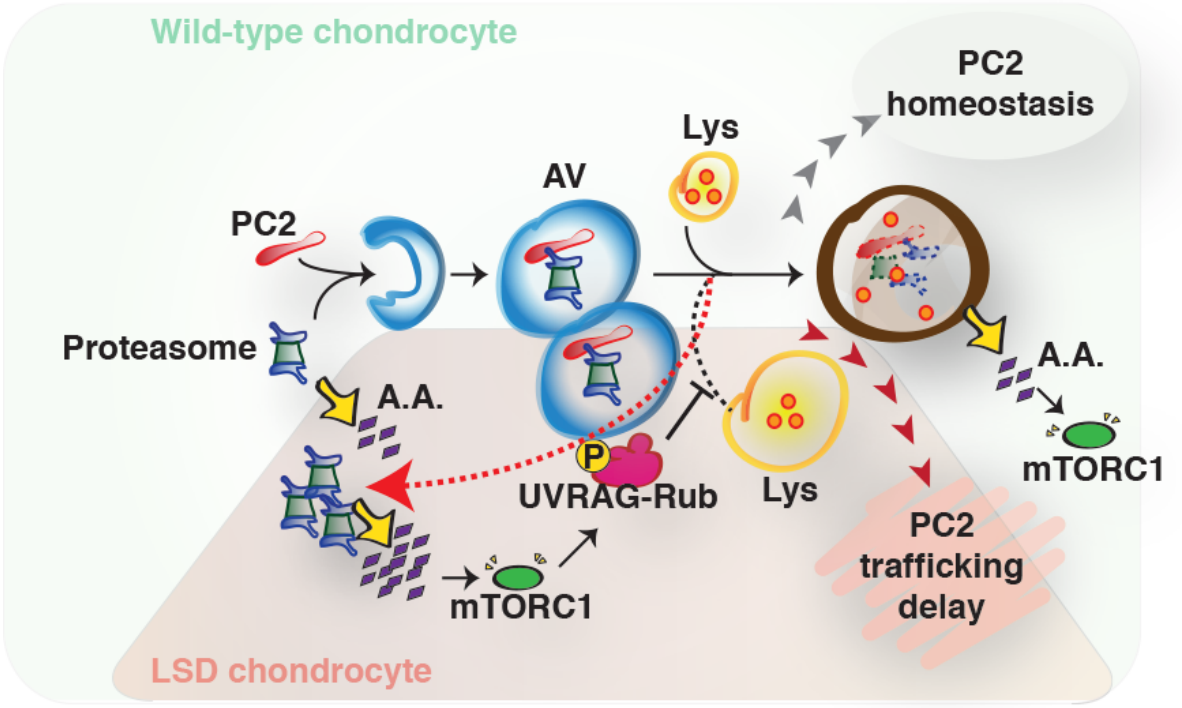

Figure 45. Model proposed for enhanced mTORC1 signaling in LSD chondrocytes.
In wild-type chondrocytes (upper green part) an equilibrium exists between the intracellular pool of amino acids (A.A.) produced by lysosomal (Lys) and proteasomal (P) activities. This source of energy activates mTORC1 to physiological levels required for different activities within the growth plate. The fine-tuned mTORC1 activity is particularly important for autophagy regulation, autophagosome (AV) biogenesis, AV-Lys fusion and, in turn, procollagen2 (PC2) homeostasis. Lysosomal impairment in case of LSD (lower red part) creates an imbalance between the two catalytic organelles (Lys and P). In particular, proteasome amount and/or activity are enhanced, leading to an excess of intracellular A.A. responsible for abnormal mTORC1 signaling. Among the autophagy targets of mTORC1, UVRAG activity is particular sensitive to mTORC1 phosphorylation. Thus in case of LSD a stable complex between UVRAG and Rubicon is found; this affects primarily AV-Lys fusion leading to AV accumulation and subsequent delay in procollagen trafficking.

In the second part of my PhD thesis, I extended the findings obtained *in vitro* trying to propose the underlying mechanism for bone growth retardation in mouse models of LSDs.

As expected, a block of autophagy and an upregulation of mTORC1 signaling were found in femoral growth plates derived from MPS VII mice. Moreover, these mice show severe long bone retardation when compared to control mice up to 1 month of age.

The work done by our lab in the last year showed that a sustained inhibition of autophagy might impair bone growth at least in part by affecting type II collagen trafficking and secretion[30]. Accordingly, we found a significant reduction in the amount of collagen within the growth plate of MPS VII mice. In particular, we found a reduction in type X collagen and in turn an impairment of hypertrophic zone thickness, main marker of healthy bone growth.

Consistent with the model we investigated *in vitro*, we show that genetic limitation of mTORC1 signaling (*Gusb*$^{-/-}$;*Rpt*$^{+/-}$) improved collagen levels in the cartilages and in turn bone growth retardation in MPS VII mice followed up to 1 month of age. This rescue clearly demonstrate that through the block of autophagy flux, mTORC1 exerts a tight regulation within the growth plate, extending the significance of the autophagic process in terms of the functional demands of the skeleton in growth and homeostasis.

Moreover, we were able to show that enhancing autophagy by daily injections of Tat-Beclin-1 peptide improved collagen levels in the cartilages and in turn bone growth retardation in two different mouse models of MPSs (MPS VII and MPS VI).

This rescue occurred even without reverting lysosomal phenotype in chondrocytes, suggesting that targeting secondary pathways, which are altered as consequence of lysosomal storage, may represent an appealing therapeutic approach for the treatment of

MPS disease features that are currently unresponsive to therapy, such as bone growth retardation.

In conclusion our data indicate a role for autophagy and mTORC1 in the genetic disorders affecting the skeleton, hence extending the list of diseases that can benefit from development of therapeutic agents targeting these two pathways.

Acknowledgements

Carmine Settembre is a young, enthusiastic researcher and good food & wine connoisseur. The latter is usually a characteristic difficult to manage within the hard work of research, however these two abilities in Carmine are perfectly combined, strengthening its passion and the ability to recognize “the good” in any field.
My meetings with him were always impromptu and happened at my bench (DAILY) thus this PhD experience has been, above all, dynamic!
I’m very grateful to him and I’m extremely satisfied for the good work we have done together.

I would like to thank his entire research group: Laura, Chiara, Annachiara, Alison, Carmen, Maria and Marilina for their encouragement, their help and for all the fun we have had in the last three years.

Besides my supervisor, I’m also thankful to my former mentor Alberto Auricchio for his kindness and helpfulness. I still owe Alberto a great deal of gratitude for helping me to develop into the scientist that I am today.

I have to thank R., the Rainbow who shone colored light in my PhD tunnel.

My family and my nephews, most of my life is for them.

Bibliography

[1] H. M. Kronenberg, “Developmental regulation of the growth plate,” *Nature*, vol. 423, no. 6937, pp. 332–336, May 2003.

[2] E. F. Wagner and G. Karsenty, “Genetic control of skeletal development,” *Curr. Opin. Genet. Dev.*, vol. 11, no. 5, pp. 527–532, Oct. 2001.

[3] M. B. Goldring, K. Tsuchimochi, and K. Ijiri, “The control of chondrogenesis,” *J. Cell. Biochem.*, vol. 97, no. 1, pp. 33–44, Jan. 2006.

[4] S. Provot and E. Schipani, “Molecular mechanisms of endochondral bone development,” *Biochem. Biophys. Res. Commun.*, vol. 328, no. 3, pp. 658–665, Mar. 2005.

[5] E. Minina, C. Kreschel, M. C. Naski, D. M. Ornitz, and A. Vortkamp, “Interaction of FGF, Ihh/Pthlh, and BMP signaling integrates chondrocyte proliferation and hypertrophic differentiation,” *Dev. Cell*, vol. 3, no. 3, pp. 439–449, Sep. 2002.

[6] J. Kaur and J. Debnath, “Autophagy at the crossroads of catabolism and anabolism,” *Nat. Rev. Mol. Cell Biol.*, vol. 16, no. 8, pp. 461–472, Aug. 2015.

[7] D. Glick, S. Barth, and K. F. Macleod, “Autophagy: cellular and molecular mechanisms,” *J. Pathol.*, vol. 221, no. 1, pp. 3–12, May 2010.

[8] M. Laplante and D. M. Sabatini, “mTOR signaling in growth control and disease,” *Cell*, vol. 149, no. 2, pp. 274–293, Apr. 2012.

[9] S. F. Funderburk, Q. J. Wang, and Z. Yue, “The Beclin 1-VPS34 complex--at the crossroads of autophagy and beyond,” *Trends Cell Biol.*, vol. 20, no. 6, pp. 355–362, Jun. 2010.

[10] J. M. Backer, “The regulation and function of Class III PI3Ks: novel roles for Vps34,” *Biochem. J.*, vol. 410, no. 1, pp. 1–17, Feb. 2008.

[11] R. C. Russell *et al.*, “ULK1 induces autophagy by phosphorylating Beclin-1 and activating VPS34 lipid kinase,” *Nat. Cell Biol.*, vol. 15, no. 7, pp. 741–750, Jul. 2013.

[12] J. Kim, M. Kundu, B. Viollet, and K.-L. Guan, “AMPK and mTOR regulate autophagy through direct phosphorylation of Ulk1,” *Nat. Cell Biol.*, vol. 13, no. 2, pp. 132–141, Feb. 2011.

[13] K. Matsunaga *et al.*, “Two Beclin 1-binding proteins, Atg14L and Rubicon, reciprocally regulate autophagy at different stages,” *Nat. Cell Biol.*, vol. 11, no. 4, pp. 385–396, Apr. 2009.

[14] S. Pattingre *et al.*, “Bcl-2 antiapoptotic proteins inhibit Beclin 1-dependent autophagy,” *Cell*, vol. 122, no. 6, pp. 927–939, Sep. 2005.

[15] C. A. Lamb, T. Yoshimori, and S. A. Tooze, “The autophagosome: origins unknown, biogenesis complex,” *Nat. Rev. Mol. Cell Biol.*, vol. 14, no. 12, pp. 759–774, Dec. 2013.

[16] C. Liang *et al.*, “Beclin1-binding UVRAG targets the class C Vps complex to coordinate autophagosome maturation and endocytic trafficking,” *Nat. Cell Biol.*, vol. 10, no. 7, pp. 776–787, Jul. 2008.

[17] Y.-M. Kim *et al.*, “mTORC1 phosphorylates UVRAG to negatively regulate autophagosome and endosome maturation,” *Mol. Cell*, vol. 57, no. 2, pp. 207–218, Jan. 2015.

[18] Q. Sun *et al.*, “The RUN Domain of Rubicon Is Important for hVps34 Binding, Lipid Kinase Inhibition, and Autophagy Suppression,” *J. Biol. Chem.*, vol. 286, no. 1, pp. 185–191, Jan. 2011.

[19] J. D. Rabinowitz and E. White, “Autophagy and Metabolism,” *Science*, vol. 330, no. 6009, pp. 1344–1348, Dec. 2010.

[20] J. Huang and B. D. Manning, “A complex interplay between Akt, TSC2, and the two mTOR complexes,” *Biochem. Soc. Trans.*, vol. 37, no. Pt 1, pp. 217–222, Feb. 2009.

[21] Y. Sancak *et al.*, “The Rag GTPases bind raptor and mediate amino acid signaling to mTORC1,” *Science*, vol. 320, no. 5882, pp. 1496–1501, Jun. 2008.

[22] A. Efeyan, R. Zoncu, and D. M. Sabatini, “Amino acids and mTORC1: from lysosomes to disease,” *Trends Mol. Med.*, vol. 18, no. 9, pp. 524–533, Sep. 2012.

[23] E. Kim, P. Goraksha-Hicks, L. Li, T. P. Neufeld, and K.-L. Guan, “Regulation of TORC1 by Rag GTPases in nutrient response,” *Nat. Cell Biol.*, vol. 10, no. 8, pp. 935–945, Aug. 2008.

[24] Y. Sancak, L. Bar-Peled, R. Zoncu, A. L. Markhard, S. Nada, and D. M. Sabatini, “Ragulator-Rag Complex Targets mTORC1 to the Lysosomal Surface and Is Necessary for Its Activation by Amino Acids,” *Cell*, vol. 141, no. 2, pp. 290–303, Apr. 2010.

[25] R. Zoncu, L. Bar-Peled, A. Efeyan, S. Wang, Y. Sancak, and D. M. Sabatini, “mTORC1 senses lysosomal amino acids through an inside-out mechanism that requires the vacuolar H(+)-ATPase,” *Science*, vol. 334, no. 6056, pp. 678–683, Nov. 2011.

[26] M. Sardiello *et al.*, “A gene network regulating lysosomal biogenesis and function,” *Science*, vol. 325, no. 5939, pp. 473–477, Jul. 2009.

[27] C. Settembre *et al.*, “A lysosome-to-nucleus signalling mechanism senses and regulates the lysosome via mTOR and TFEB,” *EMBO J.*, vol. 31, no. 5, pp. 1095–1108, Mar. 2012.

[28] A. Roczniak-Ferguson *et al.*, “The transcription factor TFEB links mTORC1 signaling to transcriptional control of lysosome homeostasis,” *Sci. Signal.*, vol. 5, no. 228, p. ra42, Jun. 2012.

[29] C. Settembre *et al.*, "TFEB links autophagy to lysosomal biogenesis," *Science*, vol. 332, no. 6036, pp. 1429–1433, Jun. 2011.

[30] L. Cinque *et al.*, "FGF signalling regulates bone growth through autophagy," *Nature*, vol. 528, no. 7581, pp. 272–275, Dec. 2015.

[31] D. M. Ornitz and P. J. Marie, "FGF signaling pathways in endochondral and intramembranous bone development and human genetic disease," *Genes Dev.*, vol. 16, no. 12, pp. 1446–1465, Jun. 2002.

[32] N. Ohbayashi *et al.*, "FGF18 is required for normal cell proliferation and differentiation during osteogenesis and chondrogenesis," *Genes Dev.*, vol. 16, no. 7, pp. 870–879, Apr. 2002.

[33] S. Shoji-Kawata *et al.*, "Identification of a candidate therapeutic autophagy-inducing peptide," *Nature*, vol. 494, no. 7436, pp. 201–206, Feb. 2013.

[34] B. Yan *et al.*, "mTORC1 regulates PTHrP to coordinate chondrocyte growth, proliferation and differentiation," *Nat. Commun.*, vol. 7, p. 11151, 2016.

[35] L. P. Lai, B. N. Lilley, J. R. Sanes, and A. P. McMahon, "Lkb1/Stk11 regulation of mTOR signaling controls the transition of chondrocyte fates and suppresses skeletal tumor formation," *Proc. Natl. Acad. Sci. U. S. A.*, vol. 110, no. 48, pp. 19450–19455, Nov. 2013.

[36] Ó. Álvarez-García *et al.*, "Growth Hormone Improves Growth Retardation Induced by Rapamycin without Blocking Its Antiproliferative and Antiangiogenic Effects on Rat Growth Plate," *PLoS ONE*, vol. 7, no. 4, Apr. 2012.

[37] A. Ciechanover, "Proteolysis: from the lysosome to ubiquitin and the proteasome," *Nat. Rev. Mol. Cell Biol.*, vol. 6, no. 1, pp. 79–87, Jan. 2005.

[38] V. I. Korolchuk, F. M. Menzies, and D. C. Rubinsztein, “Mechanisms of cross-talk between the ubiquitin-proteasome and autophagy-lysosome systems,” *FEBS Lett.*, vol. 584, no. 7, pp. 1393–1398, Apr. 2010.

[39] J. P. Luzio, P. R. Pryor, and N. A. Bright, “Lysosomes: fusion and function,” *Nat. Rev. Mol. Cell Biol.*, vol. 8, no. 8, pp. 622–632, Aug. 2007.

[40] A. H. Futerman and G. van Meer, “The cell biology of lysosomal storage disorders,” *Nat. Rev. Mol. Cell Biol.*, vol. 5, no. 7, pp. 554–565, Jul. 2004.

[41] L. A. Clarke and C. E. M. Hollak, “The clinical spectrum and pathophysiology of skeletal complications in lysosomal storage disorders,” *Best Pract. Res. Clin. Endocrinol. Metab.*, vol. 29, no. 2, pp. 219–235, Mar. 2015.

[42] E. NEUFELD, “The Mucopolysaccharidoses,” *Metab. Mol. Bases Inherit. Dis.*, pp. 3421–3452, 2001.

[43] D. J. Rowan, S. Tomatsu, J. H. Grubb, A. M. Montaño, and W. S. Sly, “Assessment of bone dysplasia by micro-CT and glycosaminoglycan levels in mouse models for mucopolysaccharidosis type I, IIIA, IVA, and VII,” *J. Inherit. Metab. Dis.*, vol. 36, no. 2, pp. 235–246, Mar. 2013.

[44] S. Tomatsu *et al.*, “Therapies for the bone in mucopolysaccharidoses,” *Mol. Genet. Metab.*, vol. 114, no. 2, pp. 94–109, Feb. 2015.

[45] D. J. Rowan *et al.*, “Long circulating enzyme replacement therapy rescues bone pathology in mucopolysaccharidosis VII murine model,” *Mol. Genet. Metab.*, vol. 107, no. 1–2, pp. 161–172, Sep. 2012.

[46] J. J. Boelens, “Trends in haematopoietic cell transplantation for inborn errors of metabolism,” *J. Inherit. Metab. Dis.*, vol. 29, no. 2–3, pp. 413–420, Apr. 2006.

[47] S. Tomatsu *et al.*, “Missense models [Gustm(E536A)Sly, Gustm(E536Q)Sly, and Gustm(L175F)Sly] of murine mucopolysaccharidosis type VII produced

by targeted mutagenesis," *Proc. Natl. Acad. Sci. U. S. A.*, vol. 99, no. 23, pp. 14982–14987, Nov. 2002.

[48] M. Evers *et al.*, "Targeted disruption of the arylsulfatase B gene results in mice resembling the phenotype of mucopolysaccharidosis VI," *Proc. Natl. Acad. Sci. U. S. A.*, vol. 93, no. 16, pp. 8214–8219, Aug. 1996.

[49] J. L. Suarez-Guerrero, P. J. I. Gómez Higuera, J. S. Arias Flórez, and G. A. Contreras-García, "[Mucopolysaccharidosis: clinical features, diagnosis and management]," *Rev. Chil. Pediatr.*, vol. 87, no. 4, pp. 295–304, Aug. 2016.

[50] S. Bruni, L. Loschi, C. Incerti, O. Gabrielli, and G. Coppa, "Update on treatment of lysosomal storage diseases," *Acta Myol.*, vol. 26, no. 1, pp. 87–92, Jul. 2007.

[51] A. Ballabio and V. Gieselmann, "Lysosomal disorders: from storage to cellular damage," *Biochim. Biophys. Acta*, vol. 1793, no. 4, pp. 684–696, Apr. 2009.

[52] A. P. Lieberman, R. Puertollano, N. Raben, S. Slaugenhaupt, S. U. Walkley, and A. Ballabio, "Autophagy in lysosomal storage disorders," *Autophagy*, vol. 8, no. 5, pp. 719–730, May 2012.

[53] C. Settembre *et al.*, "A block of autophagy in lysosomal storage disorders," *Hum. Mol. Genet.*, vol. 17, no. 1, pp. 119–129, Jan. 2008.

[54] F. Pan *et al.*, "The regulation-of-autophagy pathway may influence Chinese stature variation: evidence from elder adults," *J. Hum. Genet.*, vol. 55, no. 7, pp. 441–447, Jul. 2010.

[55] L. Bonafe *et al.*, "Nosology and classification of genetic skeletal disorders: 2015 revision," *Am. J. Med. Genet. A.*, vol. 167A, no. 12, pp. 2869–2892, Dec. 2015.

[56] A. Hershko and and A. Ciechanover, "The Ubiquitin System," *Annu. Rev. Biochem.*, vol. 67, no. 1, pp. 425–479, 1998.

[57] J. Driscoll, “The role of the proteasome in cellular protein degradation,” *Histol. Histopathol.*, vol. 9, no. 1, pp. 197–202, Jan. 1994.

[58] Y. Zhang and B. D. Manning, “mTORC1 signaling activates NRF1 to increase cellular proteasome levels,” *Cell Cycle Georget. Tex*, vol. 14, no. 13, pp. 2011–2017, 2015.

[59] E. V. Polishchuk *et al.*, “Wilson Disease Protein ATP7B Utilizes Lysosomal Exocytosis to Maintain Copper Homeostasis,” *Dev. Cell*, vol. 29, no. 6, pp. 686–700, Jun. 2014.

[60] K. B. King and J. H. Kimura, “The establishment and characterization of an immortal cell line with a stable chondrocytic phenotype,” *J. Cell. Biochem.*, vol. 89, no. 5, pp. 992–1004, Aug. 2003.

[61] H. E. J. Polson *et al.*, “Mammalian Atg18 (WIPI2) localizes to omegasome-anchored phagophores and positively regulates LC3 lipidation,” *Autophagy*, vol. 6, no. 4, pp. 506–522, May 2010.

[62] D. J. Klionsky *et al.*, “Guidelines for the use and interpretation of assays for monitoring autophagy (3rd edition),” *Autophagy*, vol. 12, no. 1, pp. 1–222, 2016.

[63] S. Kimura, T. Noda, and T. Yoshimori, “Dissection of the autophagosome maturation process by a novel reporter protein, tandem fluorescent-tagged LC3,” *Autophagy*, vol. 3, no. 5, pp. 452–460, Oct. 2007.

[64] P. T. Newton, K. K. Vuppalapati, T. Bouderlique, and A. S. Chagin, “Pharmacological inhibition of lysosomes activates the MTORC1 signaling pathway in chondrocytes in an autophagy-independent manner,” *Autophagy*, vol. 11, no. 9, pp. 1594–1607, 2015.

[65] A. Pievani *et al.*, “Comparative analysis of multilineage properties of mesenchymal stromal cells derived from fetal sources shows an advantage of

mesenchymal stromal cells isolated from cord blood in chondrogenic differentiation potential," *Cytotherapy*, vol. 16, no. 7, pp. 893–905, Jul. 2014.

[66] T. Zhang, S. Shen, J. Qu, and S. Ghaemmaghami, "Global Analysis of Cellular Protein Flux Quantifies the Selectivity of Basal Autophagy," *Cell Rep.*, vol. 14, no. 10, pp. 2426–2439, Mar. 2016.

[67] V. Cohen-Kaplan *et al.*, "p62- and ubiquitin-dependent stress-induced autophagy of the mammalian 26S proteasome," *Proc. Natl. Acad. Sci. U. S. A.*, vol. 113, no. 47, pp. E7490–E7499, Nov. 2016.

[68] D.-H. Kim *et al.*, "mTOR interacts with raptor to form a nutrient-sensitive complex that signals to the cell growth machinery," *Cell*, vol. 110, no. 2, pp. 163–175, Jul. 2002.

[69] S. Sengupta, T. R. Peterson, M. Laplante, S. Oh, and D. M. Sabatini, "mTORC1 controls fasting-induced ketogenesis and its modulation by ageing," *Nature*, vol. 468, no. 7327, pp. 1100–1104, Dec. 2010.

[70] B. Ronan *et al.*, "A highly potent and selective Vps34 inhibitor alters vesicle trafficking and autophagy," *Nat. Chem. Biol.*, vol. 10, no. 12, pp. 1013–1019, Dec. 2014.

[71] S. Tomatsu *et al.*, "Impairment of Body Growth in Mucopolysaccharidoses," in *Handbook of Growth and Growth Monitoring in Health and Disease*, V. R. Preedy, Ed. Springer New York, 2012, pp. 2091–2117.

[72] A. Ballabio, "Disease pathogenesis explained by basic science: lysosomal storage diseases as autophagocytic disorders," *Int. J. Clin. Pharmacol. Ther.*, vol. 47 Suppl 1, pp. S34-38, 2009.

[73] "Ragulator-Rag Complex Targets mTORC1 to the Lysosomal Surface and Is Necessary for Its Activation by Amino Acids: Cell." [Online]. Available:

http://www.cell.com/abstract/S0092-8674(10)00177-7. [Accessed: 27-Dec-2016].

[74] J. Zhao, B. Zhai, S. P. Gygi, and A. L. Goldberg, "mTOR inhibition activates overall protein degradation by the ubiquitin proteasome system as well as by autophagy," *Proc. Natl. Acad. Sci.*, vol. 112, no. 52, pp. 15790–15797, Dec. 2015.

[75] A. M. Cuervo, A. Palmer, A. J. Rivett, and E. Knecht, "Degradation of proteasomes by lysosomes in rat liver," *Eur. J. Biochem. FEBS*, vol. 227, no. 3, pp. 792–800, Feb. 1995.

[76] P. N. Quy, A. Kuma, P. Pierre, and N. Mizushima, "Proteasome-dependent activation of mammalian target of rapamycin complex 1 (mTORC1) is essential for autophagy suppression and muscle remodeling following denervation," *J. Biol. Chem.*, vol. 288, no. 2, pp. 1125–1134, Jan. 2013.

[77] D. Ebrahimi-Fakhari *et al.*, "Impaired Mitochondrial Dynamics And Mitophagy In Neuronal Models Of Tuberous Sclerosis Complex," *Cell Rep.*, vol. 17, no. 8, p. 2162, Nov. 2016.